

MODEL OF A FRESHWATER POND USED
FOR COLLECTION AND STORAGE
OF SOLAR ENERGY

By

DENNIS LEROY DATIN

Bachelor of Science

Oklahoma State University

Stillwater, Oklahoma

1972

Submitted to the Faculty of the Graduate College
of the Oklahoma State University
in partial fulfillment of the requirements
for the Degree of
MASTER OF SCIENCE
December, 1979

Thesis
1979
D2345m
cop. 2



MODEL OF A FRESHWATER POND USED
FOR COLLECTION AND STORAGE
OF SOLAR ENERGY

Thesis Approved:

Bobby L. Clay

Thesis Adviser

Charles E. Rice

George H. Maloney

Norman N. Durham

Dean of the Graduate College

1042931

ACKNOWLEDGMENTS

The author expresses his gratitude to his major adviser, Dr. Bobby L. Clary, for his patience and guidance throughout the study. Special appreciation is extended to the other advisory members, Dr. Charles E. Rice and Dr. George W. A. Mahoney, both of the Agricultural Engineering Department. Thanks goes to the former head of the department, Professor Jay G. Porterfield; the present head of the department, Dr. C. T. Haan; and Dr. Bobby L. Clary for obtaining funds to support this project.

I thank Mr. Jack Fryrear for his excellent assistance in the photography and preparation of figures. I am grateful to Mr. Norvil Cole and Mr. David Farmer for their guidance and assistance during this project. I am also grateful to Douglas R. Devoe, Patrick Jackson, Gene Miiller, Brian Anderson, and Philip Hurst for their help in construction and data analysis.

I am grateful to Mrs. Darlene Richardson for her laboring efforts in typing the rough and final draft of this thesis. I extend a special appreciation to my fellow graduate students who put up with me during my high and low times. I want to thank the Lord for providing me with the health and ability needed to accomplish this task.

For their many sacrifices and encouragement throughout my educational experience, I am grateful to my parents, Marion and Alice Datin. I wish to thank my lovely wife, Colette, for her help and encouragement throughout the writing of this thesis. To my wife and parents, I dedicate this thesis.

TABLE OF CONTENTS

Chapter	Page
I. INTRODUCTION	1
II. LITERATURE REVIEW.	2
Solar Collectors.	2
Storage Mediums	9
III. EXPERIMENTAL APPARATUS AND DESIGN.	13
Apparatus	13
Transmittance	17
Plastic Absorber.	21
IV. THEORETICAL DEVELOPMENT.	28
V. DATA ANALYSIS AND RESULTS.	47
Temperature Distribution.	47
Average Water Temperature	70
Efficiency.	80
VI. SUMMARY AND CONCLUSIONS.	91
Summary	91
Conclusions	92
SELECTED BIBLIOGRAPHY	93

LIST OF TABLES

Table	Page
I. Experimental Performance of Curved-Cover, Bicurved-Absorber Solar Collector at Wooster, Ohio.	8
II. Selected Summary of Test Data for Three Water Solar Collectors	10
III. Data for Transmittance Tests (Millivolts).	20
IV. Results of Comparative Tests on Solar Film Stills for Polyethylene Under Different Meteorological Conditions	24
V. Constant Values for Specific Heat, Thermal Conductivity, and Density for Water and Air Between 60° and 135° F	30
VI. Data for Solar Radiation, Heat Loss Due to Convection and Radiation, Air Infiltration Losses, and Wind Velocities for 24 Hour Period on June 16, 1978, with Beginning Time Being 6:00 a.m. (CDT).	48
VII. Observed Water Temperatures and Average Water Temperatures in the Freshwater Solar Storage Model for 24 Hour Period on June 16, 1978, with Beginning Time Being 6:00 a.m. (CDT)	49
VIII. Summary of Storage Efficiency for Freshwater Storage Model.	89

LIST OF FIGURES

Figure	Page
1. Styles of Plastic Film Solar Collectors Used in Grain Drying	3
2. Schematic of Solar Collector Model	5
3. Solar Collector Performance for Noon Hour Operation.	6
4. Solar Collector Performance for Full Day Operation	7
5. Schematic of Freshwater Solar Storage Model.	15
6. Freshwater Solar Storage Model in Operation.	16
7. Correction Factor Curve for Dropwise Condensation on Glass	22
8. Correction Factor Curve for Transmittance Through Six Mil, Clear Polyethylene with 0 to 100% Coverage of Surface Area by Condensation.	23
9. Condition of the Six Mil, Black Polyethylene After Deteriorating from the Ultra-violet Rays of the Sun.	26
10. White-film Build Up on the Surface of the Six Mil, Black Polyethylene Absorber Surface.	27
11. Nodal-point Arrangement in Storage Model for Transient Condition.	39
12. Energy Balance on Surface Node	40
13. Energy Balance on Interior Node.	43
14. Energy Balance on Bottom Node.	45
15. Comparison Between Predicted and Observed Surface Temperatures in a Freshwater Solar Storage Model for June 16, 1978. Time Is Measured from 6:00 a.m. (CDT) of This Day	50
16. Comparison Between Predicted and Observed Temperatures One Inch Below the Surface in a Freshwater Solar Storage Model for June 16, 1978. Time Is Measured from 6:00 a.m. (CDT) of This Day	51
17. Comparison Between Predicted and Observed Temperatures Six Inches Below the Surface in the Freshwater Solar Storage Model for June 16, 1978. Time Is Measured from 6:00 a.m. (CDT) of This Day.	52

Figure	Page
18. Comparison Between Predicted and Observed Temperatures 10 Inches Below the Surface in the Freshwater Solar Storage Model for June 16, 1978. Time Is Measured from 6:00 a.m. (CDT) of This Day.	53
19. Comparison Between Predicted and Observed Temperatures 36 Inches Below the Surface in the Freshwater Solar Storage Model for June 16, 1978. Time Is Measured from 6:00 a.m. (CDT) of This Day.	54
20. Comparison Between Predicted and Observed Temperatures 72 Inches Below the Surface of the Freshwater Solar Storage Model for June 16, 1978. Time Is Measured from 6:00 a.m. (CDT) of This Day.	55
21. Temperature Profile in Freshwater Solar Storage Model for 6:00 a.m. (CDT) on June 16, 1978	57
22. Comparison Between Predicted and Observed Average Water Temperature in the Freshwater Solar Storage Model for June 16, 1978. Time Is Measured from 6:00 a.m. (CDT) of This Day.	58
23. Temperature Profile in Freshwater Solar Storage Model for Both Predicted and Observed Temperatures at 5:00 a.m. (CDT) on June 16, 1978.	59
24. Temperature Profile in Freshwater Solar Storage Model for Predicted and Observed Temperatures at 7:00 a.m. (CDT) on June 16, 1978	60
25. Comparison Between Predicted and Observed Solar Radiation for June 16, 1978. Time Is Measured from 6:00 a.m. (CDT) of This Day.	62
26. Comparison Between Predicted and Observed Heat Loss Due to Convection and Radiation for June 16, 1978. Time Is Measured from 6:00 a.m. (CDT) of This Day	63
27. Comparison Between Newly Predicted and Observed Average Water Temperature in the Freshwater Solar Storage Model for June 16, 1978. Time Is Measured from 6:00 a.m. (CDT) of This Day	65
28. Comparison Between Newly Predicted and Observed Surface Temperatures in the Freshwater Solar Storage Model for June 16, 1978. Time Is Measured from 6:00 a.m. (CDT) of This Day.	66

Figure	Page
29. Comparison Between Newly Predicted and Observed Temperatures One Inch Below the Surface in the Freshwater Solar Storage Model for June 16, 1978. Time Is Measured from 6:00 a.m. (CDT) of This Day.	67
30. Comparison Between Newly Predicted and Observed Temperatures Six Inches Below the Surface in the Freshwater Solar Storage Model for June 16, 1978. Time Is Measured from 6:00 a.m. (CDT) of This Day.	68
31. Comparison Between Newly Predicted and Observed Temperatures 10 Inches Below the Surface in the Freshwater Solar Storage Model for June 16, 1978. Time Is Measured from 6:00 a.m. (CDT) of This Day.	69
32. Temperature Profile in Freshwater Solar Storage Model for 3:00 p.m. (CDT) on June 26, 1978	71
33. Temperature Profile in Freshwater Solar Storage Model for 3:00 a.m. (CDT) on June 26, 1978	72
34. Temperature Profile in Freshwater Solar Storage Model for 3:00 p.m. (CDT) on June 18, 1978	73
35. Temperature Profile in Freshwater Solar Storage Model for 3:00 a.m. (CDT) on June 18, 1978	74
36. Solar Radiation Received at Stillwater, Oklahoma, on June 26, 1978. Time Is Measured from Midnight of Previous Day (CDT)	75
37. Solar Radiation Received at Stillwater, Oklahoma, on June 18, 1978. Time Is Measured from Midnight of Previous Day (CDT)	76
38. Average Water Temperature in Freshwater Solar Storage Model for Time of 6:00 a.m. (CDT).	77
39. Average Water Temperature in Freshwater Solar Storage Model for Time of 9:00 p.m. (CDT).	78
40. Solar Radiation Received for May and June of 1978 in Stillwater, Oklahoma, with the Blank Spaces Representing Times of No Data Being Recorded.	79
41. Daily Collection and Storage Efficiency for a 24 Hour Day Beginning at 12:00 a.m. as a Function of Average Water Temperature Difference in Storage Media Between Beginning and End of Each Period	82

Figure	Page
42. Daily Collection and Storage Efficiency for a 24 Hour Day Beginning at 12:00 a.m. with Infiltration Losses Included as a Function of Average Water Temperature Difference in Storage Media Between Beginning and End of Period.	84
43. Daily Collection and Storage Efficiency for a 15 Hour Day Beginning at 6:00 a.m. as a Function of Average Temperature Difference in Storage Media Between Beginning and End of Period.	86
44. Daily Collection and Storage Efficiency for a 18 Hour Day Beginning at 6:00 a.m. with Infiltration Losses Included as a Function of Average Water Temperature Difference in Storage Media Between Beginning and End of Period.	87

NOMENCLATURE

a	= absorptance of black polyethylene.
A_S	= surface area of black polyethylene absorber, ft^2 .
A_d	= cross-sectional area of air duct, ft^2 .
c_A	= specific heat of air, $\text{BTU/lbm-}^\circ\text{F}$.
c_w	= specific heat of water, $\text{BTU/lbm-}^\circ\text{F}$.
C_T	= correction factor for transmittance.
D_S	= diameter of polyethylene sphere, ft.
E	= vertical thermal eddy diffusivity, ft^2/hr .
F	= local radiative flux, BTU/hr-ft^2 .
FR	= fraction of cover covered by condensation.
g	= gravitational constant, ft/sec^2 .
Gr_L	= Grashof number based upon plate spacing, $\frac{g\beta(t_s-t_c)L^3}{\nu^2}$.
h	= convective heat transfer coefficient, $\text{BTU/hr-ft}^2\text{-}^\circ\text{F}$.
$h_{c,p-c}$	= convective heat transfer coefficient from surface plate to cover, $\text{BTU/hr-ft}^2\text{-}^\circ\text{F}$.
$h_{r,c-sky}$	= radiative heat transfer coefficient from the cover of the collector to the sky, $\text{BTU/hr-ft}^2\text{-}^\circ\text{F}$.
$h_{r,p-c}$	= radiative heat transfer coefficient from surface plate to cover, $\text{BTU/hr-ft}^2\text{-}^\circ\text{F}$.
h_w	= convective heat transfer coefficient from the cover due to wind, $\text{BTU/hr-ft}^2\text{-}^\circ\text{F}$.
HR	= pyranometer reading with cover, MV.
HR_N	= pyranometer reading without cover, MV.

k_A	= thermal conductivity of air, BTU/hr-ft ² -°F.
k_w	= thermal conductivity of water, BTU/hr-ft ² -°F.
L	= plate spacing between polyethylene cover and absorber, BTU/hr-ft ² -°F.
m_A	= mass flow rate of air, lbm/hr.
m_w	= mass of water, lbm.
M	= thermal molecular diffusivity, ft ² /hr.
\bar{Nu}_D	= Nusselt number based upon diameter, hD_s/k_A .
\bar{Nu}_L	= Nusselt number based upon plate spacing, hL/k_A .
Pr	= Prandlt number.
q'''	= internal energy generated, BTU/hr-ft ³ .
q'''_{RAD}	= rate of heat generated per unit volume by internal absorp- tion of solar radiation, BTU/hr-ft ³ .
Q_{AIR}	= quantity of air needed to keep polyethylene dome inflated, ft ³ /min.
Q_{CON}	= energy conducted in medium, BTU/hr.
Q_{CR}	= heat loss due to convection and radiation, BTU/hr-ft ² .
Q_{CRC}	= constant heat loss due to convection and radiation for 24 hour period, BTU/hr-ft ² .
Q_{CRD}	= maximum heat loss in daytime due to convection and radiation minus constant heat loss due to convection and radiation for 24 hour period, BTU/hr-ft ² .
Q_{INF}	= heat loss due to air infiltration, BTU/hr-ft ² .
Q_{RAD}	= solar radiation received, BTU/hr-ft ² .
Q_s	= energy stored in medium, BTU/hr.
$Q_{n+1,n}$	= energy conducted from node n+1 to n, BTU/hr.
$Q_{n-1,n}$	= energy conducted from node n-1 to n, BTU/hr.

Q_{sn}	= energy stored in the n^{th} node, BTU/hr.
Q_{S1}	= energy stored in node 1, BTU/hr.
Q_{S175}	= energy stored in node 175, BTU/hr.
Q_u	= useful energy gained by storage medium, BTU/day-ft ² .
Q_{21}	= energy conducted from node 2 to node 1, BTU/hr.
$Q_{174-175}$	= energy conducted from node 174 to node 175, BTU/hr.
Re_D	= Reynolds number based upon diameter, $V_0 D_s / \nu$.
t	= temperature of fluid at time θ or depth x , °F.
t_A	= temperature of air inside polyethylene dome, °F.
t_{AVE}	= average water temperature, °F.
t_c	= temperature of polyethylene cover, °F.
t_f	= final average water temperature at 12:00 a.m., °F.
t_i	= initial average water temperature at 1:00 a.m., °F.
t_n	= temperature of the n^{th} node, °F.
t'_n	= new temperature of the n^{th} node, °F.
t_{n+1}	= temperature of the $n+1$ node, °F.
t_{n-1}	= temperature of the $n-1$ node, °F.
t_0	= ambient air temperature, °F.
t_s	= temperature of polyethylene absorber surface, °F.
t_1	= temperature of node 1, °F.
t'_1	= new temperature of node 1, °F.
t_2	= temperature of node 2, °F.
t_{144}	= temperature of node 144, °F.
t_{145}	= temperature of node 145, °F.
t'_{145}	= new temperature of node 145, °F.
T_c	= temperature of polyethylene cover, °R.

T_o	= ambient air temperature, °R.
T_s	= temperature of polyethylene absorber, °R.
T_{sky}	= sky temperature, °R.
U_o	= overall heat transfer coefficient, BTU/hr-ft ² -°F.
V	= volume of storage medium, ft ³ .
V_d	= velocity of air in duct, ft/min.
V_o	= velocity of outside air over outside cover, ft/sec.
V_1	= volume of each node, ft ³ .
x	= x-direction (vertical direction with down as positive), ft.
y	= y-direction, ft.
z	= z-direction, ft.
β	= volumetric coefficient of thermal expansion for air, 1/°F.
ϵ_c	= emissivity of clear polyethylene.
ϵ_s	= emissivity of black polyethylene.
θ	= time, hr.
ν	= kinematic viscosity of air, ft ² /sec.
ρ_A	= density of air, lbm/ft ³ .
ρ_w	= density of water, lbm/ft ³ .
σ	= Stefan-Boltzman constant, BTU/hr-ft ² -°R ⁴ .
η_1	= total efficiency for 24 hour period.
η_2	= net efficiency for 24 hour period.
η_3	= total efficiency for 15 hour period.
η_4	= net efficiency for 15 hour period.
τ_c	= transmittance of polyethylene cover without condensation.
τ_p	= transmittance of polyethylene cover.
τ_w	= transmittance of polyethylene cover with condensation.
ω	= 0.2094, rad/hr.

Δx = distance between each node, ft.

$\Delta \theta$ = time interval, hr.

Δt = difference between initial and final average temperature,
°F.

CHAPTER I

INTRODUCTION

Solar energy has been used for drying of farm crops for several years. Flat-plate solar collectors have utilized either air or water and have provided part of the heat energy needed for drying crops. Drying by solar energy was generally conducted during periods of high solar radiation with conventional systems being used during periods of low solar radiation.

To make a solar crop drying system cost effective, a method of storage for the heat energy supplied by solar radiation needs to be developed to allow usage of the heat energy at times of low solar radiation. A medium that has been used for storage of solar energy is water due to its high specific heat and low cost.

In the crop producing areas of Oklahoma where drying is utilized, freshwater ponds are available for use as storage mediums. An experiment was developed to determine the feasibility of using a freshwater pond for collection and storage of solar energy. The objectives of this study are to develop methods for predicting temperature distributions in a freshwater pond utilizing existing heat transfer theory and to determine efficiency of six mil, black polyethylene as a solar absorber on the surface of a freshwater pond.

CHAPTER II

LITERATURE REVIEW

Solar Collectors

Solar energy can be collected by use of a flat-plate solar collector during periods of high solar radiation and stored in a medium for use at a time when solar radiation is zero or less. The flat-plate collectors are constructed from such materials as copper, aluminum, and plastics while the storage mediums can be water, rocks, or eutectic salts.

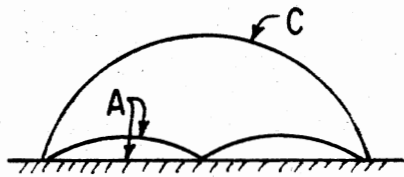
Figure 1 shows the styles of collectors used by Keener (13) where plastic was used for both the cover and absorber. He lists the following advantages and disadvantages of plastics as collector covers.

The advantages are:

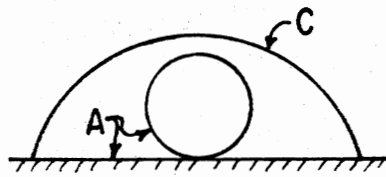
1. Lightweight - a specific gravity as low as 0.91 compared to about 2.72 for glass.
2. Flexibility - highly elastic and exceedingly strong which enables easy fabrication of various shaped collectors.
3. High radiation transmissivity - clear plastic films, such as polyethylene, have solar transmittance as high as 0.93 compared to about 0.9 for clear glass.
4. High absorptivity - opaque films have absorptivity near one.

The disadvantages are:

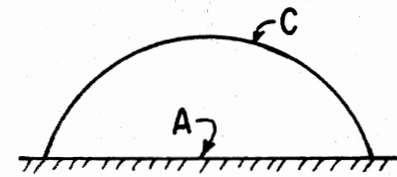
1. Long wave radiation transmissivity.
2. Aging effects associated with ultraviolet radiation.



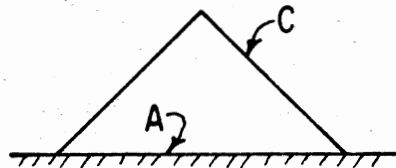
1a. Curved cover,
biconcave absorber



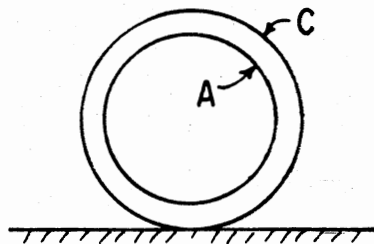
1b. Curved cover,
tubular absorber



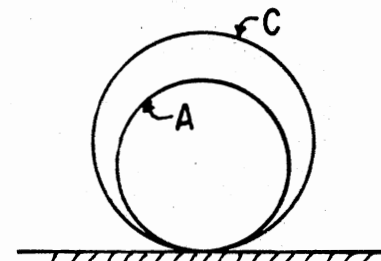
1c. Curved cover,
flat absorber



1d. Triangular



1e. Concentric tubular



1f. Eccentric tubular

A = absorber, C = cover

SOURCE: Keener (13, p. 94).

Figure 1. Styles of Plastic Film Solar Collectors Used in Grain Drying

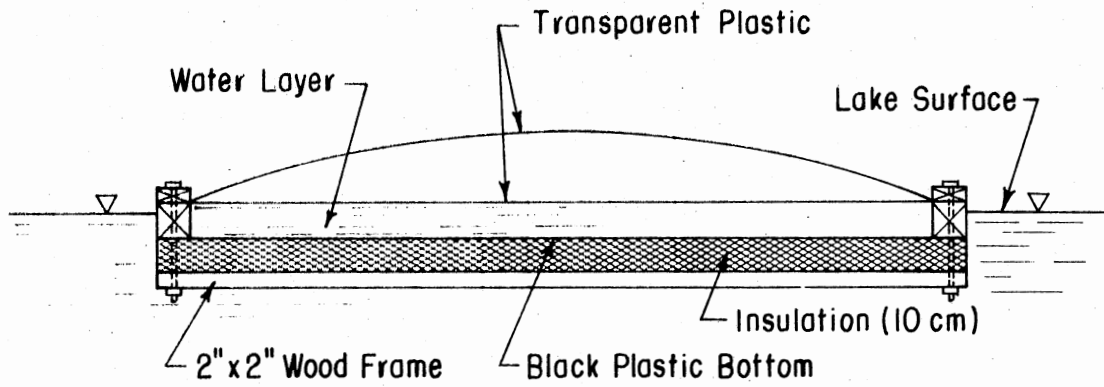
3. Fragility (subject to slashing and tearing).

Grevskott (10) in 1976 used black plastic as an absorber by placing it under a water layer and having the water surface covered with two transparent layers of plastic separated by an airspace. On the underside of black plastic, insulation was placed to reduce heat loss by conduction. Figure 2 shows the construction of the model on the surface of a lake. No data were reported on the effectiveness of this model.

Black polyethylene was placed over a water surface in Alaska (7) to retard freezing of water, but when it was discovered that covering the reservoirs made no appreciable effect on retardation of freezing, no further studies were conducted.

Kline (14) showed the performance of air collectors of various shapes using polyethylene as the cover and absorber where efficiency was lower on a collector made purely out of polyethylene versus one made out of plywood and polyethylene. These efficiencies ranged from 14 to 60% while the collector with the highest efficiency used corrugated fiberglass as the cover and deep groove formed metal as the absorber. The efficiencies for several different types of collectors are shown for the noon hour and for a full day in Figures 3 and 4, respectively. Table I shows performance of the curved-cover, bicurved absorber collector studied by Keener (13).

San Martin and Fjeld (18) conducted experiments on three different types of flat-plate water collectors: a water trickle collector where water flows down a sheet of corrugated aluminum coated on the surface with a highly absorbing material, a typical tube-in-sheet collector, and the thermal trap collector which uses a transparent solid (methyl methacrylate) adjacent to the fluid cooled collector absorber plate. The



SOURCE: Grevskott (10, p. 93).

Figure 2. Schematic of Solar Collector Model

SOLAR COLLECTOR EFFICIENCIES

NOON HOUR










Fall-Winter, 1975-76

South Facing

21 Days, Sky Clear

Optimum Angle

Air Flow - 8 CFM/FT²

Shape	COLLECTOR			COLLECTOR EFFICIENCY %
	Cover Plate	Absorber	Back Plate	
	Bare	Poly	----	17
	Poly	Poly	Ground	18
	Poly	Poly	Poly	31
	Bare	Metal	Plywood	14
	Plexiglass	Plywood	----	30
	Fiberglass	Ply-Insul	(W/Reflect)	49
	Poly	Poly	Plywood	53
	Glass	Metal	Ply-Insul	74
	Fiberglass	60° Metal	Ply-Insul	83

SOURCE: Kline (14, p. 94).

Figure 3. Solar Collector Performance for Noon Hour Operation

SOLAR COLLECTOR EFFICIENCIES

FULL DAY

Fall-Winter, 1975-76




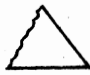





South Facing

15 Days

Optimum Angle - Noon

Sky Clear to Pt. Cldy

Air Flow - 8 CFM/FT²

Shape	COLLECTOR			OVERALL COLLECTOR EFFICIENCY %
	Cover Plate	Absorber	Back Plate	
	Bare	Poly	----	14
	Poly	Poly	Ground	12
	Poly	Poly	Poly	24
	Bare	Metal	Plywood	12
	Plexiglass	Plywood	----	22
	Fiberglass	Ply-Insul	(W/Reflect)	34
	Poly	Poly	Plywood	36
	Glass	Metal	Ply-Insul	55
	Fiberglass	60° Metal	Ply-Insul	62

SOURCE: Kline (14, p. 94).

Figure 4. Solar Collector Performance for Full Day Operation

TABLE I
 EXPERIMENTAL PERFORMANCE OF CURVED-COVER,
 BICURVED-ABSORBER^a SOLAR COLLECTOR
 AT WOOSTER, OHIO

Air Flow Rate	Test Period	Average ^b Solar Radiation	Average Heat Gained	Eff.	Average Temp. Rise
m ³ /s		MJ/day	MJ/day	%	C
1.04 ^c	10/4 - 7/74	1184 ± 328	424 ± 57	35.8	4.17 ± 0.50
1.04 ^c	11/16 - 23/74	616 ± 377	259 ± 83	42.0	2.50 ± 1.06
1.04 ^{c,d}	11/16 - 23/74	645 ± 394	227 ± 68	35.3	2.06 ± 0.89
0.44 ^e	9/17 - 23/75	808 ± 362	247 ± 98	30.6	5.35 ± 2.07
0.89	9/17 - 23/75	798 ± 358	368 ± 126	46.1	3.85 ± 1.31
0.77 ^e	10/16 - 21/75	633 ± 473	256 ± 125	40.4	3.30 ± 1.94
0.89	10/16 - 21/75	626 ± 467	353 ± 225	56.4	3.28 ± 1.36
0.61 ^e	11/23 - 27/75	433 ± 284	151 ± 95	34.1	3.81 ± 2.24

a - Trademark Soloron - mfg. by Solar Energy Products Co., Avon Lake, Ohio.

b - Based on incident radiation on a flat horizontal collector. Absorber dimensions 3.7m x 24.4m.

c - Soil temperatures rising during October and November 1974. Falling in 1975.

d - Collector oriented north-south, while in all other tests the collector was oriented east-west.

e - Collector insulated from ground with 25 mm beaded styrofoam.

SOURCE: Keener (13, p. 94).

absorbing surface of these three collectors was aluminum painted with 3M Nexten Velvet Coating No. 101-C10. The water trickle collector had good efficiency at operating temperatures below 125° F while at operating temperatures above 145° F the thermal trap collector is more than twice as efficient as the water trickle collector. Table II shows a selected summary of test data where the water trickle collector is collector number one, the thermal trap collector is collector number two, and the standard tube-in-sheet collector is collector number three, with efficiencies ranging from 10 to 65%.

Storage Mediums

The concept of using water as a storage medium for heat energy supplied by solar radiation has advantages of being low cost with a high specific heat and less volume needed for rock storage. The disadvantage is that a water to air heat exchanger is needed for heating of air.

A solar pond and a freshwater pond are two kinds of water storage mediums that can be used to store heat energy with the solar pond requiring a density gradient produced by a salt concentration while a freshwater pond requires no additional additives. Temperatures as high as 194° F have been recorded in solar ponds, Tabor (21).

Chepurniy and Savage (3) in a study of a laboratory solar pond model to predict the time-dependent temperature distribution in the pond, studied the effects of pond depth, intensity and wavelength distribution of the incident radiation, and the effect of the concentration gradient. Using an implicit finite temperature difference scheme, they found good correlation between measured and predicted temperature profiles. They included heat flux losses due to evaporation, conduction, surface

TABLE II
 SELECTED SUMMARY OF TEST DATA FOR THREE
 WATER SOLAR COLLECTORS

Date	Collector	Maximum Solar Rad. BTU/hr. ft ²	Flow Rate lb/min. ft ²	Maximum Collection Temp. °F	Average Efficiency %	Hours of Useful Collection hrs.
Jan. 1, 1974	1	297	0.30	121.1	35.2	7.0
	2	297	0.34	126.9	65.6	(1)
	3	297	0.33	125.3	64.5	(1)
Jan. 29	1	315	0.22	149.5	24.8	7.0
	2	315	0.27	153.5	52.9	8.8
	3	315	0.13	162.3	49.3	8.8
Feb. 5	1	316	0.20	140.7	20.3	6.0
	2	316	0.27	150.8	56.4	8.6
	3	316	0.13	161.5	53.9	8.6
Feb. 23	1	327	0.19	144.5	17.4	6.4
	2*	327	0.34	153.1	60.3	9.0
	3	327	0.33	149.5	48.3	8.6
Feb. 28	2*	338	0.34	181.0	59.8	(2)
	3	338	0.33	177.4	55.1	(2)
Mar. 1	1	330	0.16	171.9	9.4	(3)
	2*	330	0.34	177.8	53.1	(3)
	3	330	0.33	175.0	50.9	(3)
Mar. 25	1	322	0.10	160.3	16.2	6.0
	2	322	0.34	165.9	59.2	9.4
	3	322	0.33	162.3	53.4	9.2
Mar. 28	1	315	0.10	153.5	8.7	4.6
	2	315	0.34	159.9	51.3	9.4
	3	315	0.33	157.5	48.3	8.8

* without glazing

(1) collectors only operated for 8 hrs.

(2) collectors only operated for 7 hrs.

(3) collectors only operated for 4.8 hrs.

SOURCE: San Martin and Fjeld (18, p. 94).

absorption, back radiation at the surface, heat losses through side walls, and heat losses through the bottom surface.

Weinberger (24) states that to evaluate the temperature distribution and heat flow in a solar pond it is essential to know the thermal properties of the salt-water solution, adjacent soil, and heat transfer rates to the atmosphere at the site of the pond.

Snider and Viskanta (20) studied a stagnant water pond heated by solar radiation and found good agreement between measured and predicted temperature profiles. A finite difference method was used to solve the governing differential equation (1) for temperature distribution.

$$\rho_w C_w \frac{\partial t}{\partial \theta} = - \frac{\partial}{\partial x} (-k_w \frac{\partial T}{\partial x} + F) \quad (1)$$

where,

ρ_w = density of water, lbm/ft³.

C_w = specific heat, BTU/lbm-°F.

t = temperature, °F.

θ = time, hr.

x = length coordinate measured from the water surface, ft.

k_w = thermal conductivity, BTU/hr-ft-°F.

F = local radiative flux, BTU/hr-ft².

Dake and Harleman (4) made a study of thermal stratification in lakes heated by solar radiation. Their solution to the governing second order heat transfer equation was solved by superposition of solutions for the surface absorbed radiation and the internally absorbed radiation. Their measurements for constant solar radiation are in good agreement with predicted temperatures. The differential equation they used was:

$$\frac{\partial t}{\partial \theta} = M \left(\frac{\partial^2 t}{\partial x^2} \right) + \left(\frac{\partial}{\partial x} \right) [E \left(\frac{\partial t}{\partial x} \right)] + (q_{int}' / \rho_w C_w) \quad (2)$$

where,

t = temperature, °F.

θ = time, hr.

x = vertical coordinate measured downward from the water surface, ft.

E = vertical thermal eddy diffusivity, ft^2/hr .

q_{int}''' = rate of heat generated per unit volume by internal absorption of solar radiation, $\text{BTU}/\text{hr}\text{-ft}^3$.

M = thermal molecular diffusivity, ft^2/hr .

ρ_w = density of the water, lbm/ft^3 .

C_w = specific heat of the water, $\text{BTU}/\text{lbm}\text{-}^\circ\text{F}$.

CHAPTER III

EXPERIMENTAL APPARATUS AND DESIGN

Apparatus

A model was developed to represent a vertical section of a small freshwater pond having a surface area of 10,000 square feet and a depth of six feet. The pond was heated at the surface by solar radiation and was assumed to have one dimensional heat flow in the vertical direction.

To represent a vertical section of a small freshwater pond, a circular steel tank, 6.78 feet in diameter and 6.17 feet in depth, was chosen as the experimental model. This model was filled with 72° F water to a depth of six feet and insulated around the circumference with seven inches of fiberglass insulation (R-22) to minimize heat loss through the side walls by conduction. By minimizing heat loss through the side walls, the model would be able to approximate one dimensional heat flow in the vertical direction. The overall heat transfer coefficient for the side walls was 0.0489 BTU/hr-ft²-°F. Two layers of clear, six mil polyethylene were used to protect the insulation from the weather.

The model was set above ground on a platform, eight feet by eight feet, made from 1/2" plywood and 2" x 4" beams with 3 1/2 inches of fiberglass insulation (R-11) between the bottom of the model and the surface of the ground. The insulation on the bottom of the model helps

stabilize the temperature of the water at the bottom by reducing the heat flow to the ground by conduction.

A cover of six mil, clear polyethylene was placed over the surface of the model to provide a decrease in heat loss due to convection and evaporation. The cover was in the shape of a hemisphere with a diameter of 44 1/4 inches and was air supported using a pressure of 0.1 inch of water provided by a 1/16 horsepower centrifugal fan. It was necessary to continuously supply air at the rate of 44.4 cfm due to air leakage where the plastic dome was connected to the model tank.

The 36.1 square foot solar collector absorber was constructed of six mil, black polyethylene and placed on the surface of the water. The absorber was allowed to float on the water surface to maintain constant contact with the water, thus supplying by conduction heat energy from the absorber to the water surface. Therefore, the heat energy is conducted one dimensionally through the water.

A schematic of the model is shown in Figure 5 and Figure 6 shows the experimental model in operation.

A multipoint data logger was used to record temperatures of air and water at various depths using 24 gauge copper-constantan thermocouple wire. Temperatures of the air inside the polyethylene dome, ambient air, surface of the water, and depths of 1 inch, 6 inches, 10 inches, 18 inches, 24 inches, 36 inches, and 72 inches below the water surface were recorded.

Solar radiation data were collected by the Agronomy Research Station located on the campus of Oklahoma State University in Stillwater, Oklahoma. The distance from the experimental site to the Agronomy Research Station was approximately two miles.

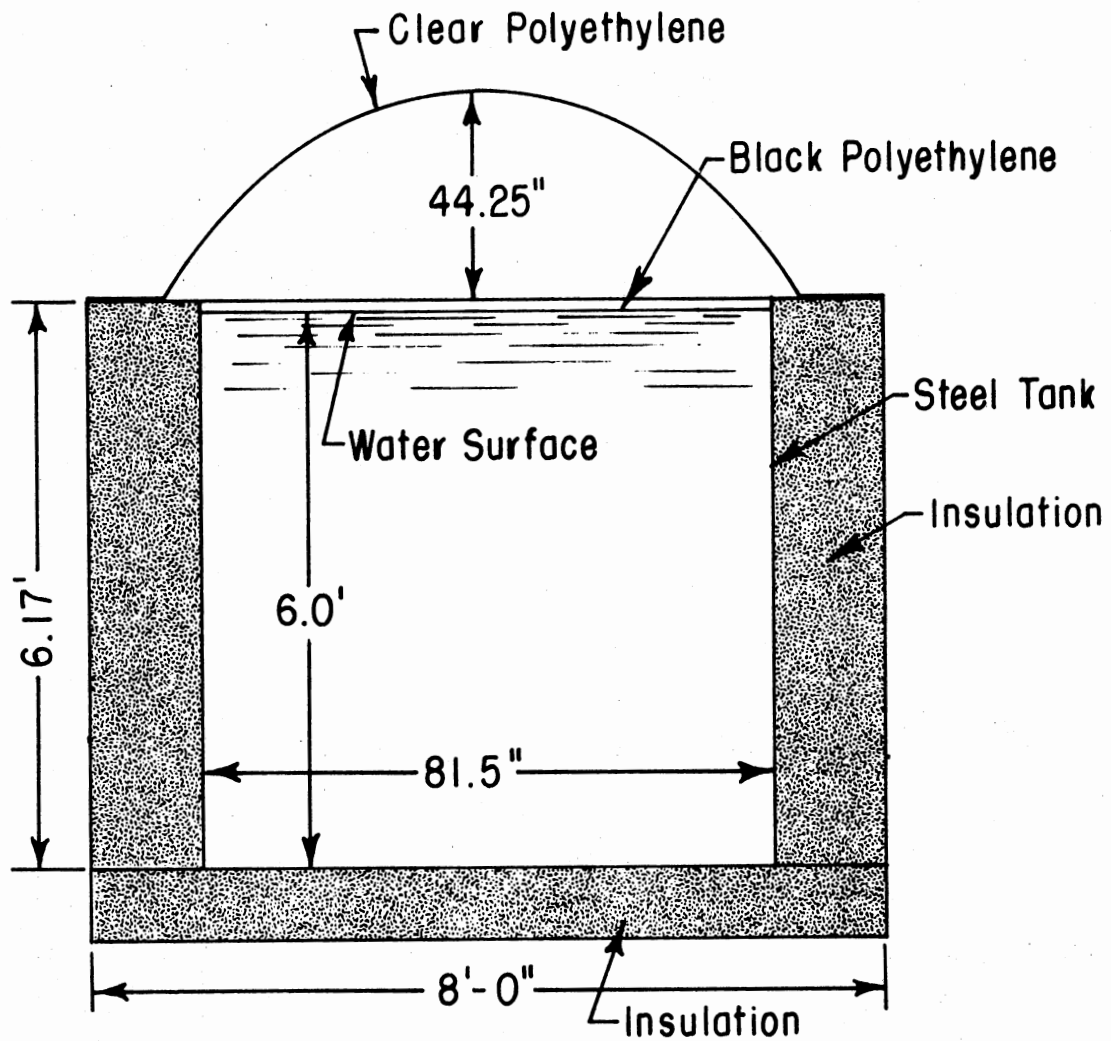


Figure 5. Schematic of Freshwater Solar Storage Model

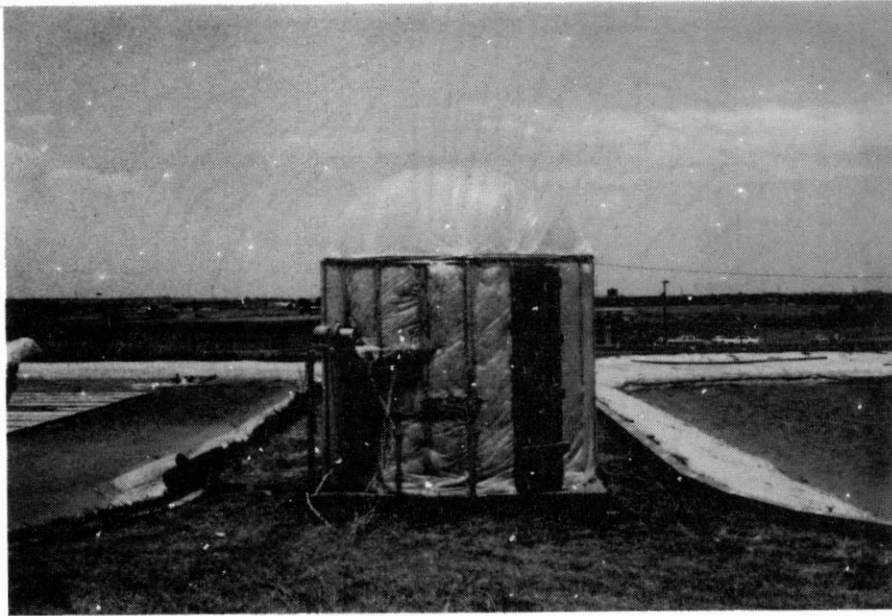


Figure 6. Freshwater Solar Storage Model in Operation

Transmittance

Transmittance is defined as the incident solar radiation transmitted through a non-opaque medium divided by the total incident solar radiation received. It is affected by the following four factors: (a) the type of material used in construction (9), (b) the amount of dust collected on the surface (8), (c) the angle of incident of the solar radiation (9), and (d) condensation on the underside of the surface cover (11).

The transmittance through a sheet of clear, six mil polyethylene and through the same sheet covered with condensation on the underside was measured in this experiment because they represent the conditions of the cover in the experimental model while the amount of dust collected on the top surface of the collector cover was neglected.

An Eppley Pyranometer, Model 8.48, was placed into a box that was 17 inches wide, 20 inches long, and 11 1/2 inches deep. A cover for the box was constructed of six mil, clear polyethylene on a wooden frame and was attached to the top of the box and removed by hand. With the cover in place, the box was sealed so that no light would penetrate into the box. The top of the pyranometer was two inches below the surface plane of the box, allowing 2 1/2 inches between the top of the pyranometer and the underside of the polyethylene cover. The test for transmittance compares with ASTM Standard, E 424-71, except that the inside of the box was not painted flat black.

Condensation on the underside of the polyethylene cover was produced by a steam generator to represent the condensation formed under the polyethylene dome on the experimental model. The percent of coverage was 100%, determined by viewing the cover and shutting off the steam

generator when the cover was totally coated with condensation. Dropwise condensation developed on the pyranometer dome when the condensation was produced, but no effort was made to determine the effect of this condensation on the pyranometer readings.

When a cover is placed over a free surface of water, condensation occurs because of evaporation from the surface of the water. The evaporation causes the air inside to become saturated with water vapor and condensation on the inside surface occurs when ambient air temperature is cooler than the air on the inside of the cover. Condensation is a problem associated with transmittance because of two factors as stated by Hsieh and Rajvanshi (11). The first factor is rapid variation of the water absorption coefficient with wavelength. The second factor is that, when radiation enters into the water droplet and crosses the water-air interface, total reflection will take place for the rays of large incident angles because of the smaller refractive index occurring at the air side.

Three replications were run measuring the transmittance values for the clear polyethylene cover and for the cover with 100% condensation on the underside. The average ambient air temperature was 61.1° F when the tests were run with time being at 1:30 p.m. on December 5, 1978. The transmittance values for the cover were determined by equation (3).

$$\tau_p = \frac{HR}{HR_N} \quad (3)$$

where,

τ_p = transmittance of polyethylene cover.

HR_N = pyranometer reading without cover (MV).

HR = pyranometer reading with cover (MV).

Table III shows the transmittance data collected for both the clear cover and the cover with condensation on the underside with the transmittance values calculated from equation (3).

The transmittance value for the clear cover is 0.786 which is 11% lower than the reported value of 0.88 by Walker and Slack (23) for a clear sheet of polyethylene. While for 100% coverage of the underside surface by condensation, the transmittance value is 0.67 which is 2% higher than the value of 0.66 reported by Umarov et al. (22) for polyethylene with condensation on the underside surface and is 22% higher than that reported by Hsieh and Rajvanshi (11) concerning dropwise condensation on glass. The reason for the discrepancy between the measured value for clear polyethylene and the value reported in literature could be due to differences in the polyethylene.

A correction factor for coverage of condensation on the underside of a polyethylene cover can be predicted from the transmittance data. Hsieh and Rajvanshi (11) used equation (4) to determine the correction factor for glass.

$$C_{\tau} = (1 - FR) + FR (\tau_w / \tau_c) \quad (4)$$

where,

C_{τ} = correction factor for transmittance.

FR = fraction covered by condensation.

τ_w = transmittance of polyethylene cover with condensation.

τ_c = transmittance of polyethylene cover without condensation.

The correction factor can be used in the following manner:

$$\tau_w = C_{\tau} \tau_c \quad (5)$$

TABLE III
DATA FOR TRANSMITTANCE TESTS
(MILLIVOLTS)

	No Cover	Clear Cover	Cover with Condensation
Replication 1			
Mean	5.698	4.450	3.816
S.D.	0.0117	0.00632	0.0233
Transmittance		$\tau_c = 0.781$	$\tau_w = 0.670$
Replication 2			
Mean	5.550	4.210	3.714
S.D.	0.0110	0.0385	0.0102
Transmittance		$\tau_c = 0.759$	$\tau_w = 0.669$
Replication 3			
Mean	5.452	4.466	3.672
S.D.	0.004	0.0049	0.016
Transmittance		$\tau_c = 0.819$	$\tau_w = 0.674$
Average	5.567	4.375	3.734
Average Transmittance		$\tau_c = 0.786$	$\tau_w = 0.671$

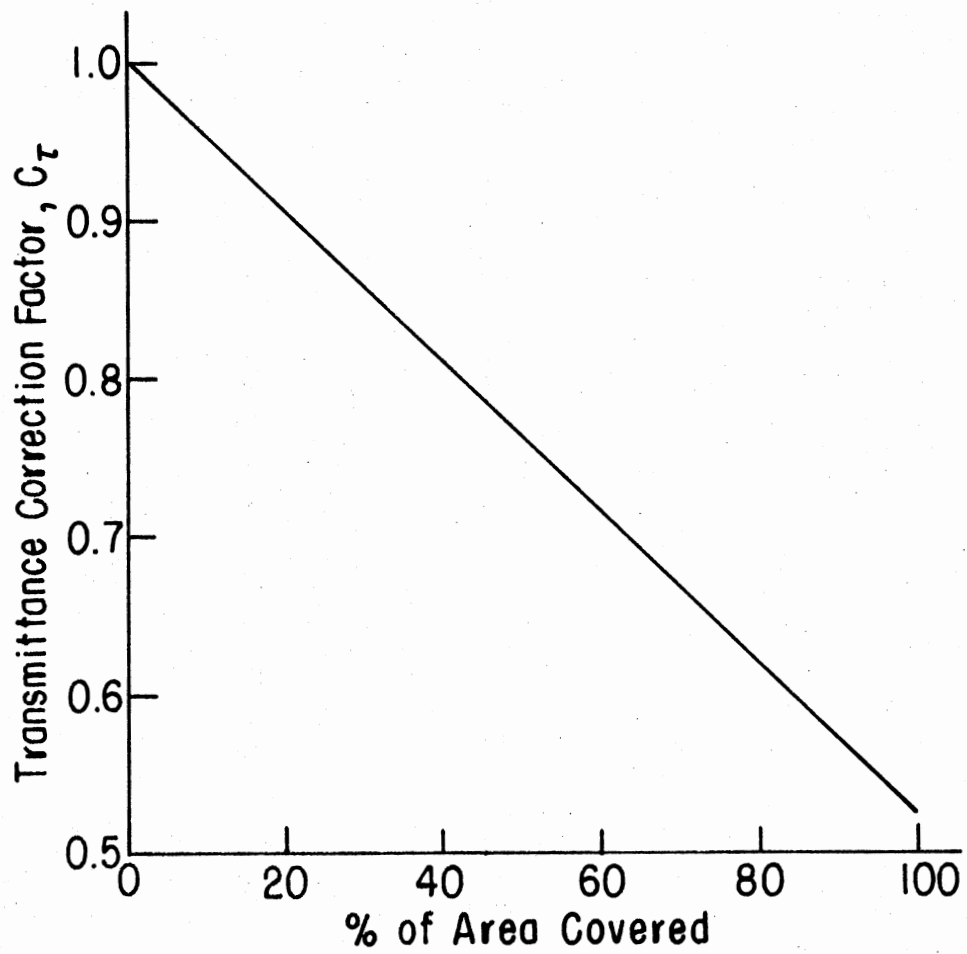
Figure 7 shows the transmittance correction factor curve by Hsieh and Rajvanshi (11) and Figure 8 shows the data for this experiment, allowing transmittance through polyethylene to be determined with 0 to 100% coverage of the underside by condensation.

Condensation does have an appreciable effect on the actual energy received by a solar collector absorber surface. Umarov (22) shows that the efficiency of a system is decreased as a result of the influence of meteorological factors and a reduction in the transparency of the film. Table IV compares a polyethylene film that is treated, where treated means that either a "sun clear" water dispersion or a polyvinyl alcohol solution was used to reduce condensation, and one that is untreated in July of 1975.

Plastic Absorber

The solar radiation absorber was constructed of six mil, black polyethylene and had a surface area of 36.1 square feet and a diameter of 6.1 feet. After 47 days of continuous use with water surface temperatures up to 138.9° F, the polyethylene became brittle and tore along the edge of the absorber because polyethylene deteriorates from ultraviolet rays received from the sun.

During this same time period, a white film developed on the surface of the absorber, caused by the evaporation of water from the surface of the absorber allowing impurities in the water to precipitate. As the film develops, the amount of solar radiation absorbed by the polyethylene is affected and probably decreases the amount of solar radiation absorbed. No effort was made to determine the effect of this film on the amount of solar radiation absorbed by the polyethylene. Figure 9 shows the



SOURCE: Hsieh and Rajvanshi (11, p. 94).

Figure 7. Correction Factor Curve for Dropwise Condensation on Glass

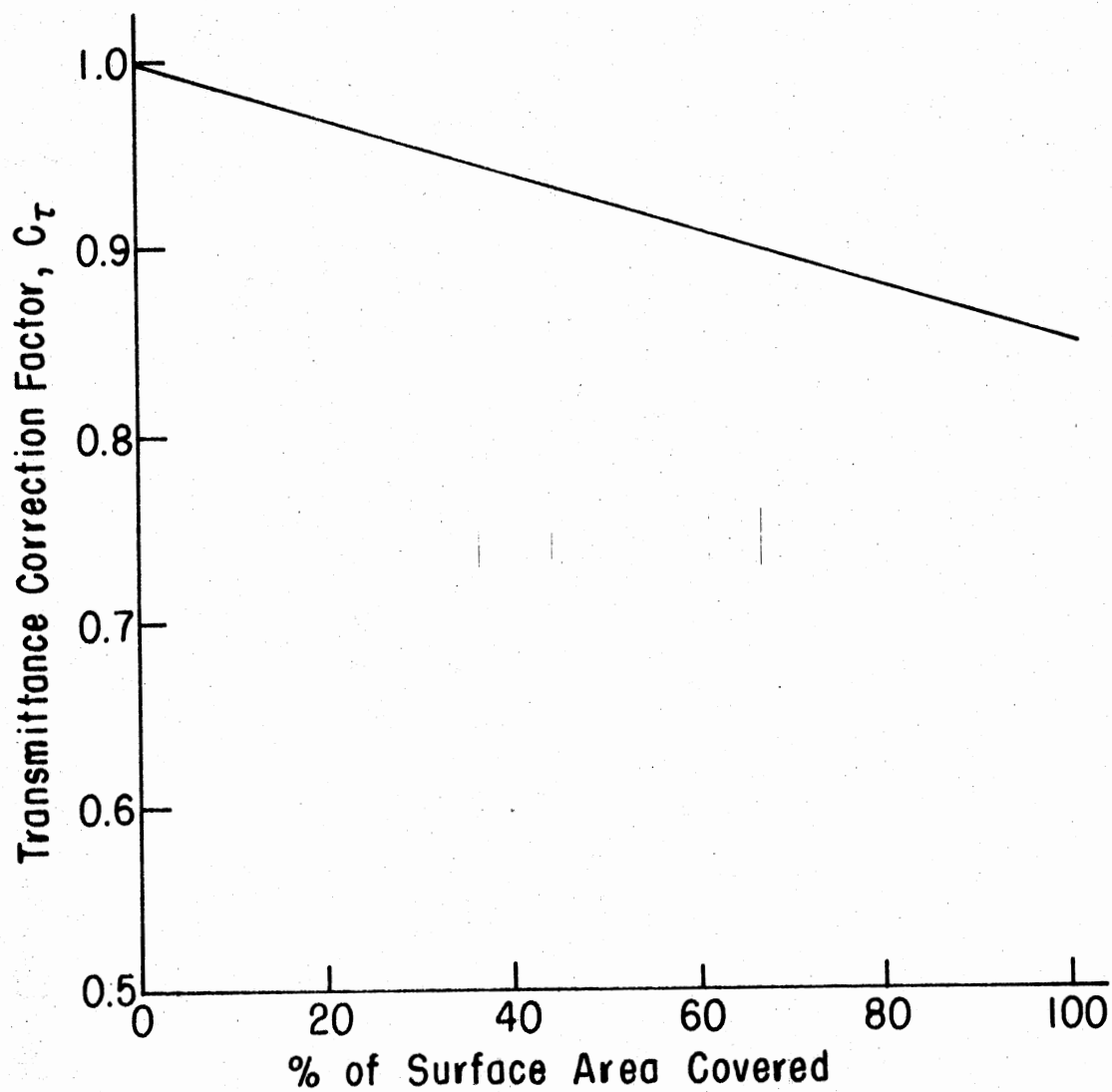


Figure 8. Correction Factor Curve for Transmittance Through Six Mil, Clear Polyethylene With 0 to 100% Coverage of Surface Area by Condensation

TABLE IV
RESULTS OF COMPARATIVE TESTS ON SOLAR FILM STILLS
UNDER DIFFERENT METEOROLOGICAL CONDITIONS

Date of Test, 1975	Incident Solar Radiation kcal/m ² · day	Polyethylene Film Treated with		Untreated Polyethylene Film Efficiency
		"Sun Clear" Water Dispersion Efficiency	Polyvinyl Alcohol Solution Efficiency	
July 1	4400	0.565	0.528	0.362
July 5	4464	0.558	0.523	0.355
July 10	4532	0.550	0.512	0.343
July 15	4600	0.535	0.498	0.341
July 20	4670	0.525	0.485	0.333
July 25	4740	0.510	0.474	0.324
July 30	4800	0.506	0.468	0.318

SOURCE: Umarov et al. (22, p. 94).

condition of the polyethylene after it had deteriorated under the ultra-violet rays of the sun and Figure 10 shows the white film on the surface of the absorber.



Figure 9. Condition of the Six Mil, Black Polyethylene After Deteriorating from the Ultra-violet Rays of the Sun



Figure 10. White-film Build Up on the Surface of the Six Mil, Black Polyethylene Absorber Surface

CHAPTER IV

THEORETICAL DEVELOPMENT

Several assumptions were made governing the heat transfer characteristics of the model storage tank to theoretically predict the temperature distributions in the storage model. It was assumed that the storage medium had one dimensional heat flow in the vertical direction with heat being added to the surface of the water by solar radiation. Only clear, sunny days were considered for solar radiation and it was assumed that the net radiation received was sinusoidal during the daytime with a constant rate of heat loss due to convection and radiation for the 24 hour period. Also, no internal generation of heat was considered.

The heat loss through the bottom of the model by conduction was considered negligible due to 3 1/2 inches of fiberglass insulation (R-11) and low temperature differences between the bottom of the model and the surface of the ground. Heat loss through the side walls was also considered negligible due to seven inches of fiberglass insulation (R-22) and the ambient air temperature being warmer than the average water temperature in the model during daylight hours.

Therefore, heat loss from the model is due to convection and radiation from the surface of the absorber and air infiltration. Air infiltration is the quantity of air needed to keep the polyethylene dome inflated to 0.1 inch of water pressure calculated from equation (6) for

the 1/16 horsepower fan that supplied the air.

$$Q_{\text{AIR}} = V_d A_d \quad (6)$$

where,

Q_{AIR} = quantity of air needed, ft³/min.

V_d = velocity of air in the duct, ft/min.

A_d = cross-sectional area of the duct, ft².

The heat loss from the polyethylene dome can be calculated by equation (7) using the property values for air in Table V.

$$Q_{\text{INF}} = \frac{m_A C_A}{A_s} (t_A - t_o) \quad (7)$$

where,

Q_{INF} = heat loss due to infiltration, BTU/hr-ft².

m_A = mass flow of air, lbm/hr.

C_A = specific heat of air, BTU/lbm-°F.

A_s = surface area of collector absorber, ft².

t_A = temperature of air inside polyethylene dome, °F.

t_o = ambient air temperature, °F.

With a temperature range of 60° F to 130° F for water and air in this experiment, the property values of density, thermal conductivity, and specific heat were considered constant.

Equation (8) was used to calculate heat loss from the surface of the collector due to convection and radiation.

$$Q_{\text{CR}} = U_o (t_s - t_o) \quad (8)$$

where,

Q_{CR} = heat loss due to convection and radiation, BTU/hr-ft².

U_o = overall heat transfer coefficient, BTU/hr-ft²-°F.

t_s = temperature of polyethylene absorber, °F.

TABLE V

CONSTANT VALUES FOR SPECIFIC HEAT, THERMAL
CONDUCTIVITY, AND DENSITY FOR
WATER AND AIR BETWEEN
60° AND 135° F

Property	Water	Air
Specific Heat (BTU/lbm-°F)	1.0	0.24
Thermal Conductivity (BTU/hr-ft-°F)	0.357	0.0156
Density (lbm/ft ³)	62.0	0.0714

t_o = ambient air temperature, °F.

For a collector cover constructed of a single layer of plastic, partially transparent to infrared radiation, equation (9) was recommended by Duffie and Beckman (6) to calculate the overall heat transfer coefficient for the surface of a collector.

$$U_o = \tau_p \epsilon_s 4\sigma T_c^3 \frac{(T_s - T_{sky})}{(T_s - T_o)} + \frac{1}{\frac{1}{h_{c,p-c}} + \frac{1}{h_{r,p-c}} + \frac{1}{h_w + h_{r,c-sky}}} \quad (9)$$

where,

U_o = overall collector top loss coefficient, BTU/hr-ft²-°F.

τ_p = transmittance of cover.

ϵ_s = emissivity of absorber plate, 0.9.

σ = Stefan-Boltzman constant, 0.1714×10^{-8} , BTU/hr-ft²-°R⁴.

T_c = temperature of polyethylene cover, °R.

T_s = temperature of polyethylene absorber, °R.

T_{sky} = sky temperature, °R.

T_o = ambient air temperature, °R.

$h_{c,p-c}$ = convective heat transfer coefficient from surface plate to cover, BTU/hr-ft²-°F.

$h_{r,p-c}$ = radiative heat transfer coefficient from surface plate to cover, BTU/hr-ft²-°F.

h_w = convective heat transfer coefficient from the cover due to wind, BTU/hr-ft²-°F.

$h_{r,c-sky}$ = radiative heat transfer coefficient from the cover of the collector to the sky, BTU/hr-ft²-°F.

To calculate the convective heat transfer coefficients, the values for the Prandlt, Reynolds, Grashof, and Nusselt numbers are needed.

The Prandlt number, Pr , is relatively constant for air having a value of 0.72. The Reynolds number, an index of the ratio of inertial forces to viscous forces, was calculated by equation (10).

$$Re_D = \frac{V_0 D_s}{\nu} \quad (10)$$

where,

Re_D = Reynolds number based upon the diameter.

V_0 = velocity of air over sphere, ft/sec.

D_s = diameter of sphere, 7.375 ft.

ν = kinematic viscosity of air, ft^2/sec .

The Grashof number, an index of the ratio of buoyancy forces to viscous forces, is described in equation (11).

$$Gr_L = \frac{g\beta(t_s - t_c) L^3}{\nu^2} \quad (11)$$

where,

Gr_L = Grashof number based upon plate spacing.

g = gravitational constant, $32.17 ft/sec^2$.

β = volumetric coefficient of expansion of air, $1/^\circ F$.

t_s = temperature of absorber surface, $^\circ F$.

t_c = temperature of collector cover, $^\circ F$.

L = plate spacing between polyethylene cover and absorber, 1.565 ft.

ν = kinematic viscosity, ft^2/sec .

The Nusselt number is used to calculate the heat transfer coefficient and is an index of the ratio of the resistance to heat transfer at the boundary to the internal resistance. It can have either the spacing between the cover and the plate or the diameter as the characteristic length dimension and was calculated by equation (12). Here L is used as

the characteristic length but can be replaced by D if the diameter of the sphere is used.

$$\bar{Nu}_L = \frac{hL}{k_A} \quad (12)$$

where,

\bar{Nu}_L = Nusselt number based upon plate spacing.

h = convective heat transfer coefficient, BTU/hr-ft²-°F.

L = plate spacing, ft.

k_A = thermal conductivity of air, BTU/hr-ft-°F.

To calculate the convective heat transfer coefficient from the absorber surface to the collector cover, $h_{c,p-c}$, the polyethylene dome was assumed to represent a horizontally enclosed space between two parallel flat-plates with the lower plate at a higher temperature than the upper plate. Parker et al. (17) states that when the ratio of the Grashof number to the square of the Reynolds is much greater than one, natural convection occurs because the motion of the fluid is due to buoyancy forces. Therefore, natural convection is assumed because Gr/Re^2 is about 26.

Equation (13) is suggested by Parker et al. (17) for calculating the Nusselt number for a horizontally enclosed space with the restrictions that the Prandlt number is greater than 0.02 and less than 8,750 and $Gr \times Pr$ is greater than 3×10^5 and less than 7×10^9 .

$$\bar{Nu}_L = 0.069 (Gr)^{1/3} Pr^{0.074} \quad (13)$$

where,

\bar{Nu}_L = Nusselt number based upon plate spacing.

Gr_L = Grashof number based upon plate spacing.

Pr = Prandlt number for air, 0.72.

It was assumed that the polyethylene dome represented a sphere to calculate the convective heat transfer coefficient due to the outside air velocity. Parker et al. (17) recommended the following equation for calculating the average Nusselt number over a sphere for Reynolds number from 25 to 100,000.

$$\bar{Nu}_D = 0.37 Re_D^{0.6} \quad (14)$$

where,

\bar{Nu}_D = Nusselt number based upon sphere diameter.

Re_D = Reynolds number based upon sphere diameter.

McAdams (15) states for Reynolds number from 1.3×10^5 to 10^6 , the average Nusselt number is 40 to 60 percent above those predicted by equation (14). Therefore, for the Reynolds number range of 1.3×10^5 to 10^6 equation (13) was modified to:

$$\bar{Nu}_D = 0.37 Re_D^{0.6} \quad (1.5) \quad (15)$$

Equations (16) and (17) were used to calculate the radiation heat transfer coefficient from the absorber plate to the cover and for the radiation heat transfer coefficient from the cover to the sky, respectively, as presented by Duffie and Beckman (6). It was assumed again that the collector absorber and cover represented a flat-plate.

$$h_{r,s-c} = \frac{\sigma(T_s^2 + T_c^2)(T_s + T_c)}{(1/\epsilon_s) + (1/\epsilon_c) - 1} \quad (16)$$

$$\text{and } h_{r,c-sky} = \epsilon_c \sigma (T_c^2 + T_{sky}^2) (T_c + T_{sky}) \quad (17)$$

where,

$h_{r,s-c}$ = radiation heat transfer coefficient from absorber surface to collector cover, BTU/hr-ft²-°F.

$h_{r,c-sky}$ = radiation heat transfer coefficient from the collector cover to the sky, BTU/hr-ft²-°F.

σ = Stefan Boltzman constant, 0.1714×10^{-8} , BTU/hr-ft²-°R⁴.

T_S = temperature of polyethylene absorber, °R.

T_C = temperature of polyethylene cover, °R.

ϵ_S = emmissivity of black polyethylene, 0.90.

ϵ_C = emmissivity of clear polyethylene, 0.90.

T_{sky} = sky temperature, °R.

The sky temperature was calculated by equation (18).

$$T_{sky} = 0.0411 (T_0)^{1.5} \quad (18)$$

where,

T_{sky} = sky temperature, °R.

T_0 = ambient air temperature, °R.

Using the assumptions that have been mentioned, the general heat conduction equation can be reduced from

$$k_w \frac{\partial^2 t}{\partial x^2} + k_w \frac{\partial^2 t}{\partial y^2} + k_w \frac{\partial^2 t}{\partial z^2} + q''' = \rho_w C_w \frac{\partial t}{\partial \theta} \quad (19)$$

to

$$\frac{\partial^2 t}{\partial x^2} = \frac{\rho_w C_w}{k_w} \frac{\partial t}{\partial \theta} \quad (20)$$

where,

k_w = thermal conductivity, BTU/hr-ft-°F.

t = temperature, °F.

x = distance in x direction, ft.

y = distance in y direction, ft.

z = distance in z direction, ft.

q''' = internal energy, BTU/hr-ft³-°F.

ρ_w = density, lbm/ft³.

C_w = specific heat, BTU/lbm-°F.

θ = time, hr.

Equation (20) is a linear, homogeneous second order differential equation which requires one initial condition and two boundary conditions to be solved. With variable initial and boundary conditions, explicit solutions to equation (19) are difficult to obtain, but it can be solved by use of a finite difference numerical solution for a transient condition.

The initial condition was that the water temperature in the model at time zero is the average water temperature that was calculated by integrating the temperature profiles for a particular time. Therefore, the initial condition is:

$$t(x,0) = t_{AVE} \quad (21)$$

where,

$$t_{AVE} = \text{average water temperature, } ^\circ\text{F.}$$

The first boundary condition requires the energy absorbed by the collector be equal to the energy conducted from the surface of the absorber into the water plus the energy loss due to convection, radiation, and air infiltration. Equation (22) defines this relationship for the time period from 6:00 a.m. to 9:00 p.m. (CDT) and equation (23) describes the surface boundary condition for the time period from 9:00 p.m. to 6:00 a.m. (CDT).

$$a\tau_p Q_{RAD} \sin\omega\theta = -k_w \left. \frac{\partial t}{\partial x} \right|_{x=0} + Q_{CR} + Q_{INF} \quad (22)$$

where,

a = absorptance of absorber.

τ_p = transmittance.

Q_{RAD} = solar radiation, BTU/hr-ft².

$$\omega = 0.2094 \text{ RAD/hr.}$$

$$\theta = \text{time, hr.}$$

$$k_w = \text{thermal conductivity, BTU/hr-ft}^2\text{-}^\circ\text{F.}$$

$$t = \text{temperature, }^\circ\text{F.}$$

$$Q_{CR} = \text{heat loss due to convection and radiation, BTU/hr-ft}^2.$$

$$Q_{INF} = \text{heat loss due to air infiltration, BTU/hr-ft}^2.$$

$$k_w \frac{\partial t}{\partial x} \Big|_{x=0} = Q_{CR} + Q_{INF} \quad (23)$$

In equation (22), Q_{CR} is assumed sinusoidal with a constant term equivalent to the rate of heat loss at night due to convection and radiation. Therefore, Q_{CR} is defined by equation (24) for the time period from 6:00 a.m. to 9:00 p.m. (CDT).

$$Q_{CR} = Q_{CRD} \sin \omega \theta + Q_{CRC} \quad (24)$$

where the amplitude of the sinusoidal wave in equation (24), Q_{CRD} , is equal to the maximum value calculated for, Q_{CR} , by equation (8) minus the constant rate of heat loss at night, Q_{CRC} , which is the average of the values calculated by equation (8) for the time period between 9:00 p.m. and 6:00 a.m. (CDT). By substituting in the values obtained from equation (24) and rearranging equation (22) and (23), these equations become:

$$\frac{\partial t}{\partial x} \Big|_{x=0} = - \frac{1}{k_w} [(a\tau_p Q_{RAD} - Q_{CRD}) \sin \omega \theta - Q_{CRC} - Q_{INF}] \quad (25)$$

and

$$\frac{\partial t}{\partial x} \Big|_{x=0} = \frac{1}{k_w} [Q_{CRC} + Q_{INF}] \quad (26)$$

The second boundary condition assumes that no heat is lost through the bottom by conduction and is described in equation (27).

$$\left. \frac{\partial t}{\partial x} \right|_{x=6} = 0 \quad (27)$$

A finite difference numerical solution for transient conduction was written with the storage model being divided into 145 different nodes having a spacing (ΔX) of 1/2 inch between each node (Figure 11). The time difference ($\Delta\theta$) was 0.1 hour letting the temperature of each node represent the temperature of a thin plane wall, ΔX thick, surrounding the node. An energy balance was written for each node.

The energy balance for the surface node states the energy received at the surface minus the energy lost at the surface plus the energy conducted from the adjacent node is equal to energy stored in the surface node. This energy balance is shown in Figure 12 and is represented by equation (28).

$$Q_{S1} = A_S Q_{RAD} + A_S Q_{CR} + A_S Q_{INF} + Q_{21} \quad (28)$$

where,

Q_{S1} = energy stored in node 1, BTU/hr.

Q_{RAD} = solar radiation received, BTU/hr-ft².

Q_{CR} = heat loss due to convection and radiation, BTU/hr-ft².

Q_{INF} = heat loss due to air infiltration, BTU/hr-ft².

Q_{21} = energy conducted from node 2 to node 1, BTU/hr.

A_S = surface area of collector, ft².

The energy conducted can be represented by Fourier's Heat Equation:

$$Q_{con} = -k_w A_S \frac{\partial t}{\partial x} \quad (29)$$

where,

Q_{con} = energy conducted in the medium, BTU/hr.

k_w = thermal conductivity of fluid, BTU/hr-ft-°F.

A_S = cross-sectional area of surface, ft².

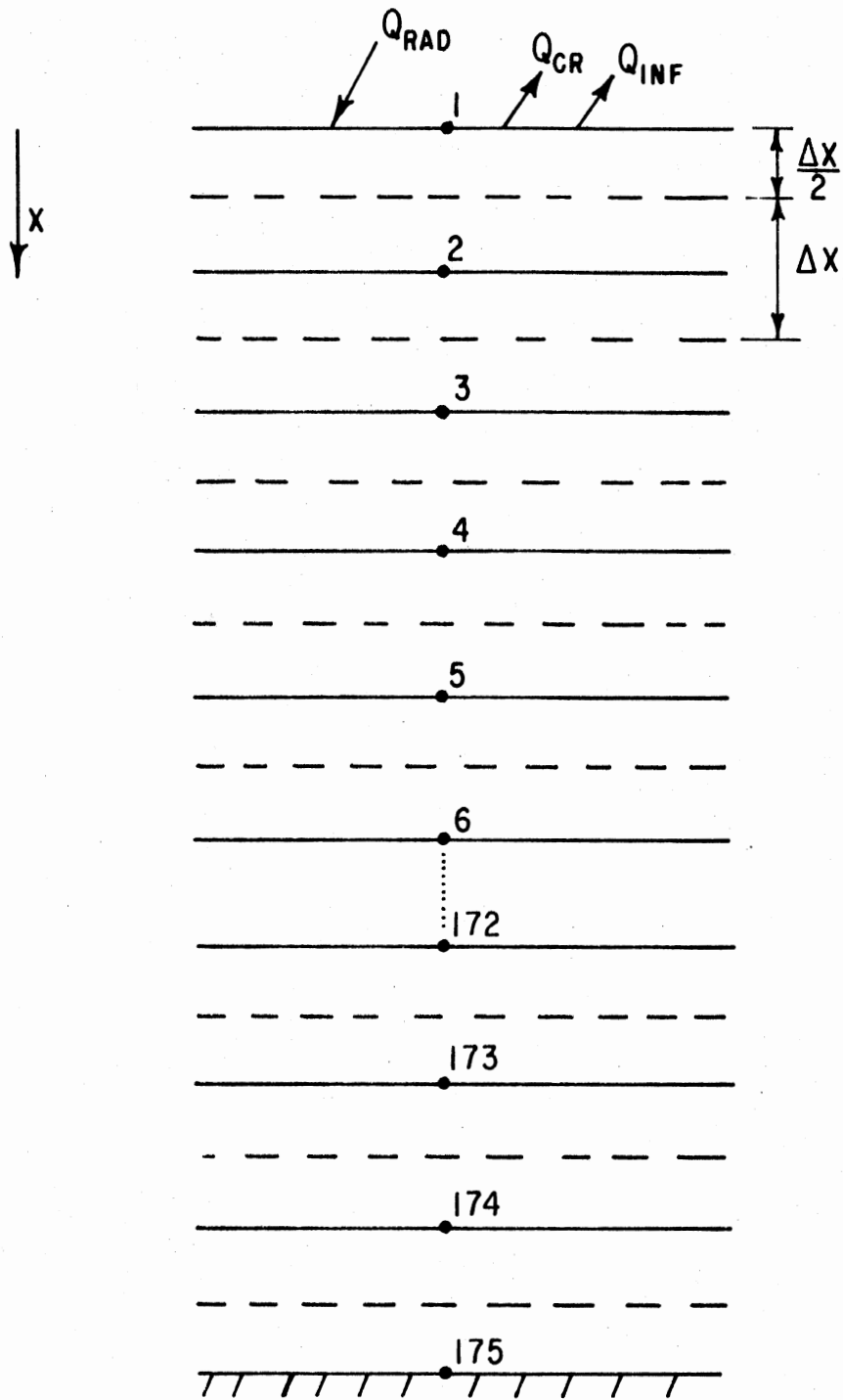


Figure 11. Nodal-point Arrangement in Storage Model for Transient Conduction

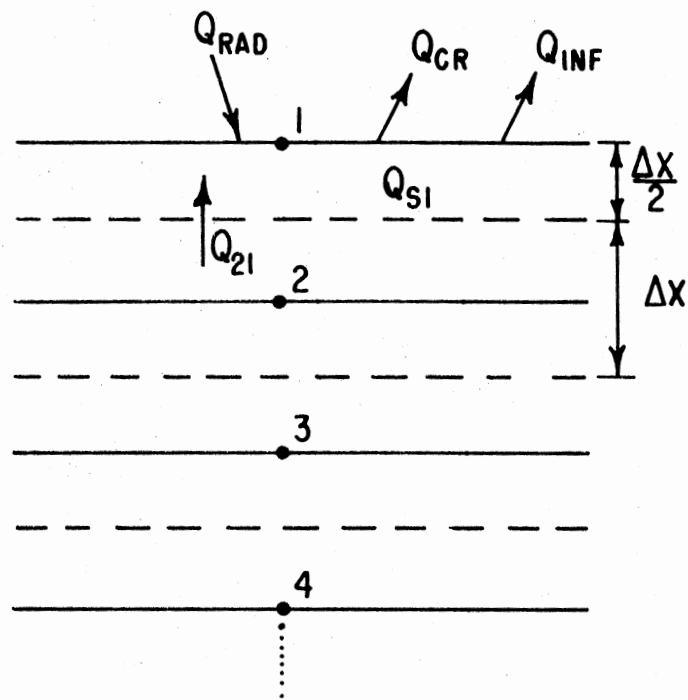


Figure 12. Energy Balance on Surface Node

t = temperature of water at depth x , °F.

x = depth below surface, ft.

The energy stored in a medium can be determined by use of equation (30).

$$Q_S = \rho_w C_w V \frac{\partial t}{\partial \theta} \quad (30)$$

where,

Q_S = energy stored, BTU/hr.

ρ_w = density, lbm/ft³.

C_w = specific heat, BTU/lbm-°F.

V = volume of medium, ft³.

t = temperature at time θ , °F.

θ = time, hr.

Therefore, a finite difference equation can be written for both the conduction and storage terms with equations (29) and (30), respectively.

$$Q_{21} = k_w A_S \frac{(t_2 - t_1)}{\Delta X} \quad (31)$$

where,

t_2 = temperature of node 2, °F.

t_1 = temperature of node 1, °F.

ΔX = distance between nodes, 1/2 inch.

and

$$Q_{S1} = \rho_w C_w V_1 \frac{t_1' - t_1}{\Delta \theta} \quad (32)$$

where,

t_1' = new temperature of the surface at new time, °F.

V_1 = volume of each node, ft³.

$\Delta \theta$ = time interval, 0.1 hour.

Substituting equation (31) and (32) into the energy balance, equation (28) becomes:

$$\rho_w C_w V_1 \frac{t_1' - t_1}{\Delta\theta} = A_S Q_{RAD} + A_S Q_{CR} + A_S Q_{INF} + \frac{k_w A_S}{\Delta X} (t_2 - t_1) \quad (33)$$

Rearranging equation (33) and letting $V_1 = \frac{\Delta X}{2} A_S$ and dividing by A_S ,

$$t_1' = t_1 + \frac{2\Delta\theta k_w}{\Delta X \rho_w C_w} (t_2 - t_1) + \frac{2(Q_{RAD} + Q_{CR} + Q_{INF})}{\rho_w C_w \Delta X} \Delta\theta \quad (34)$$

At each new time of θ , the temperature at the surface can be determined.

To determine temperature of the interior nodes, an energy balance needs to be written for each node and the new temperature calculated. Figure 13 shows a nodal point arrangement for an interior node where n represents the node. An energy balance on the n^{th} node gives

$$Q_{sn} = Q_{n-1,n} + Q_{n+1,n} \quad (35)$$

The finite difference equation for each term becomes

$$Q_{n-1,n} = k_w A_s \frac{t_{n-1} - t_n}{\Delta X} \quad (36)$$

$$Q_{n+1,n} = k_w A_s \frac{(t_{n+1} - t_n)}{\Delta X} \quad (37)$$

$$\text{and } Q_{sn} = \rho_w C_w V \frac{(t_n' - t_n)}{\Delta\theta} \quad (38)$$

where,

$Q_{n-1,n}$ = energy conducted from node $n-1$ to n , BTU/hr.

$Q_{n+1,n}$ = energy conducted from node $n+1$ to n , BTU/hr.

Q_{sn} = energy stored in node n , BTU/hr.

t_{n-1} = temperature of node $n-1$, °F.

t_n = temperature of node n , °F.

t_{n+1} = temperature of node $n+1$, °F.

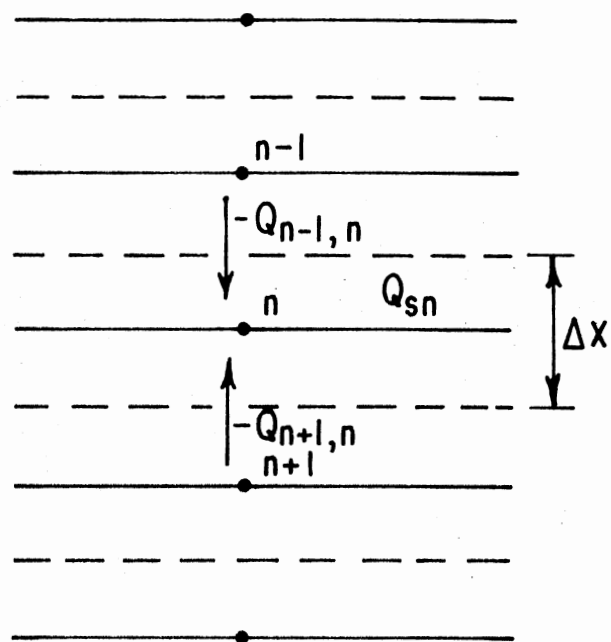


Figure 13. Energy Balance on Interior Node

t_n' = new temperature of node n, °F.

Substituting equation (36), (37), and (38) into equation (35)

gives

$$\frac{\rho_w C_w V_1 (t_n' - t_n)}{\Delta\theta} = k_w A_s \frac{(t_{n-1} - t_n)}{\Delta X} + k_w A_s \frac{(t_{n+1} - t_n)}{\Delta X} \quad (39)$$

Rearranging equation (39) and letting $V_1 = \Delta X A_s$, the equation for determining the temperature of an interior node at time θ becomes

$$t_n' = t_n + \frac{\Delta\theta}{\Delta X^2} \frac{k_w}{\rho_w C_w} (t_{n-1} - 2t_n + t_{n+1}) \quad (40)$$

Calculating the temperature of the bottom node, number 175, represented in Figure 14, an energy balance says the energy conducted into node 175 from the adjacent node, number 174, equals the energy stored in node 175 and is given by equation (41).

$$Q_{174-175} = Q_{S175} \quad (41)$$

The finite difference equations becomes

$$Q_{174-175} = k_w A_s \frac{t_{174} - t_{175}}{\Delta X} \quad (42)$$

$$\text{and } Q_{S175} = \rho_w C_w V_1 \frac{t'_{175} - t_{175}}{\Delta\theta} \quad (43)$$

where,

$Q_{174-175}$ = energy conducted from node 174 to 175, BTU/hr.

Q_{S175} = energy stored in node 175.

t_{175} = temperature of node 175, °F.

t'_{175} = new temperature of node 175, °F.

Substituting into equation (41) and again letting $V_1 = \frac{\Delta X}{2} A_s$, the energy balance gives:

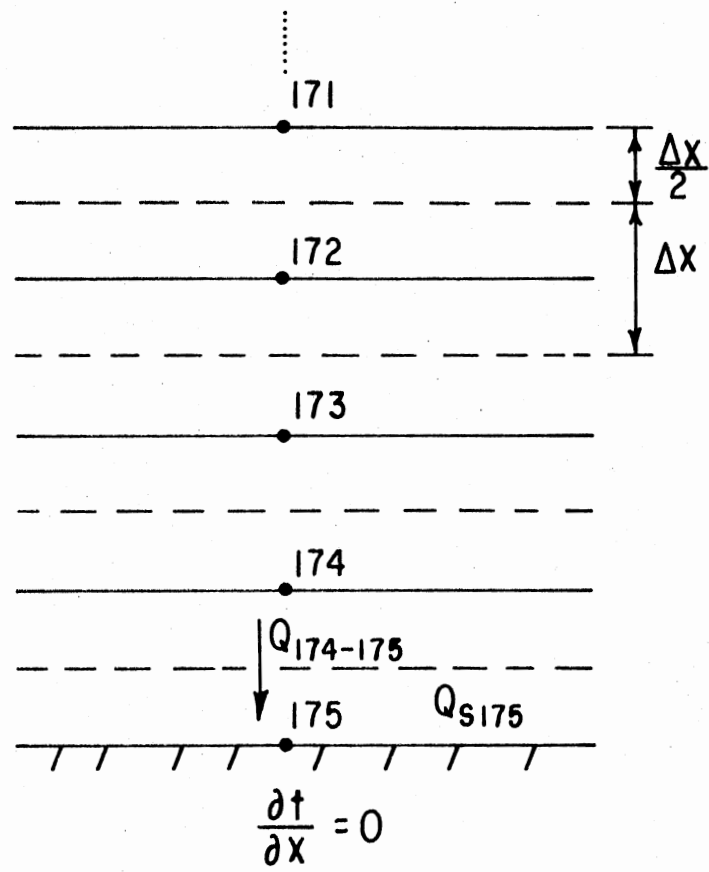


Figure 14. Energy Balance on Bottom Node

$$k \frac{t_{174} - t_{175}}{\Delta X} = \rho_w C_w \frac{\Delta X}{2} \frac{(t'_{175} - t_{175})}{\Delta \theta} \quad (44)$$

By rearranging equation (44), the temperature at the bottom node is:

$$t'_{175} = t_{175} + \frac{k_w}{\rho_w C_w} \frac{2\Delta \theta}{\Delta X^2} (t_{174} - t_{175}) \quad (45)$$

CHAPTER V

DATA ANALYSIS AND RESULTS

Temperature Distributions

The finite difference equations (34), (40), and (45) were solved to predict the temperature distribution in the storage model. The atmospheric conditions encountered, the calculation of the heat loss terms for convection, radiation, and air infiltration by equations (8) and (7) and the calculated average water temperature for this experiment were used in the theoretical numerical equations. This provides comparisons between the predicted and observed temperatures.

Comparisons between observed and predicted temperatures in June 16, 1978, for a 24 hour period beginning at 6:00 a.m. (CDT) are shown in Figures 15, 16, 17, 18, 19, and 20 for the surface temperature and for depths of 1 inch, 6 inches, 10 inches, 36 inches, and 72 inches below the water surface, respectively. The numerical data used for calculating the temperature distributions are given in Table VI with Table VII showing the observed temperatures at the different depths recorded.

Figures 15 and 16 show differences of 33% between the predicted and observed temperatures while Figure 17 shows differences of 15% between the observed and predicted temperatures toward the last half of the 24 hour period. Figure 18 shows differences of 7% toward the last three hours of the time period. The differences between the observed and

TABLE VI

DATA FOR SOLAR RADIATION, HEAT LOSS DUE TO
CONVECTION AND RADIATION, AIR INFIL-
TRATION LOSSES, AND WIND VELOCITIES
FOR 24 HOUR PERIOD ON JUNE 16,
1978, WITH BEGINNING TIME
BEING 6:00 A.M. (CDT)

Time* Hours (CDT)	$\frac{Q_{RAD}}{BTU}$ $hr\ ft^2$	$\frac{Q_{CR}}{BTU}$ $hr\ ft^2$	$\frac{Q_{INF}}{BTU}$ $hr\ ft^2$	Wind Vel. Miles hr
1	11.0	34.0	4.0	11.1
2	55.4	32.0	9.0	11.1
3	116.7	35.0	15.0	12.3
4	178.7	41.0	17.0	13.6
5	231.3	52.0	20.0	16.0
6	271.8	56.0	23.0	17.3
7	297.1	61.0	27.0	18.5
8	305.8	59.0	27.0	18.5
9	279.1	66.0	28.0	18.5
10	269.3	67.0	24.0	19.8
11	225.8	63.0	22.0	19.8
12	171.2	56.0	19.0	19.8
13	108.8	47.0	16.0	18.5
14	48.4	41.0	7.0	13.6
15	8.6	38.0	2.0	9.9
16	—	37.0	1.0	11.1
17	—	36.0	1.0	11.1
18	—	35.0	1.0	12.3
19	—	35.0	1.0	13.6
20	—	34.0	0.0	12.3
21	—	32.0	0.0	12.3
22	—	33.0	1.0	9.9
23	—	32.0	1.0	9.9
24	—	32.0	1.0	9.9

*Time = 1 is same as 7:00 a.m. (CDT) on June 16, 1978.

$Q_{RAD} = 306.0\ BTU/hr\ ft^2.$

$Q_{CRD} = 33.0\ BTU/hr\ ft^2.$

$Q_{CRC} = 34.0\ BTU/hr\ ft^2.$

$T_{AVE} = 82.1^\circ\ F.$

TABLE VII

OBSERVED WATER TEMPERATURES AND AVERAGE WATER
TEMPERATURES IN THE FRESHWATER SOLAR
STORAGE MODEL FOR 24 HOUR PERIOD
ON JUNE 16, 1978, WITH
BEGINNING TIME BEING
6:00 A.M. (CDT)

Time* Hours (CDT)	Temp. Air Inside Bubble °F	Temp. Sur- face °F	Temp. Below Surface, °F					Temp. Amb. Air °F	Temp. Ave. Water °F
			1"	6"	10"	36"	72"		
1	78.3	83.4	83.7	84.0		82.0	79.3	75.2	81.9
2	84.8	84.4	84.1	82.7		82.0	79.3	77.3	81.8
3	92.8	90.4	86.9	83.8		81.8	79.1	81.2	81.8
4	97.4	96.3	91.2	82.8	84.0	81.6	78.9	83.9	81.8
5	101.5	103.6	97.6	82.6	83.7	81.3	78.6	85.9	81.7
6	107.4	108.6	102.2	81.3	83.3	80.9	78.2	88.9	81.4
7	111.7	112.5	107.7	79.6	83.3	75.9	77.0	90.7	77.6
8	113.6	113.4	110.4	82.5	82.9	78.6	72.9	92.2	79.4
9	113.7	115.8	111.5	85.6	84.2	81.6	78.9	91.7	82.6
10	110.9	116.8	113.3	81.9	85.0	81.7	79.1	92.0	83.0
11	79.4	114.5	112.0	89.2	85.6	81.9	79.4	91.6	83.3
12	105.5	110.0	109.1	90.8	86.7	82.1	79.6	90.1	83.6
13	101.3	104.3	105.1	92.3	87.4	82.0	79.5	88.7	83.5
14	92.1	99.3	100.8	93.3	88.2	82.1	79.6	86.7	83.6
15	86.1	95.4	97.1	93.9	89.0	82.2	79.8	84.3	83.7
16	83.8	92.9	94.3	93.6	89.4	82.2	79.8	82.8	83.6
17	82.3	91.1	92.4	92.7	89.8	82.2	79.8	81.5	83.5
18	80.7	89.4	90.8	91.3	89.9	82.3	79.8	80.3	83.4
19	80.0	88.1	89.4	89.7	89.4	82.1	79.6	79.3	83.1
20	79.1	87.1	88.4	89.0	88.9	82.1	79.7	78.9	83.0
21	78.4	86.2	87.7	88.2	88.3	82.3	79.8	78.6	83.0
22	78.0	85.3	86.5	86.9	86.9	81.9	79.3	77.5	82.4
23	77.7	84.7	86.0	86.4	86.4	82.0	79.4	77.2	82.4
24	77.2	84.1	85.4	85.8	85.8	81.9	79.3	77.0	82.2

*Time = 1 is same as 7:00 a.m. (CDT) on June 16, 1978.

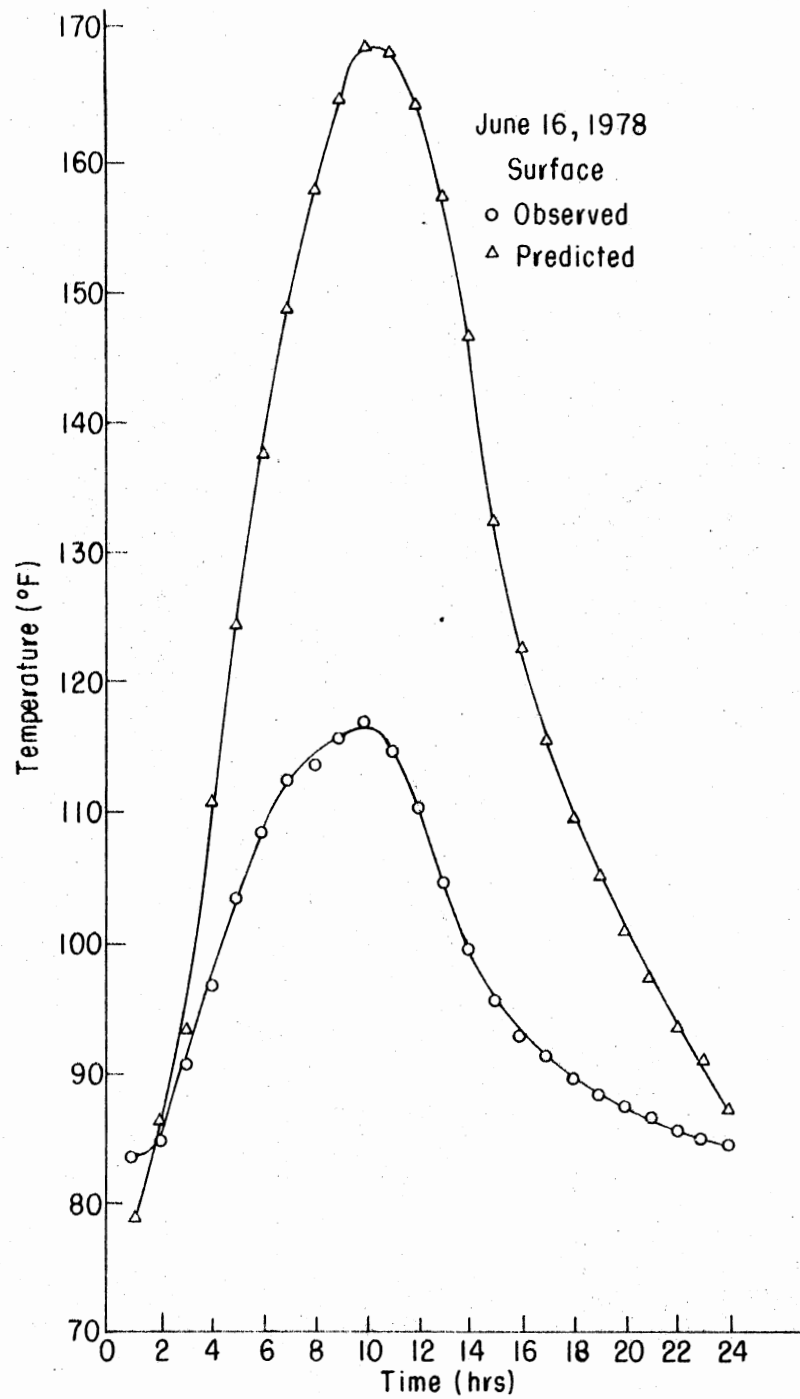


Figure 15. Comparison Between Predicted and Observed Surface Temperatures in a Freshwater Solar Storage Model for June 16, 1978. Time Is Measured from 6:00 a.m. (CDT) of This Day

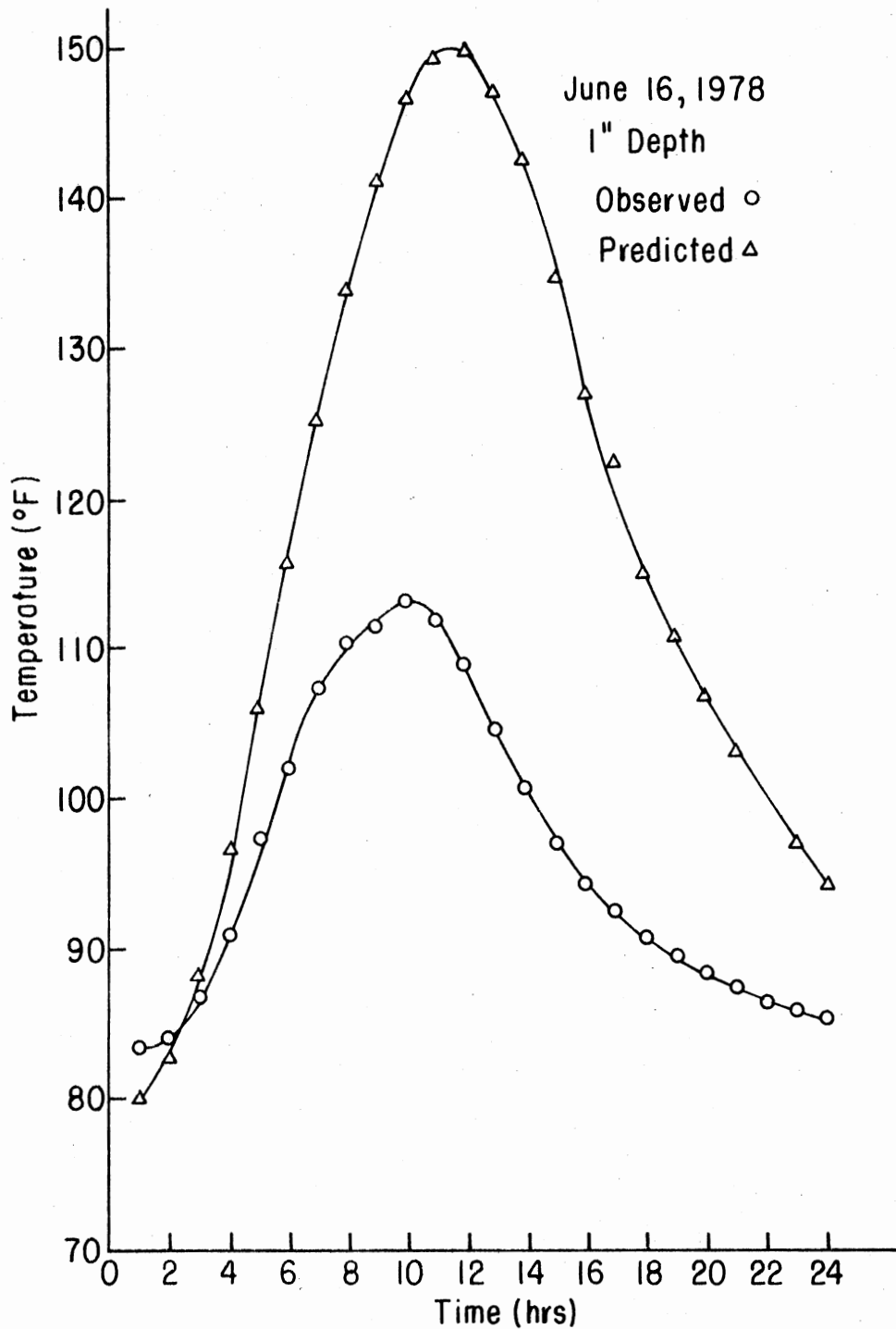


Figure 16. Comparison Between Predicted and Observed Temperatures One Inch Below the Surface in a Freshwater Solar Storage Model for June 16, 1978. Time Is Measured from 6:00 a.m. (CDT) of This Day

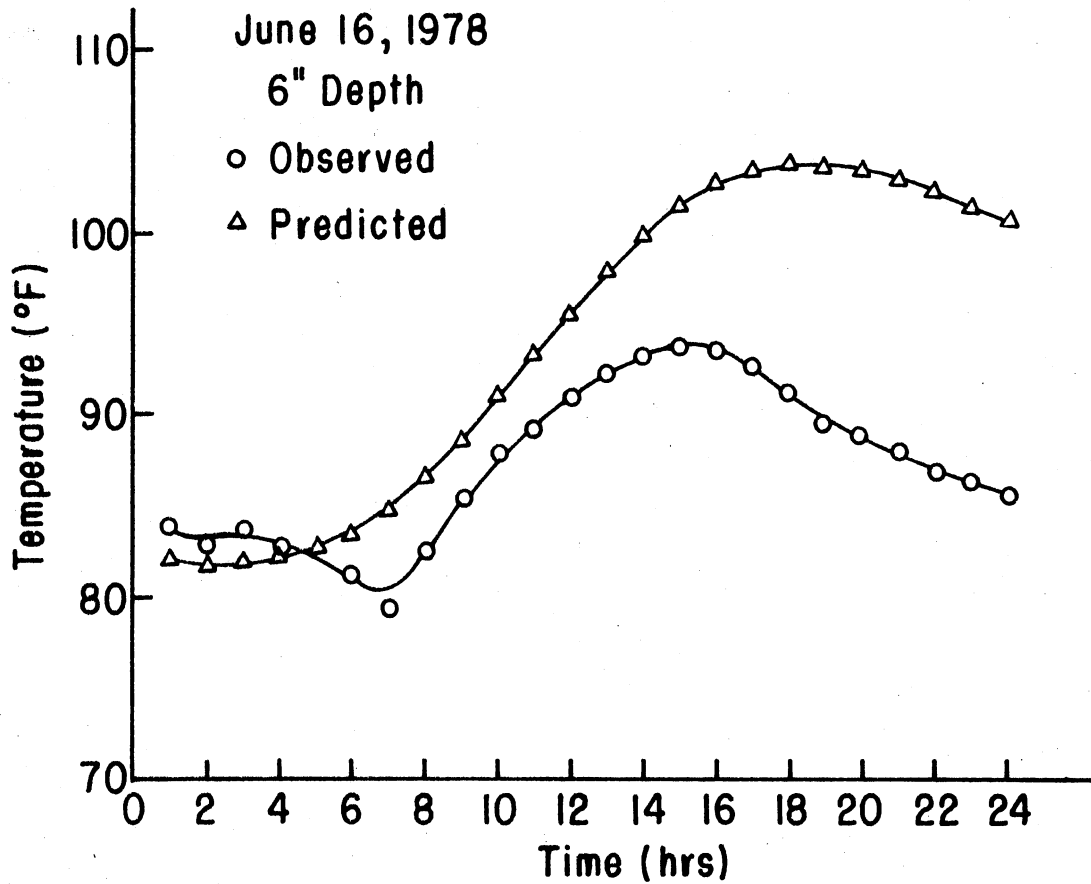


Figure 17. Comparison Between Predicted and Observed Temperatures Six Inches Below the Surface in the Freshwater Solar Storage Model for June 16, 1978. Time Is Measured from 6:00 a.m. (CDT) of This Day

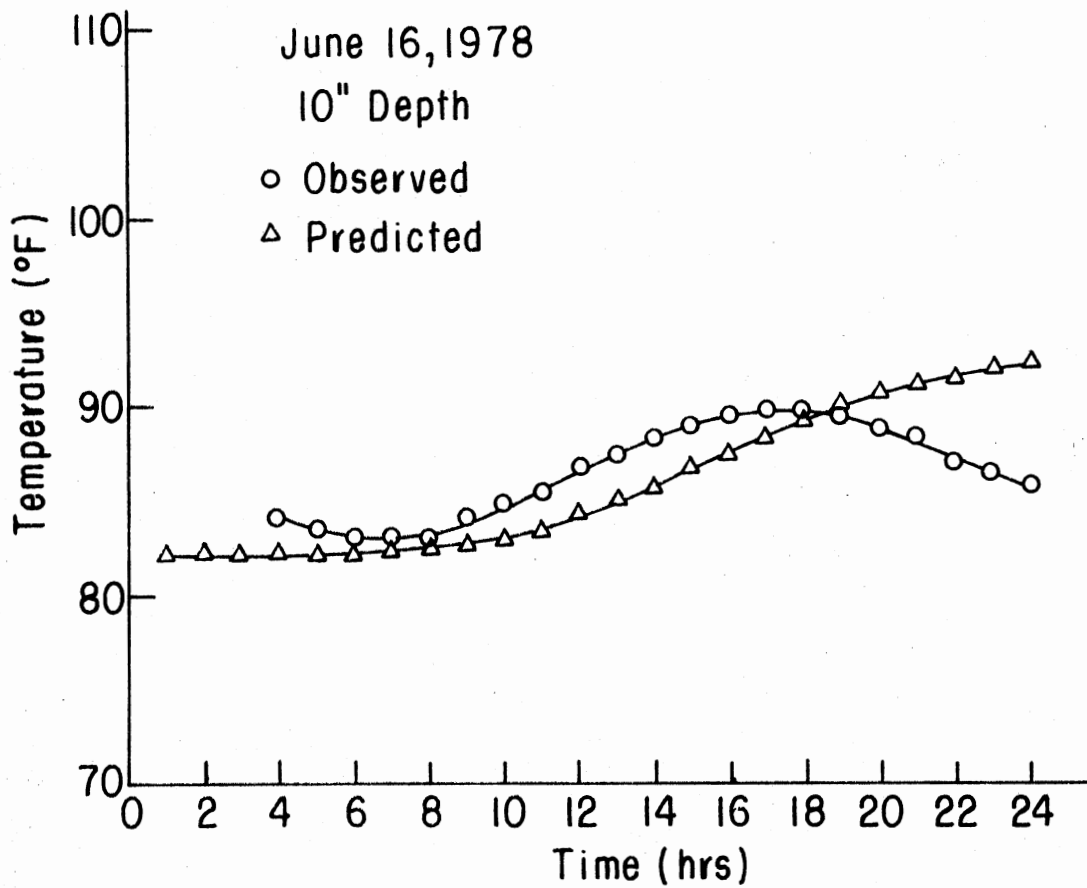


Figure 18. Comparison Between Predicted and Observed Temperatures 10 Inches Below the Surface in the Freshwater Solar Storage Model for June 16, 1978. Time Is Measured from 6:00 a.m. (CDT) of This Day

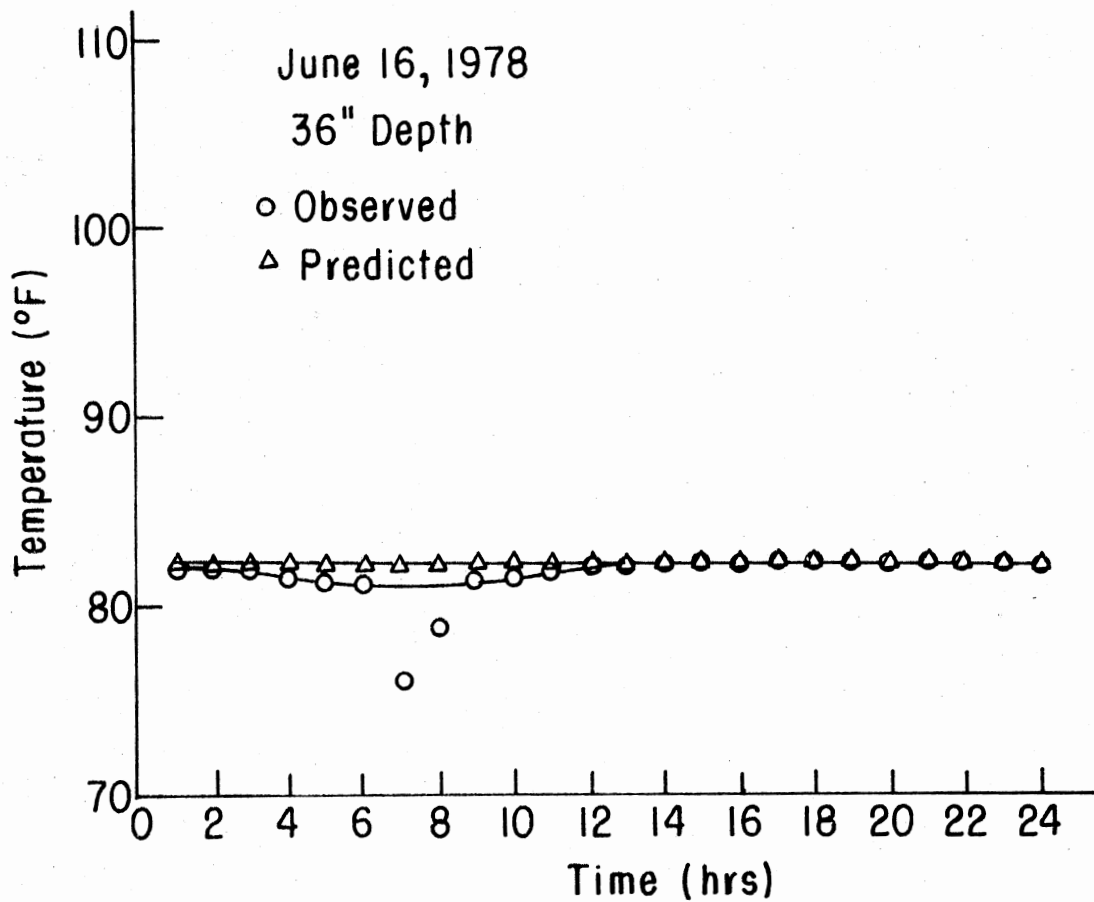


Figure 19. Comparison Between Predicted and Observed Temperatures 36 Inches Below the Surface in the Freshwater Solar Storage Model for June 16, 1978. Time Is Measured from 6:00 a.m. (CDT) of This Day

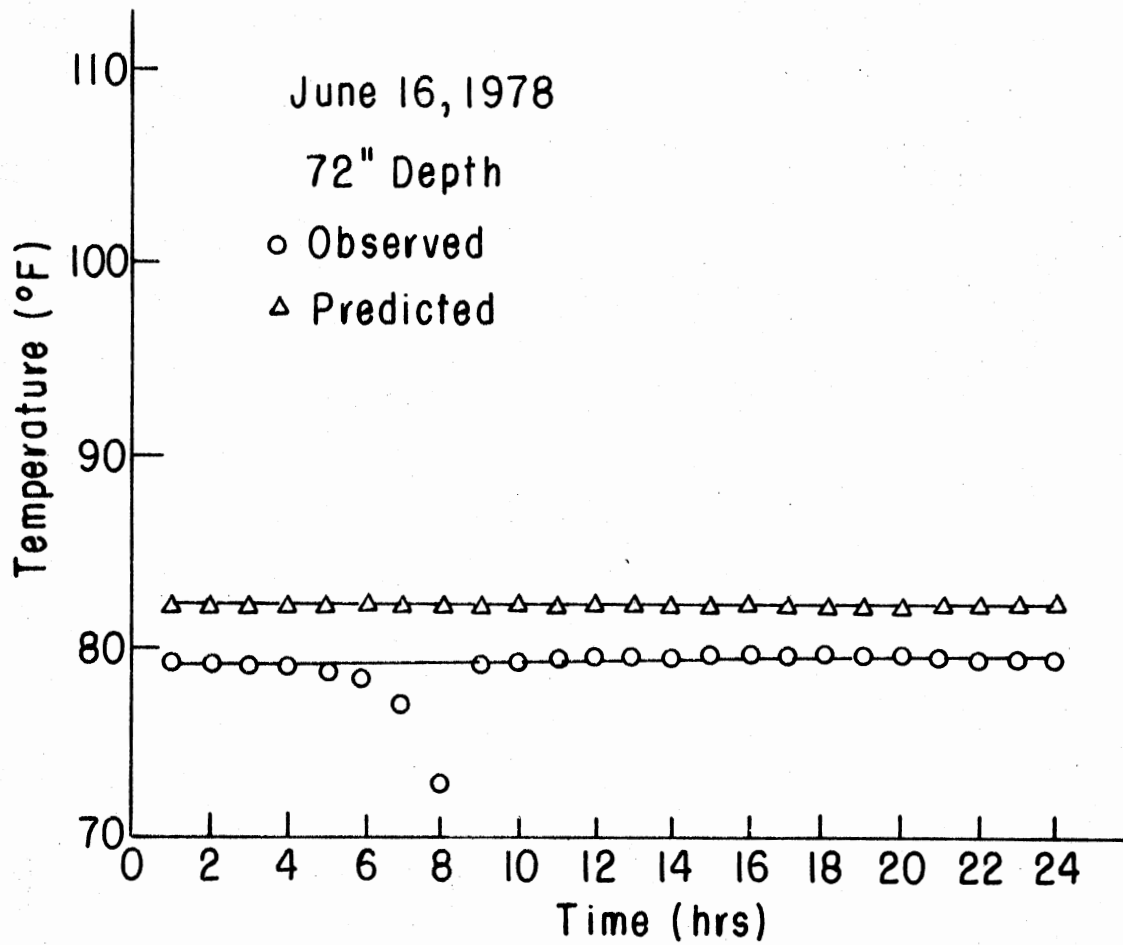


Figure 20. Comparison Between Predicted and Observed Temperatures 72 Inches Below the Surface of the Freshwater Solar Storage Model for June 16, 1978. Time Is Measured from 6:00 a.m. (CDT) of This Day

predicted temperatures in the lower depths of the storage model indicate that these temperatures are dependent upon the value chosen for the initial average water temperature. These two curves are shown in Figures 19 and 20. Therefore, the assumption of an iso-thermal temperature for an initial condition is not accurate as described in equation (21) and can be seen in Figure 21 which shows a plot of the observed temperature profile at 6:00 a.m. (CDT).

Average water temperature for June 16, 1978, is plotted in Figure 22 for the predicted and calculated temperatures with a 2.7 degree or 3% temperature difference.

In an attempt to determine what caused the error between the predicted and observed temperatures in the upper 12 inches of the storage model, temperature profiles for several hours were studied. Figure 23 shows the temperature profile at 5:00 a.m. for the observed and predicted temperatures while Figure 24 shows the same for 7:00 a.m. An unstable temperature profile exists in the upper regions of the storage model, when no surface heating is taking place due to solar radiation. This unstable condition is caused by convective currents which distribute heat energy and causes the temperatures to be unpredictable. The convection currents occur when the temperature of the water at the surface becomes cooler than the water below it. Therefore, convective mixing at the surface is one probable cause of error between the predicted and observed temperatures at the surface.

Snider and Viskanta (20) state that to accurately predict temperature distributions in water heated by solar radiation, the boundary condition at the water surface must be correctly specified. The surface boundary condition used in this model was described in equations (22)

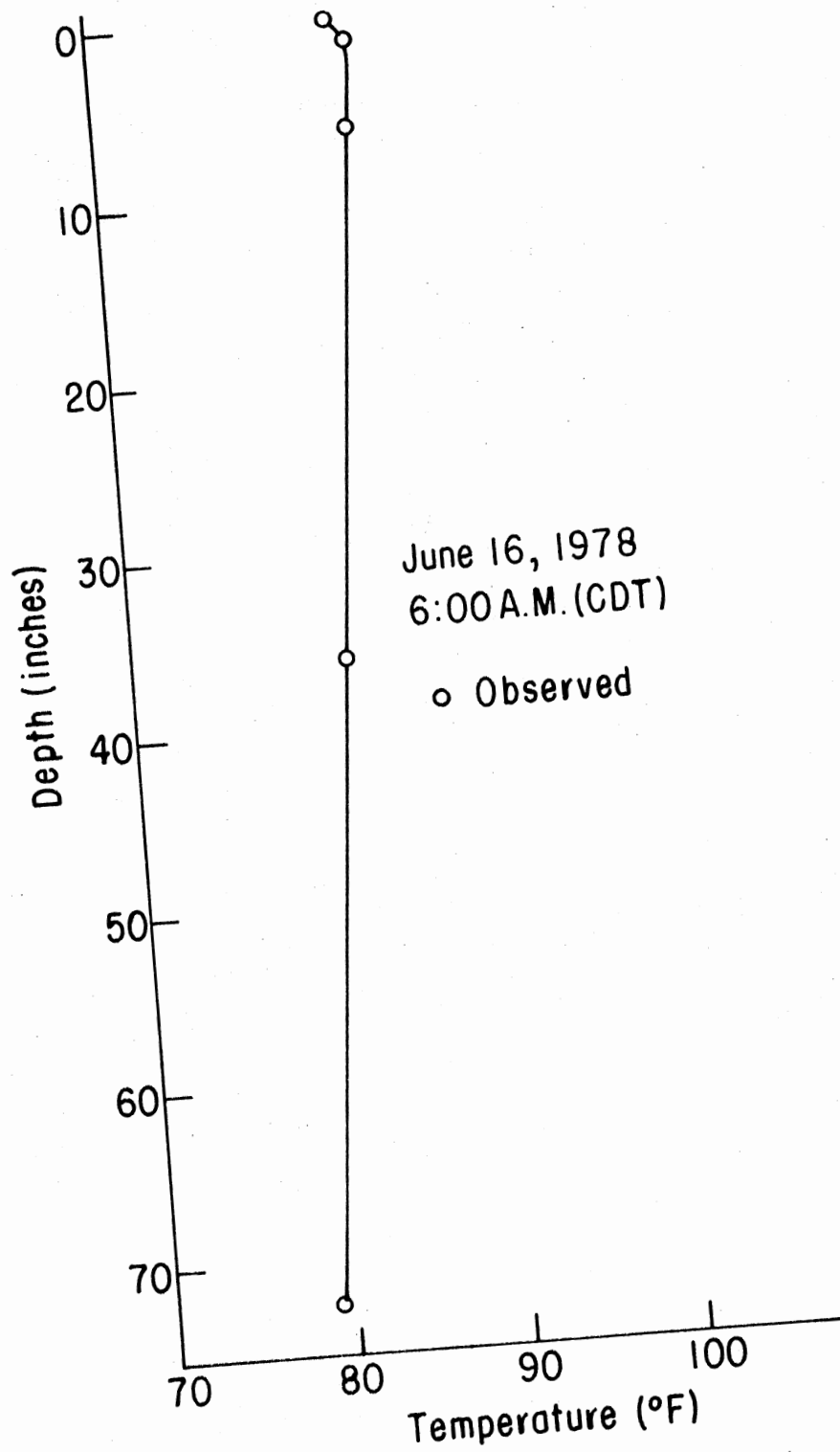


Figure 21. Temperature Profile in Freshwater Solar Storage Model for 6:00 a.m. (CDT) on June 16, 1978

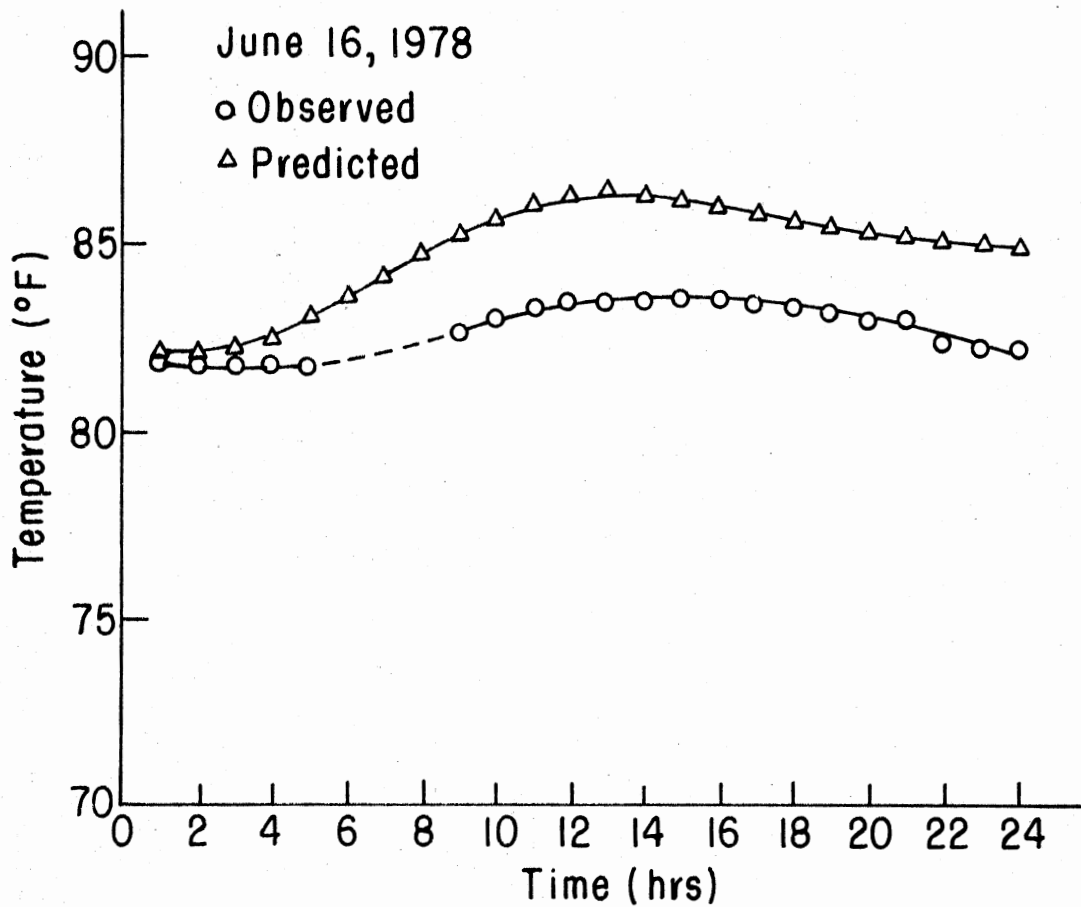


Figure 22. Comparison Between Predicted and Observed Average Water Temperature in the Freshwater Solar Storage Model for June 16, 1978. Time Is Measured from 6:00 a.m. (CDT) of This Day

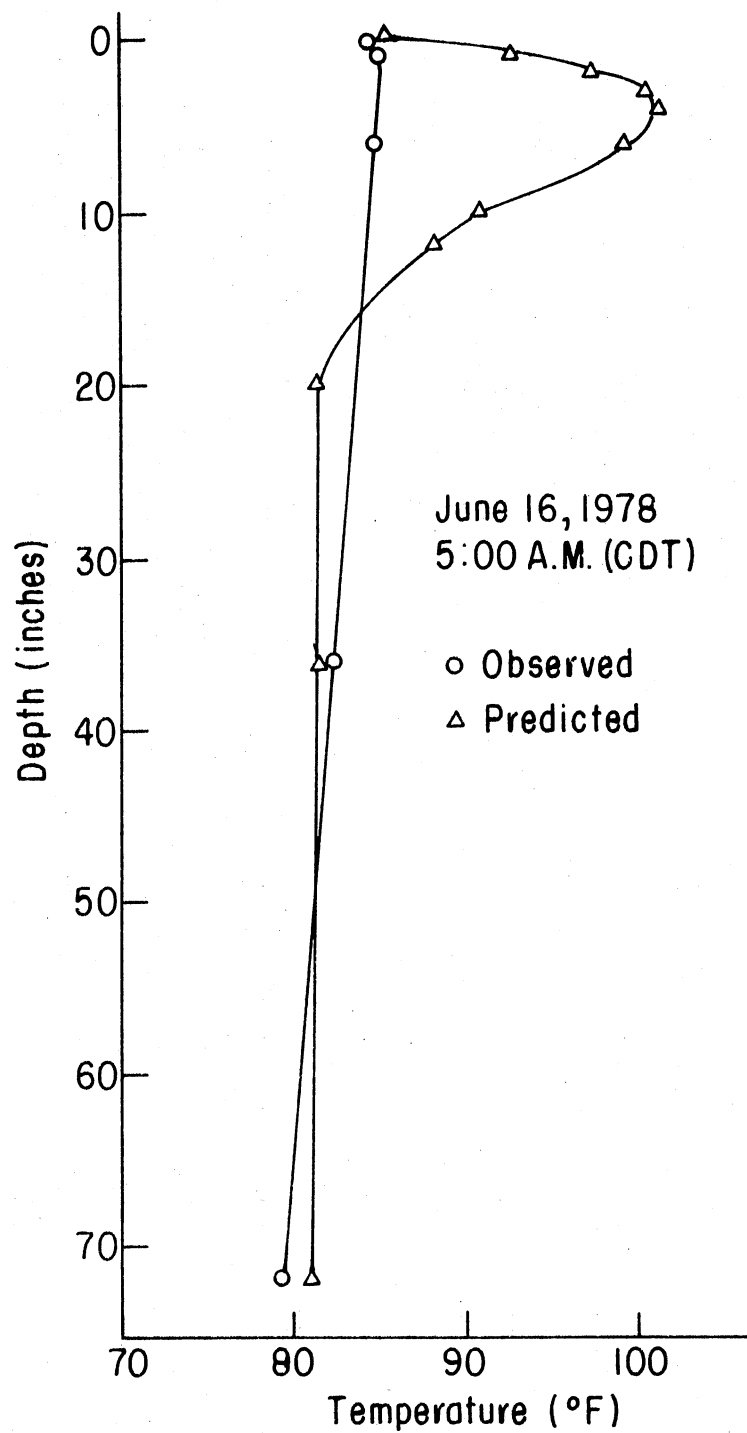


Figure 23. Temperature Profile in Fresh-water Solar Storage Model for Both Predicted and Observed Temperatures at 5:00 a.m. (CDT) on June 16, 1978

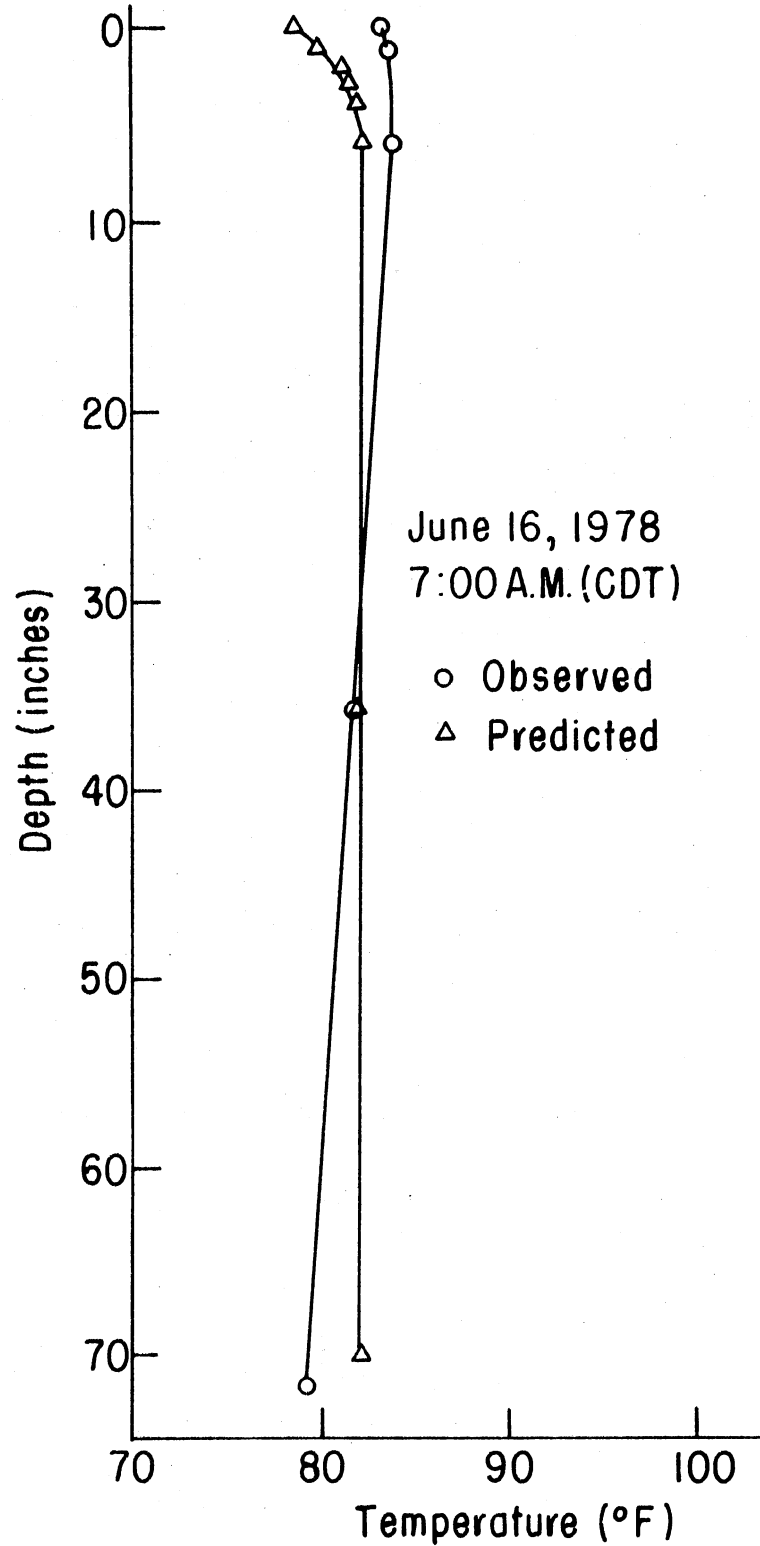


Figure 24. Temperature Profile in Fresh-water Solar Storage Model for Predicted and Observed Temperatures at 7:00 a.m. (CDT) on June 16, 1978

and (23).

Brunt (1) and Jaeger and Johnson (12) assumed that the solar radiation received at the earth's surface was sinusoidal during the daytime with a constant rate of heat loss during the day and night. In this experiment, this same assumption was made with an additional heat loss in the daytime that was sinusoidal. The predicted and observed solar radiation data for June 16 is plotted in Figure 25 and Figure 26 shows the predicted and observed heat loss data due to convection and radiation. The difference between the observed and predicted heat loss varies as much as 34% during the daytime. This could be another source of error.

Another probable cause of error in the surface boundary condition is the specification of the heat loss term due to evaporation. It is known that evaporation took place during the 47 day period of the experiment because of a decrease in the height of the water surface in the storage model. This difference was not measured, but an estimate of the heat loss due to evaporation was determined and was approximately 33% of the calculated heat loss during the daytime. The effect of this upon the predicted and observed temperatures will be discussed later.

When water changes from a saturated state to a vapor state, evaporation takes place and during this process heat energy is released at a rate between 1,060 and 1,020 BTU per pound of water evaporated for the temperature range encountered. Evaporation does not take place at a constant rate but is affected by the temperature of the water surface, relative humidity of air above the water surface, wind speed over the surface, composition of water, i.e. salt concentration, and area of evaporation (5). In this experiment, temperature of the water surface,

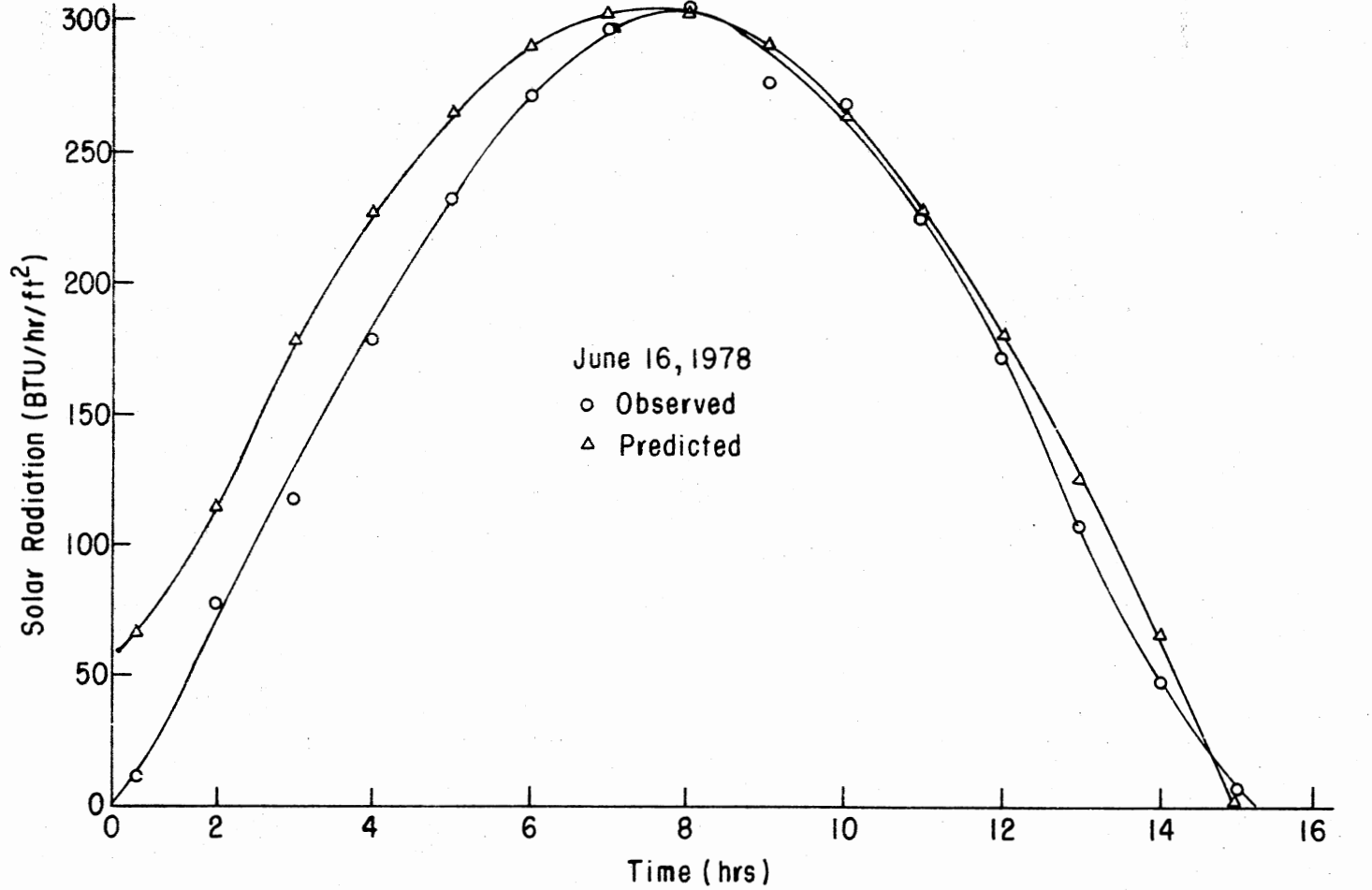


Figure 25. Comparison Between Predicted and Observed Solar Radiation for June 16, 1978. Time Is Measured from 6:00 a.m. (CDT) of This Day

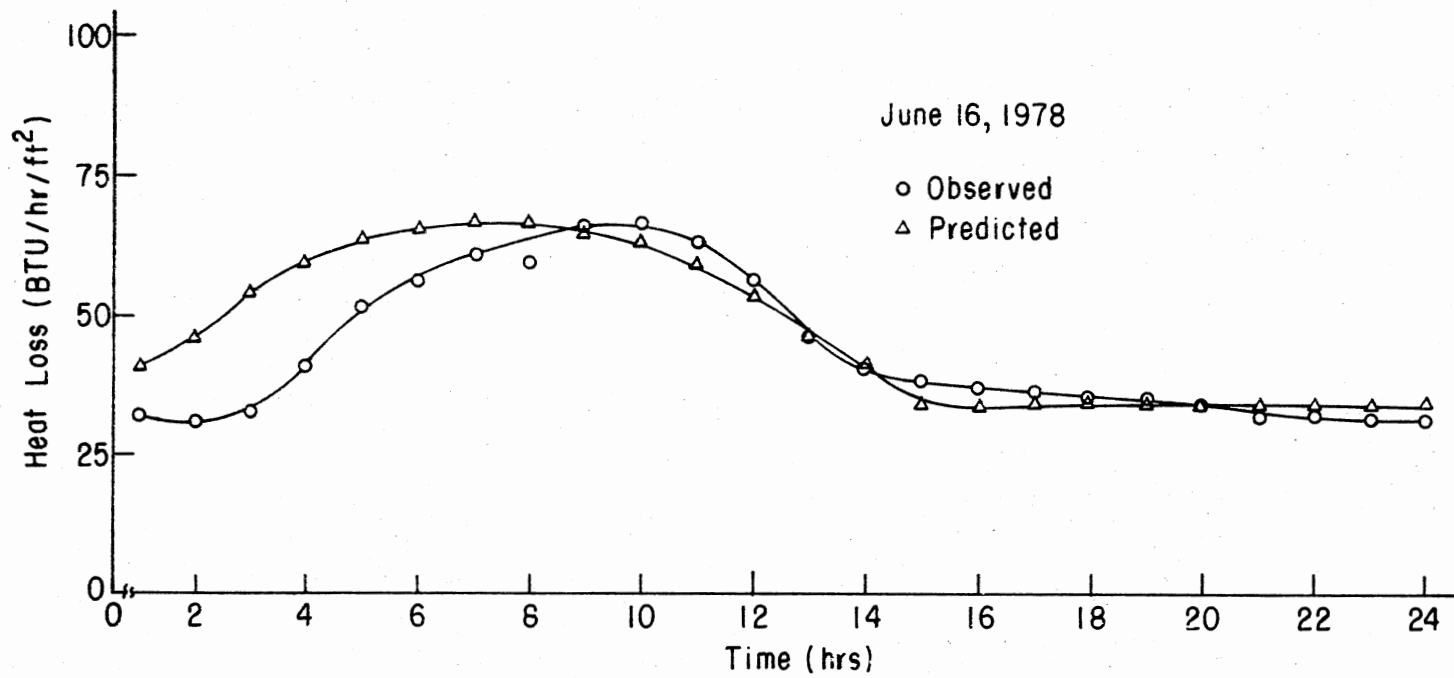


Figure 26. Comparison Between Predicted and Observed Heat Loss Due to Convection and Radiation for June 16, 1978. Time Is Measured from 6:00 a.m. (CDT) of This Day

relative humidity of the air inside the polyethylene dome, and percent coverage of the water surface by black polyethylene would affect evaporation. An increase in surface water temperature will increase the rate of evaporation while the higher the relative humidity, the lower is the evaporation loss (5). Also, Carlson (2) states that if more of the surface area is covered, the lower the rate of evaporation. Therefore, it is a reasonable assumption that greater evaporation took place in the daytime than during the night hours during this experiment.

Another possible cause of inaccurate determination of the surface boundary condition is due to the polyethylene absorber surface being partially coated with a white film as shown in Figure 10. This film affects the quantity of heat absorbed and will probably decrease the absorption of solar radiation.

To obtain an idea of what the true heat loss term should be, several different values were assumed and substituted into the surface boundary condition. A plot of the observed and newly predicted average water temperatures, where the heat loss term in the daytime was increased by a value of 66.0 or 33% and the heat loss at night decreased by 19.0 or 44%, is shown in Figure 27. Also, the observed and newly predicted temperatures at the surface and depths of 1 inch, 6 inches, and 10 inches below the surface are plotted in Figures 28, 29, 30, and 31, respectively. These newly predicted temperatures agree with the observed temperatures and reveal that the surface boundary condition is not correctly specified. The heat loss due to evaporation should be included in the surface boundary condition along with the heat loss due to convection, radiation, and air infiltration.

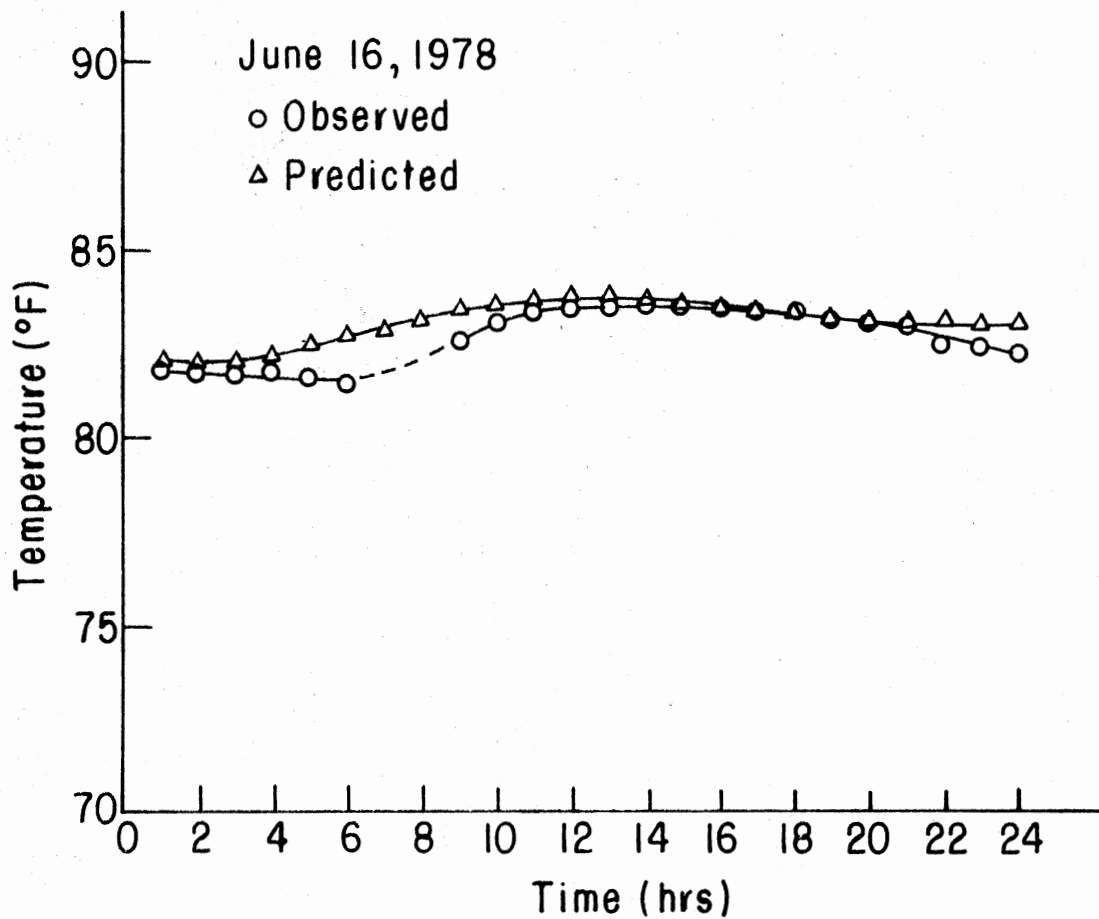


Figure 27. Comparison Between Newly Predicted and Observed Average Water Temperature in the Freshwater Solar Storage Model for June 16, 1978. Time Is Measured from 6:00 a.m. (CDT) of This Day

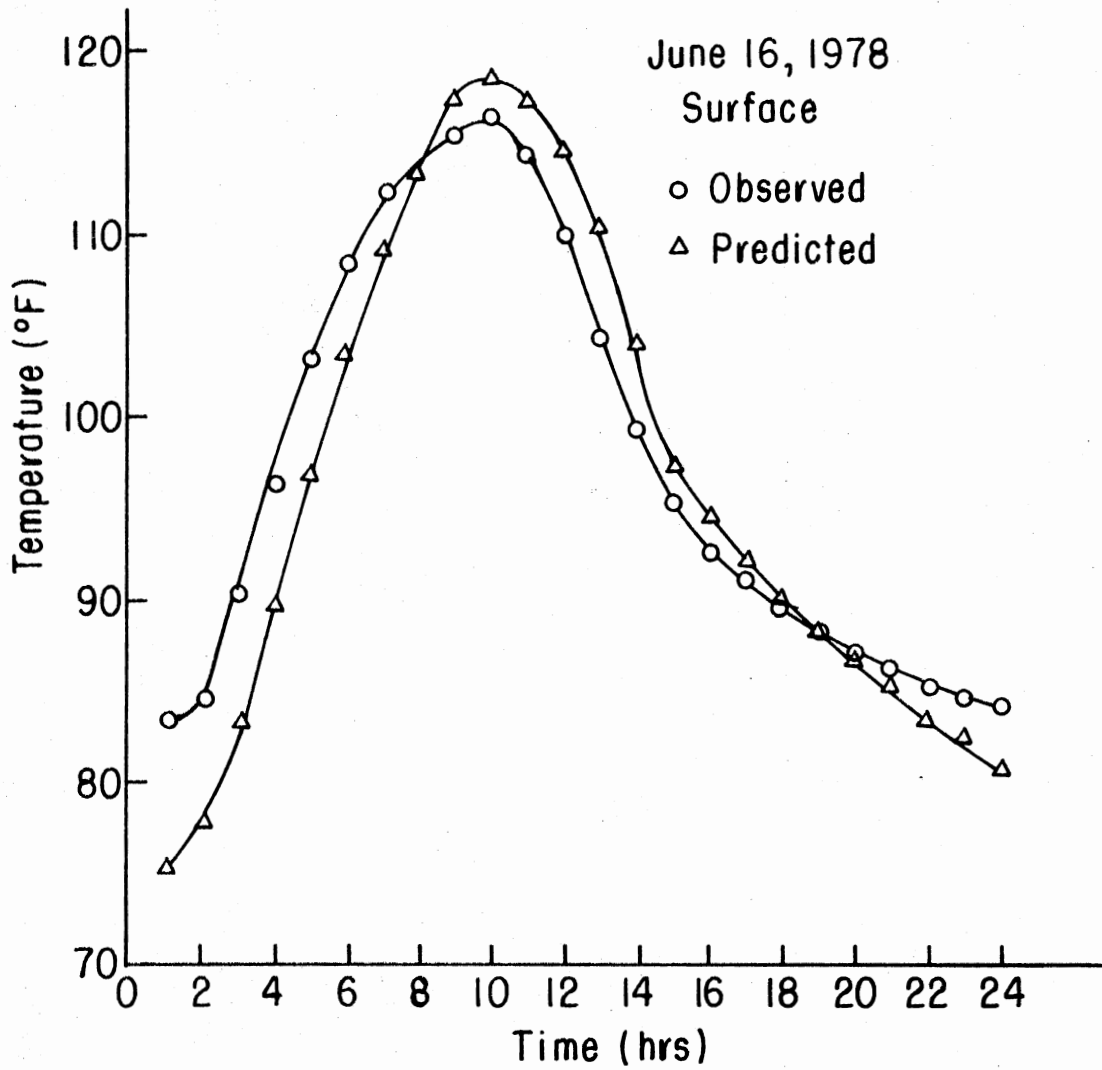


Figure 28. Comparison Between Newly Predicted and Observed Surface Temperatures in the Freshwater Solar Storage Model for June 16, 1978. Time Is Measured from 6:00 a.m. (CDT) of This Day

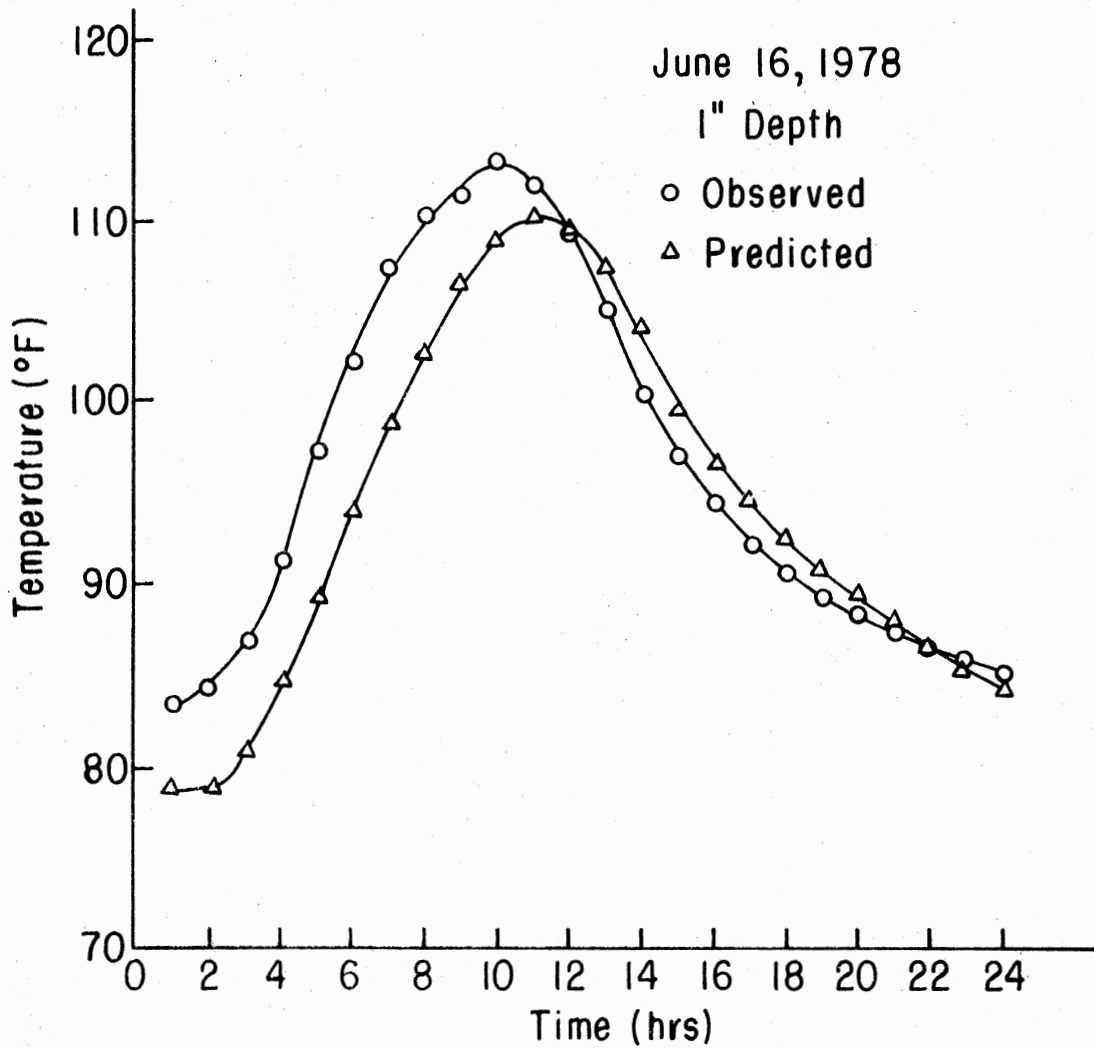


Figure 29. Comparison Between Newly Predicted and Observed Temperatures One Inch Below the Surface in the Freshwater Solar Storage Model for June 16, 1978. Time Is Measured from 6:00 a.m. (CDT) of This Day

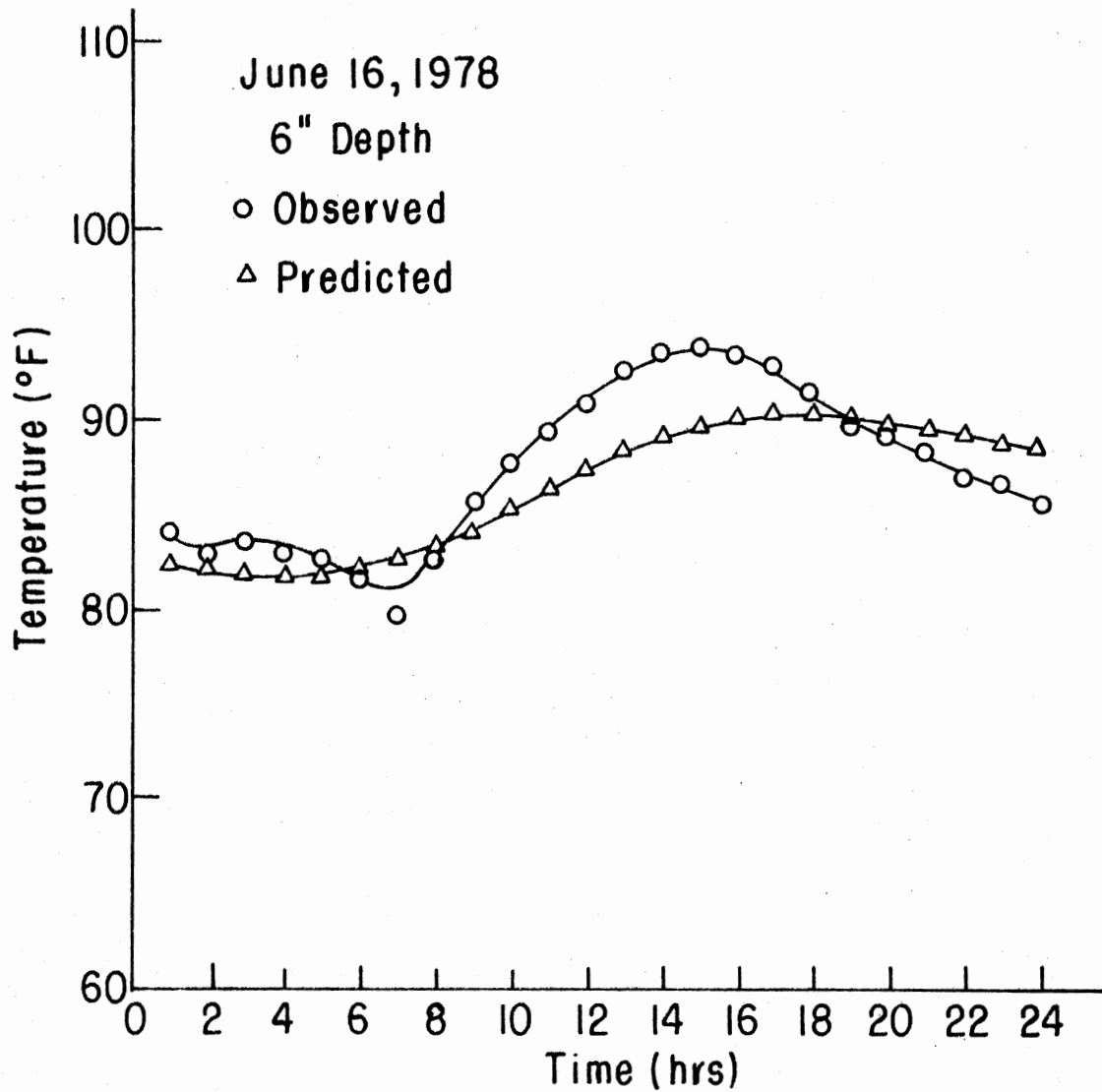


Figure 30. Comparison Between Newly Predicted and Observed Temperatures Six Inches Below the Surface in the Freshwater Solar Storage Model for June 16, 1978. Time Is Measured from 6:00 a.m. (CDT) of This Day

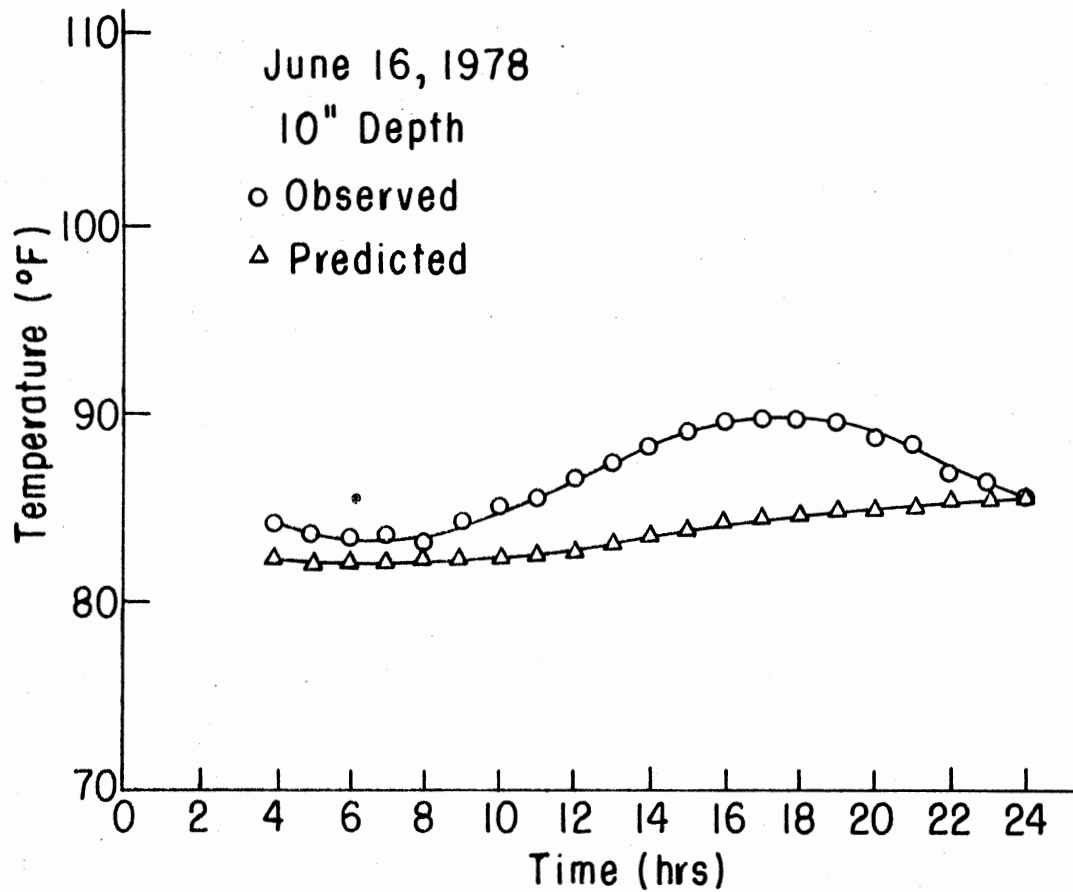


Figure 31. Comparison Between Newly Predicted and Observed Temperatures 10 Inches Below the Surface in the Freshwater Solar Storage Model for June 16, 1978. Time Is Measured from 6:00 a.m. (CDT) of This Day

Average Water Temperature

Average water temperature is the mass average temperature of the water in the model. No effort was made to agitate the water and thus a stratified condition occurred allowing the temperature profile to take on an exponential type function. To calculate the average water temperatures, the temperature profile was integrated over the entire depth of the water at each one hour time interval. Figures 32, 33, 34, and 35 show the temperature profiles for daytime and nighttime of a clear day and rainy overcast day, respectively. Also, the daily solar radiation is plotted for the clear day and a rainy overcast day in Figures 36 and 37, respectively, for Stillwater, Oklahoma.

The average water temperature in the model increased at a rate of 0.3° F per day or 9° F per month for the 47 day reporting period which is equivalent to 108 BTU per square foot per day or 3,340 BTU per square foot per month of heat energy gain.

The average water temperature plotted in Figures 38 and 39 represent the times when the largest amount of energy was lost (early morning) and when the largest amount of energy was gained (late evening), respectively. The dotted lines represent times the data logger malfunctioned or there were problems with the thermocouple wires and no temperatures were recorded.

The average daily solar radiation is plotted in Figure 40 with several days when solar radiation data is missing. There is a considerable variation in the amount of solar radiation received on a daily basis. Comparing Figures 38, 39, and 40, the days when solar radiation is lowest is the same days when the average water temperature drops,

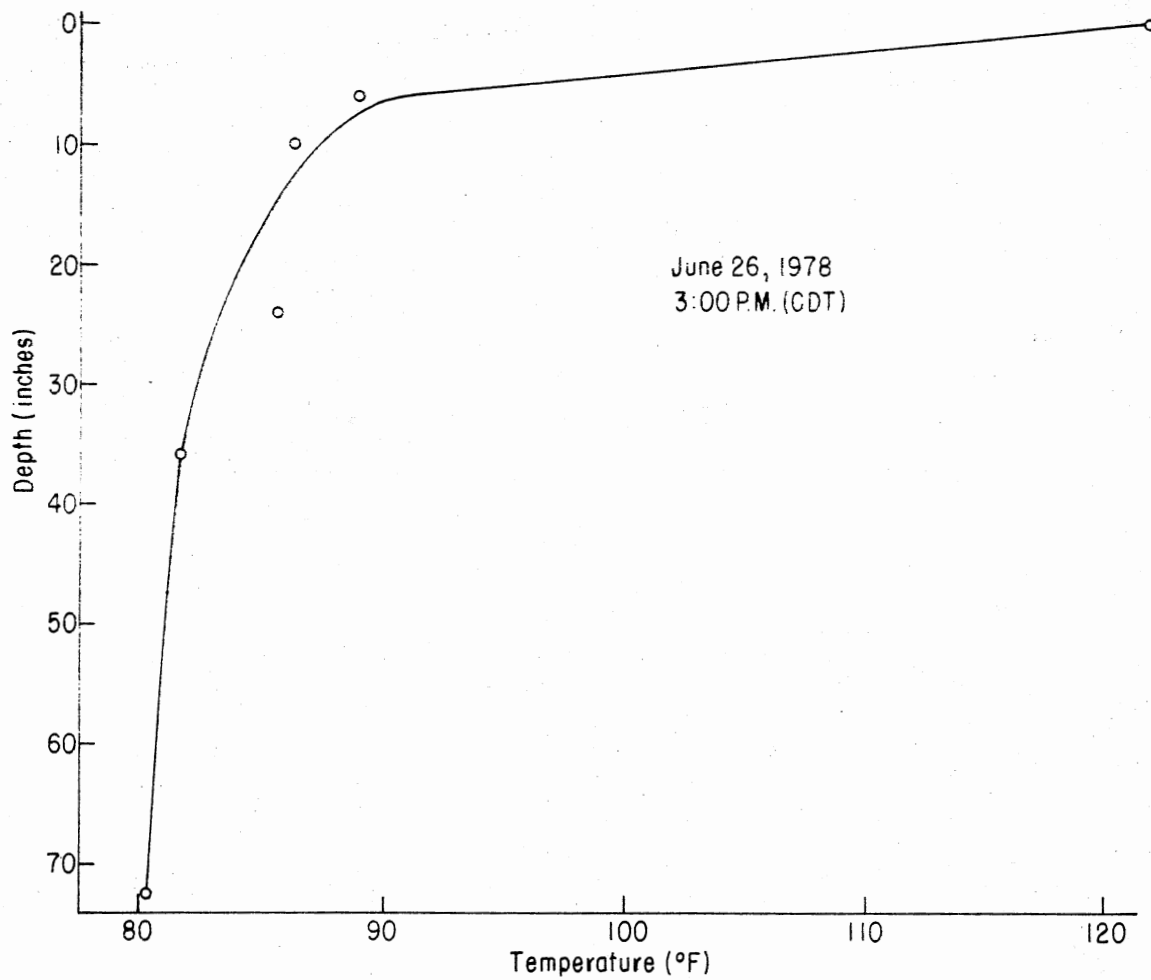


Figure 32. Temperature Profile in Freshwater Solar Storage Model for 3:00 p.m. (CDT) on June 26, 1978

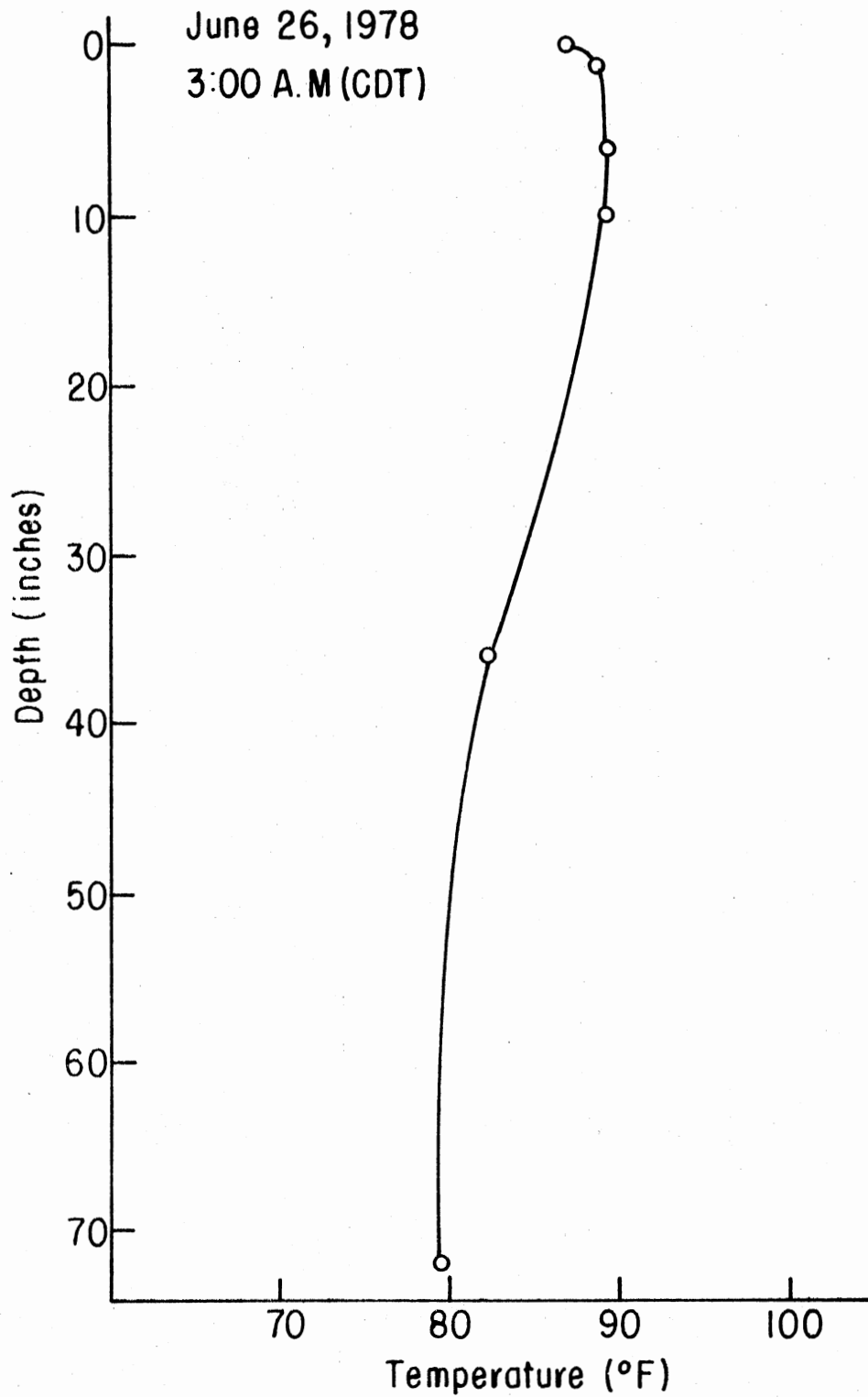


Figure 33. Temperature Profile in Freshwater Solar Storage Model for 3:00 a.m. (CDT) on June 26, 1978

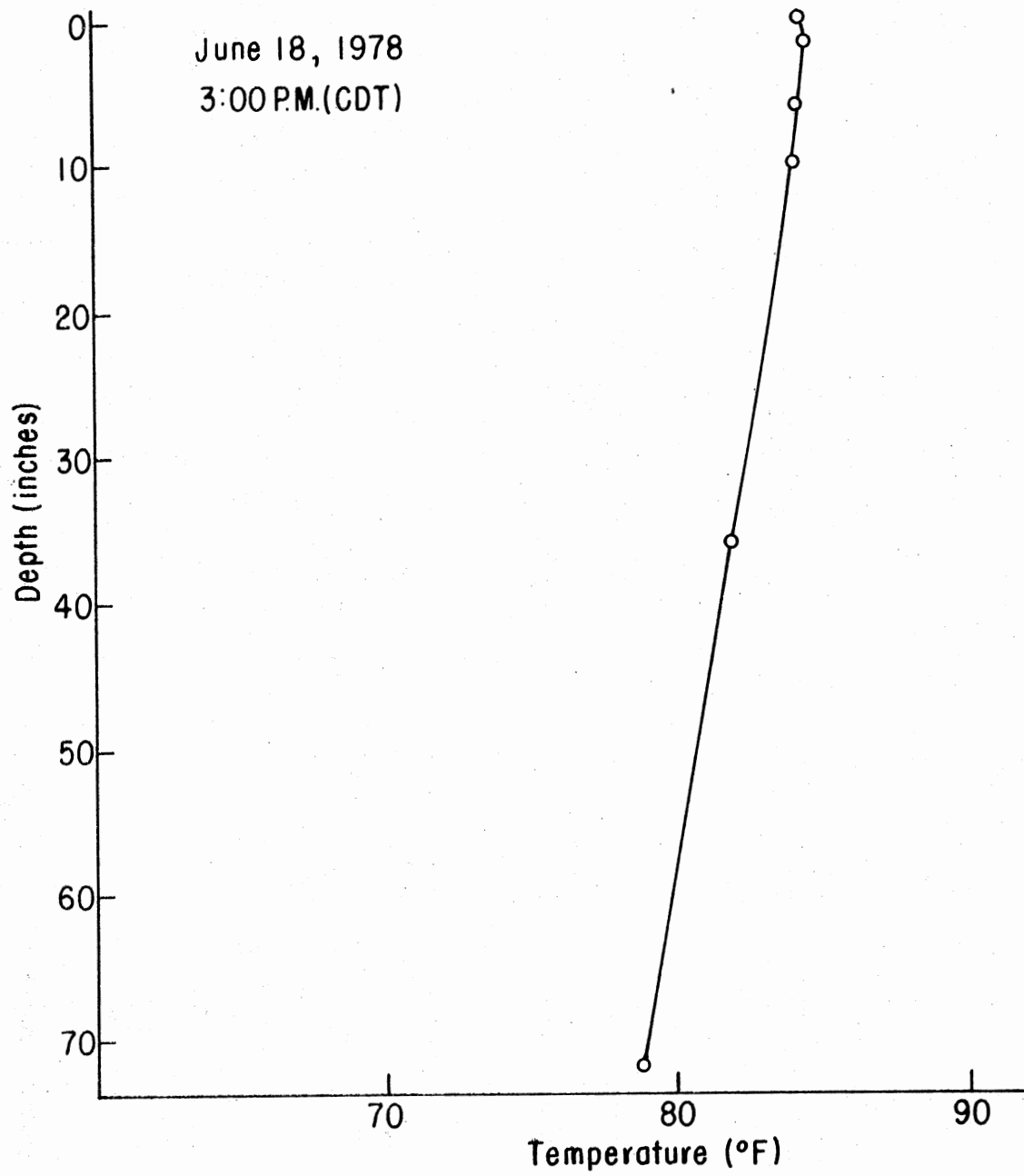


Figure 34. Temperature Profile in Freshwater Solar Storage Model for 3:00 p.m. (CDT) on June 18, 1978

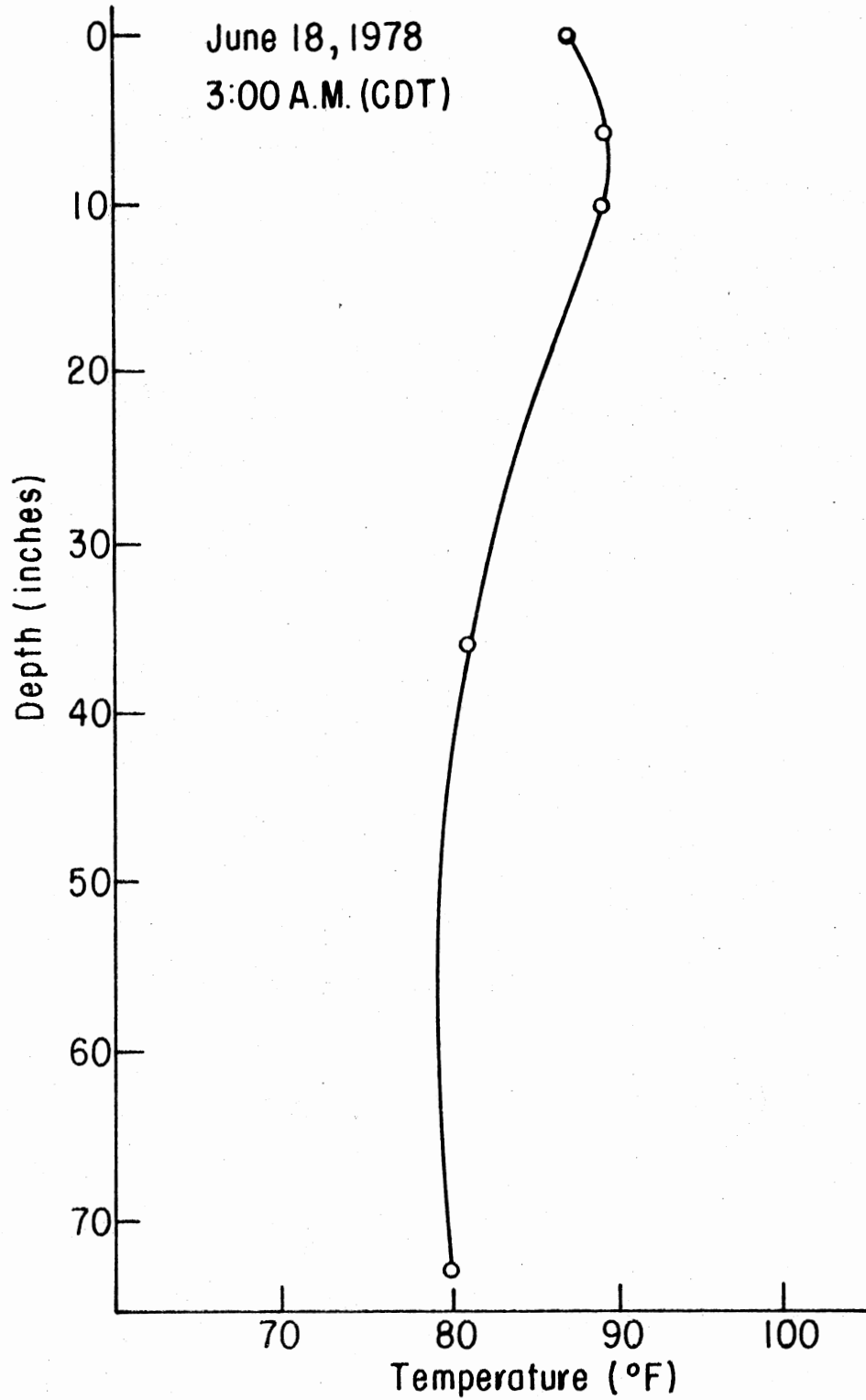


Figure 35. Temperature Profile in Freshwater Solar Storage Model for 3:00 a.m. (CDT) on June 18, 1978

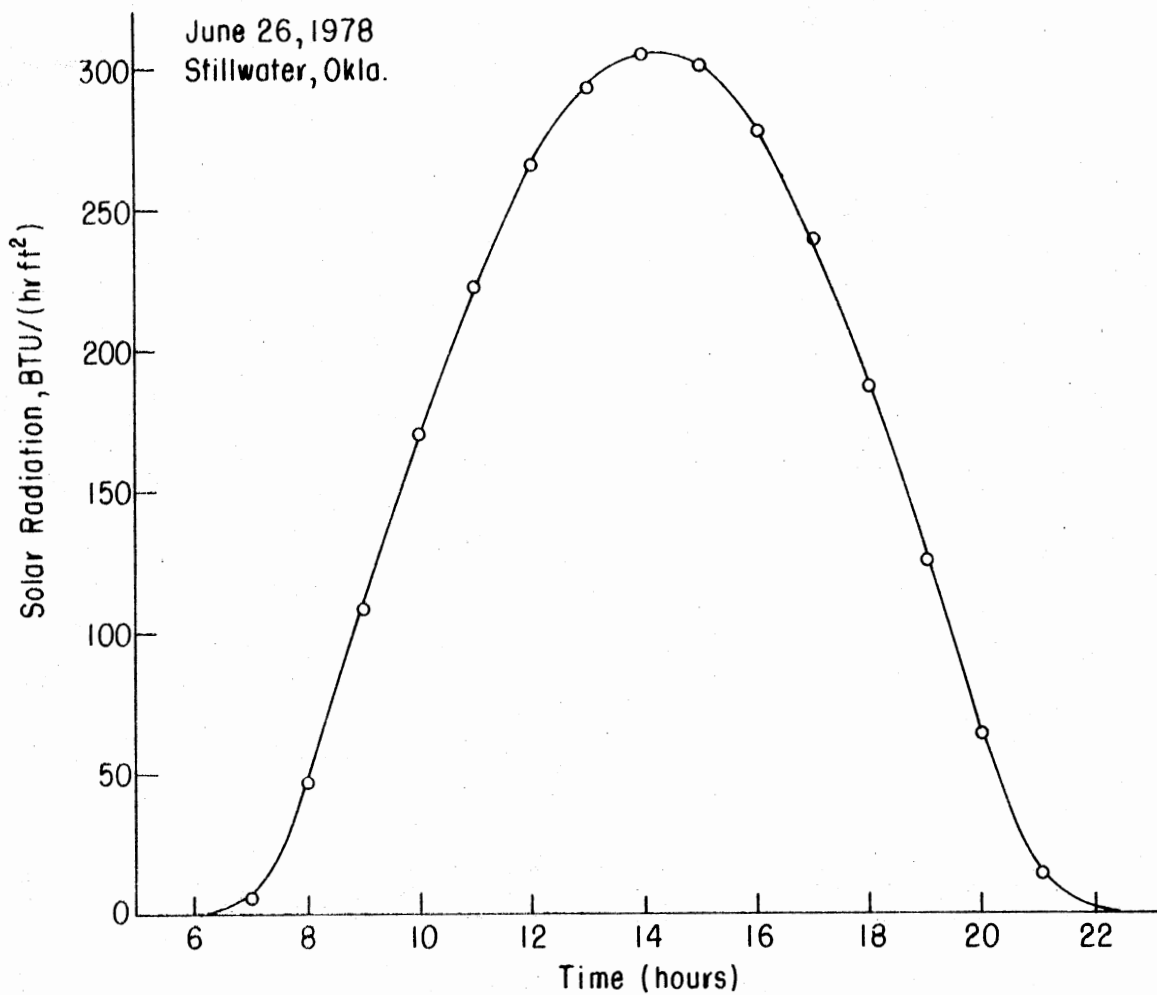


Figure 36. Solar Radiation Received at Stillwater, Oklahoma, on June 26, 1978. Time Is Measured from Midnight of Previous Day (CDT)

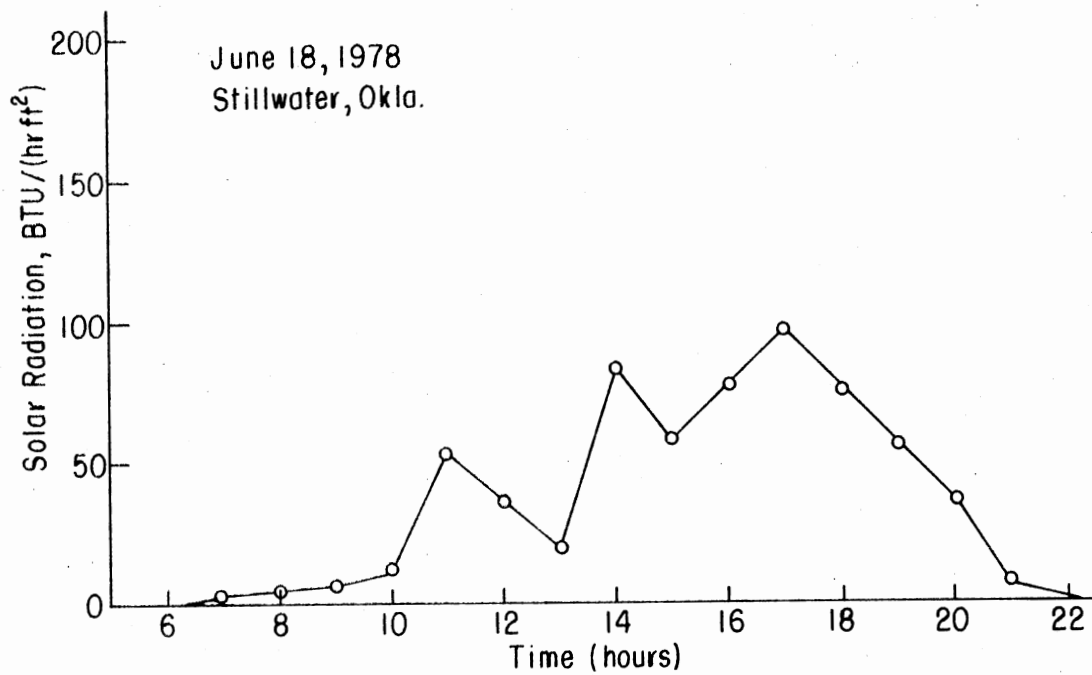


Figure 37. Solar Radiation Received at Stillwater, Oklahoma, on June 18, 1978. Time Is Measured from Midnight of Previous Day (CDT)

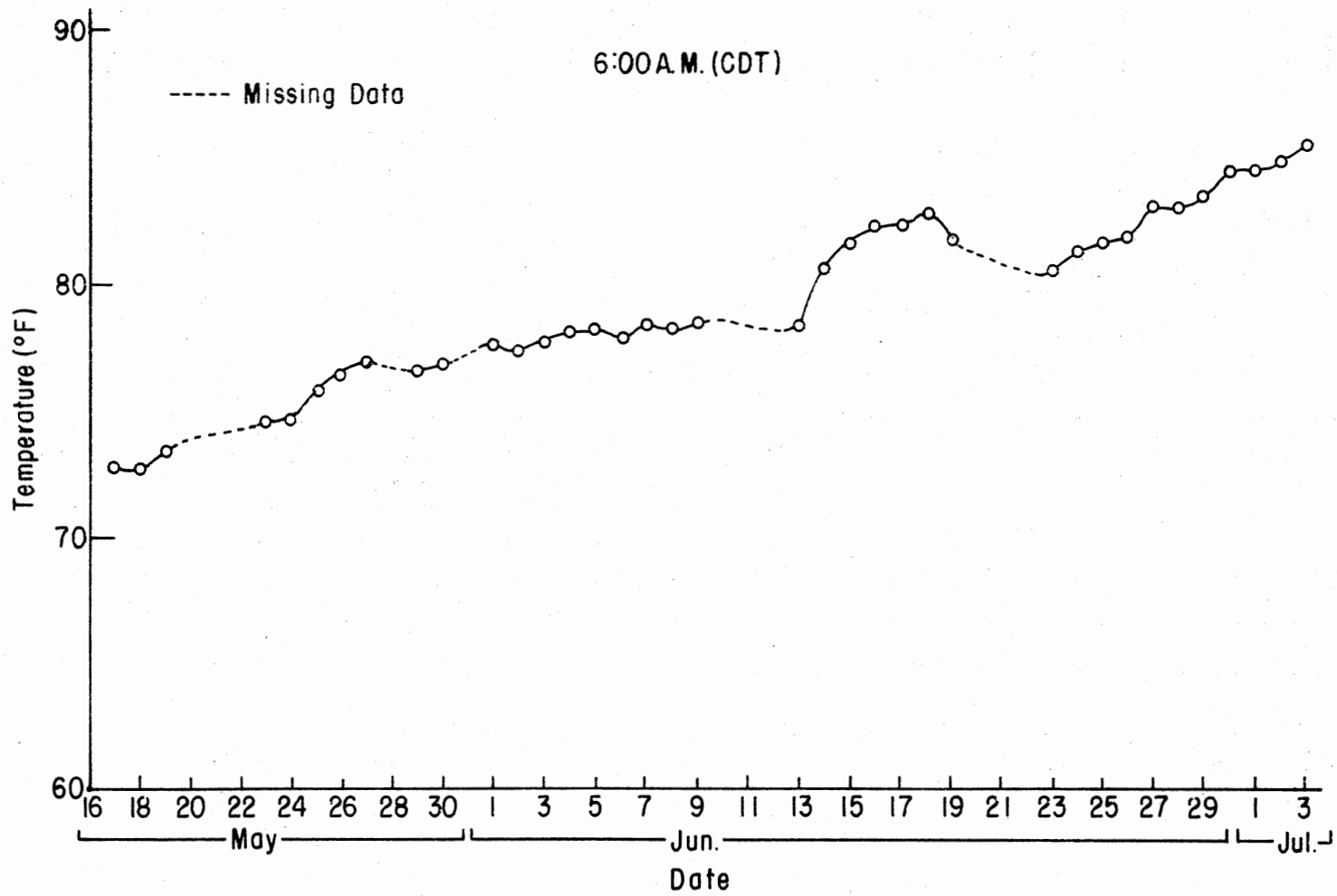


Figure 38. Average Water Temperature in Freshwater Solar Storage Model for Time of 6:00 a.m. (CDT)

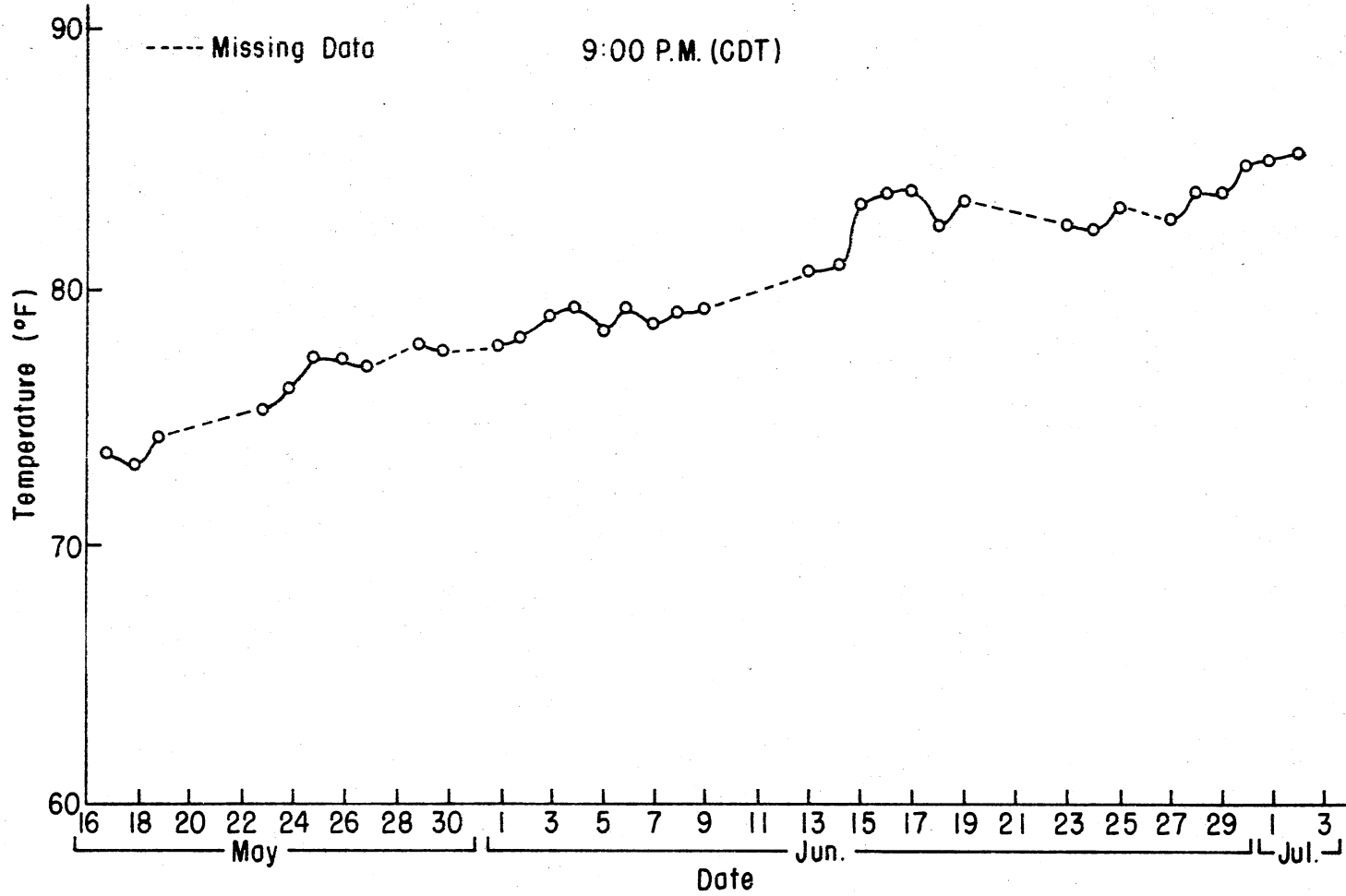


Figure 39. Average Water Temperature in Freshwater Solar Storage Model for Time of 9:00 p.m. (CDT)

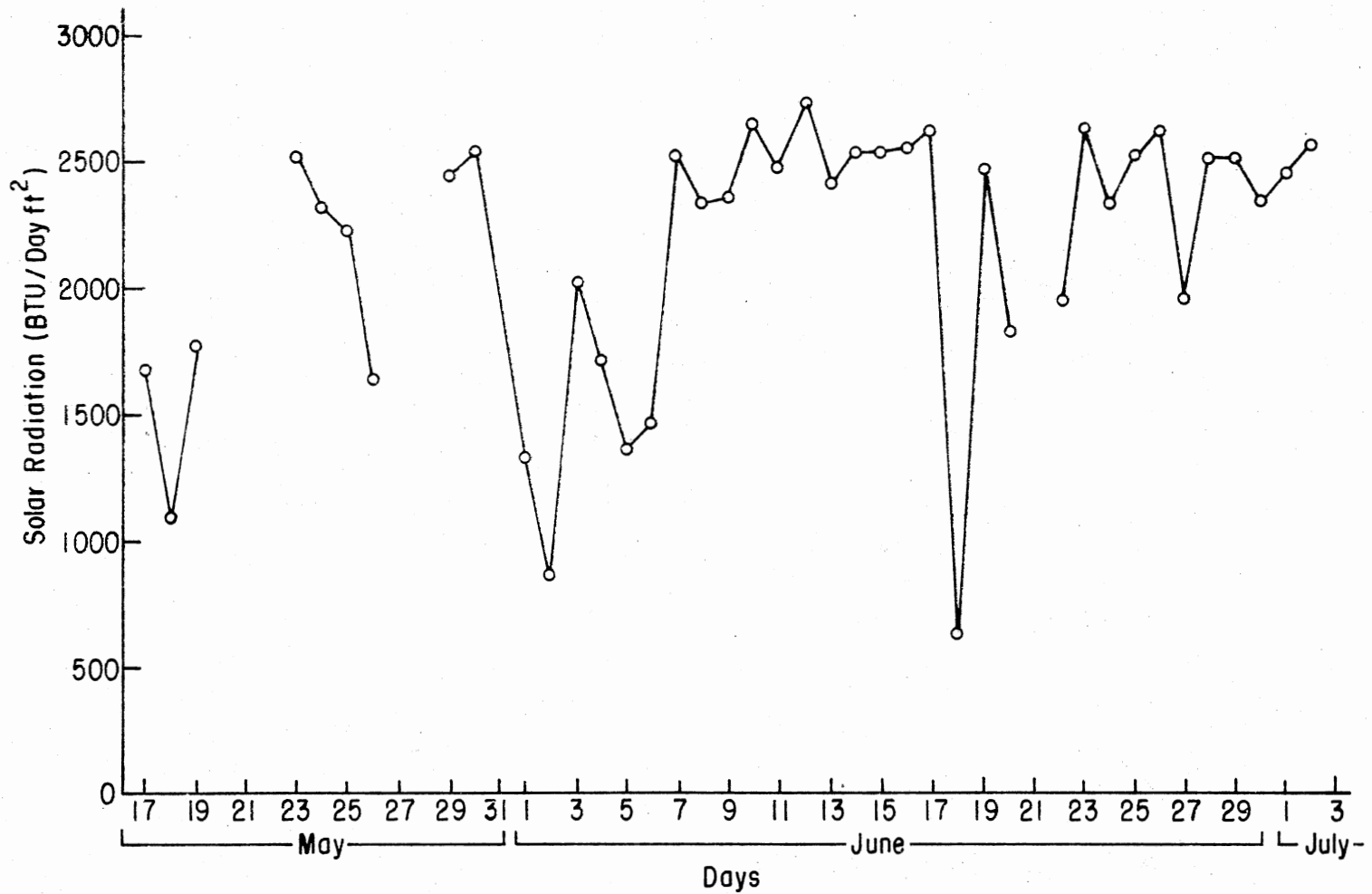


Figure 40. Solar Radiation Received for May and June of 1978 in Stillwater, Oklahoma, with the Blank Spaces Representing Times of No Data Being Recorded

while the days of increased solar radiation shows the average water temperature increasing.

The maximum average temperature the water will reach is dependent upon the vapor pressure of the water and the process by which the water is heated. An energy balance on the system will enable the maximum temperature to be calculated.

Efficiency

Efficiency is defined as the useful energy gained by the water divided by the total energy received due to solar radiation. Total efficiency for the system was determined for a 24 hour period and includes all the losses due to air infiltration, reradiation, losses through the wall and bottom of the model by conduction, and convection. The amount of energy gained by the water was calculated using equation (46).

$$Q_u = m_w C_w (t_f - t_i) \quad (46)$$

where,

Q_u = useful energy gained, BTU/day-ft².

m_w = mass of water, lbm.

C_w = specific heat of water, BTU/lbm-°F.

t_f = final average water temperature at 12:00 a.m., °F.

t_i = initial average water temperature at 1:00 a.m., °F.

The total amount of solar radiation received on a flat surface was determined from data collected at the Agronomy Research Station located at Stillwater, Oklahoma.

The total efficiency of the system was calculated by equation (47).

$$\eta_1 = \frac{Q_u}{\Sigma Q_{RAD}} \quad (47)$$

where,

η_1 = total efficiency for a 24 hour period.

Q_u = energy gained by the water, BTU/ft²-day.

ΣQ_{RAD} = summation of solar radiation received for 24 hour period, BTU/ft²-day.

Total efficiency values ranged as high as 42% with equation (48) being selected to fit the data.

$$\eta_1 = 0.0166 + 0.141\Delta t \quad (48)$$

where,

η_1 = total efficiency for 24 hours.

Δt = temperature difference between initial and final average water temperature for 24 hour period, °F.

Figure 41 is a plot of total efficiency versus temperature difference for a 24 hour time period. There were five days when the total efficiency was negative and these negative data points were not included in the regression analysis. Three of these five days were either overcast or overcast with rain which caused a loss of heat that resulted in negative efficiencies. The other two data points are negative due to the data logger malfunctioning at the time the temperatures were recorded giving erroneous temperature readings.

Net efficiency was determined to take into account the heat loss due to air infiltration, where air infiltration is the amount of air needed to keep the polyethylene dome inflated to 0.1 inch of water pressure and was calculated by equation (7).

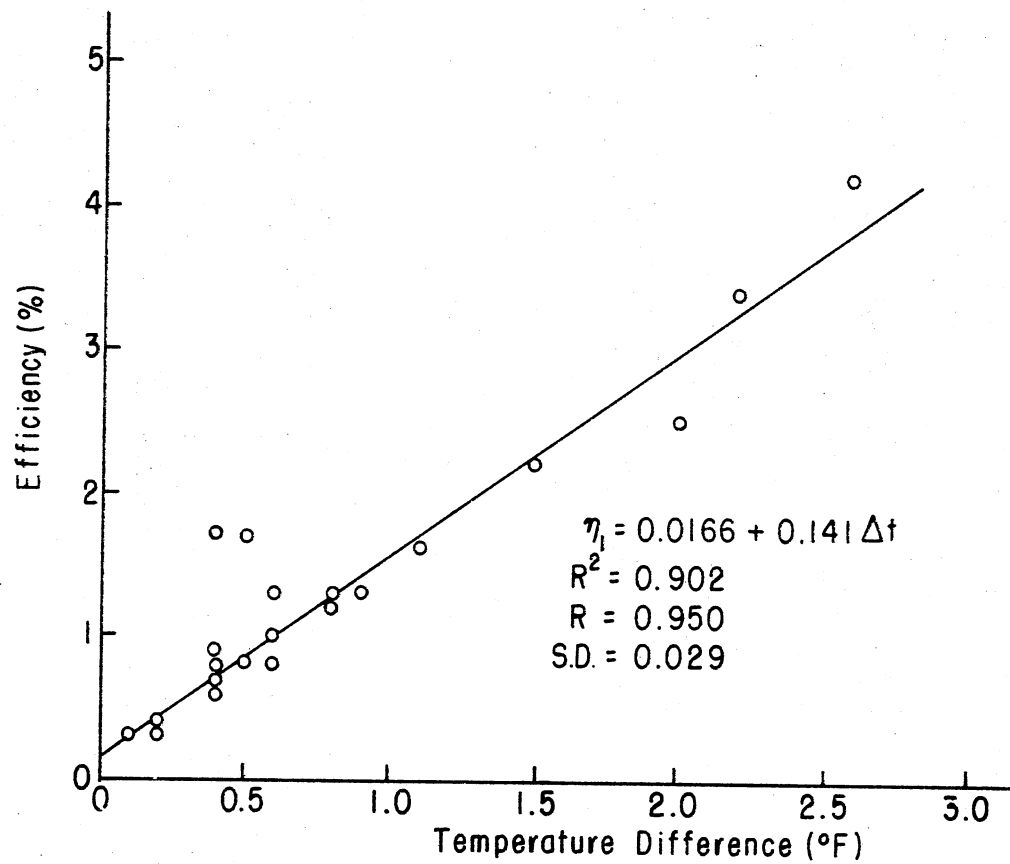


Figure 41. Daily Collection and Storage Efficiency for a 24 Hour Day Beginning at 12:00 a.m. as a Function of Average Water Temperature Difference in Storage Media Between Beginning and End of Each Period

Net efficiency was calculated using equation (49).

$$\eta_2 = \frac{Q_u}{\Sigma Q_{RAD} - Q_{AIR}} \quad (49)$$

where,

η_2 = net efficiency of system.

ΣQ_{AIR} = summation of heat loss due to air infiltration, BTU/day-ft².

The net efficiency values ranged up to 49%, 14% higher than the total efficiency values. Air infiltration does have an effect upon the efficiency of the system and a better method of eliminating air loss due to infiltration would improve the efficiency of the system and thus improve the amount of heat gained by the water.

The net efficiency versus the temperature difference for a 24 hour period is plotted in Figure 42 with equation (50) determined by linear regression to fit the data.

$$\eta_2 = 0.0246 + 0.162\Delta t \quad (50)$$

where,

η_2 = net efficiency of a system for a 24 hour period.

Δt = difference between initial and final average temperature, °F.

Efficiency was also calculated for a 15 hour period when solar radiation is received to compare these efficiencies with those calculated for a conventional flat-plate collector which is usually in operation only during periods when solar radiation can be collected. Both the total efficiency and the net efficiency for the system were calculated for the 15 hour period. By modifying equation (47) to include only the time period of 15 hours, the total efficiency of the system can be

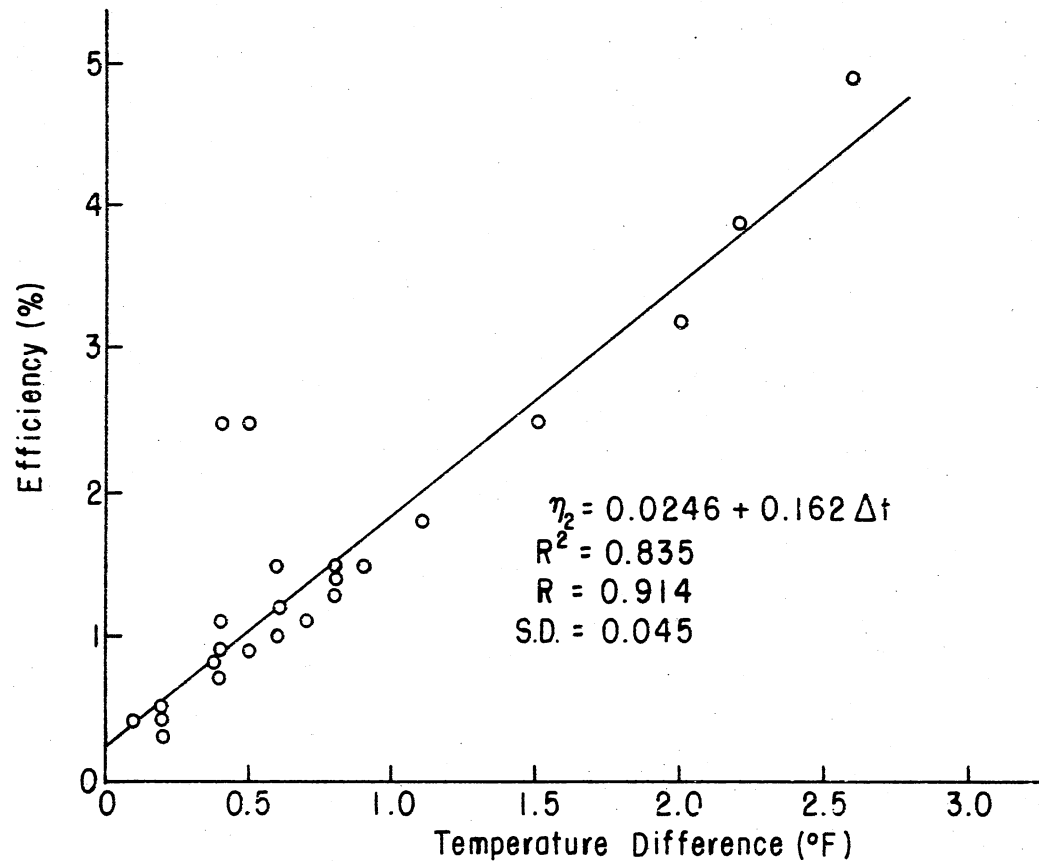


Figure 42. Daily Collection and Storage Efficiency for a 24 Hour Day Beginning at 12:00 a.m. with Infiltration Losses Included as a Function of Average Water Temperature Difference in Storage Media Between Beginning and End of Period

determined.

Figure 43 shows the plot of total efficiency versus temperature difference for a 15 hour time period with equation (51) being selected as the one to fit the data plotted in Figure 43.

$$\eta_3 = 0.0482 + 0.132\Delta t \quad (51)$$

where,

η_3 = total efficiency for a 15 hour period.

Δt = temperature difference between initial and final average water temperatures, °F.

These total efficiency values ranged up to 53% which compare quite well with conventional solar collectors for air and water having values ranging up to 60% (14).

The net efficiency was also calculated to account for the heat loss due to air infiltration for an 15 hour period and equation (49) was modified to only account for 15 hours with the data being plotted in Figure 44.

The data plotted in Figure 44 is represented by equation (52).

$$\eta_4 = 0.065 + 0.140\Delta t \quad (52)$$

where,

η_4 = net efficiency for a 15 hour period.

Δt = temperature difference between initial and final average water temperature, °F.

The net efficiency values ranged up to 59% which compared quite well for total efficiency with the values for conventional air and water solar collectors of 20 to 60% (14). Also, the net efficiency values is 10% higher than the total efficiency value for a 15 hour time period which shows that decreasing air infiltration will increase efficiency.

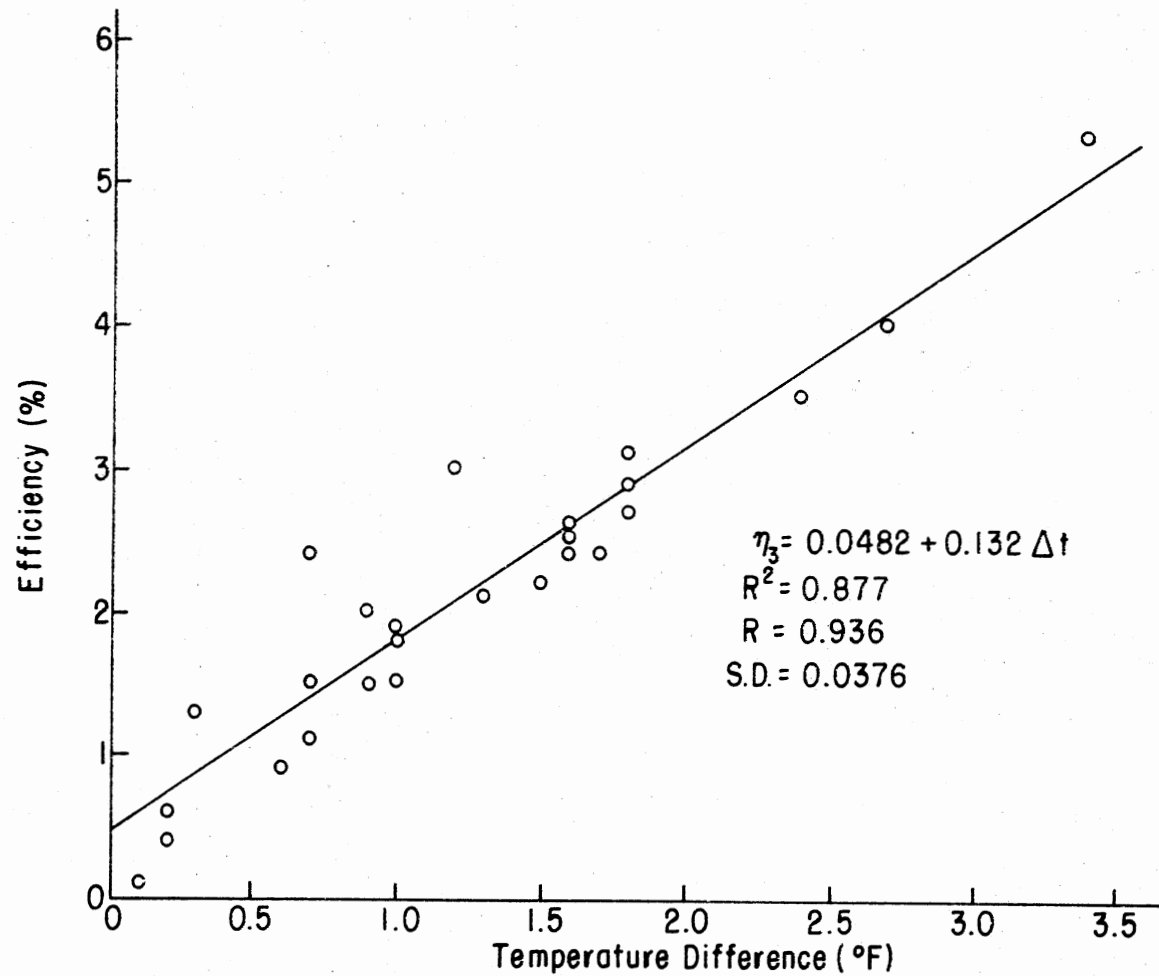


Figure 43. Daily Collection and Storage Efficiency for a 15 Hour Day Beginning at 6:00 a.m. as a Function of Average Temperature Difference in Storage Media Between Beginning and End of Period

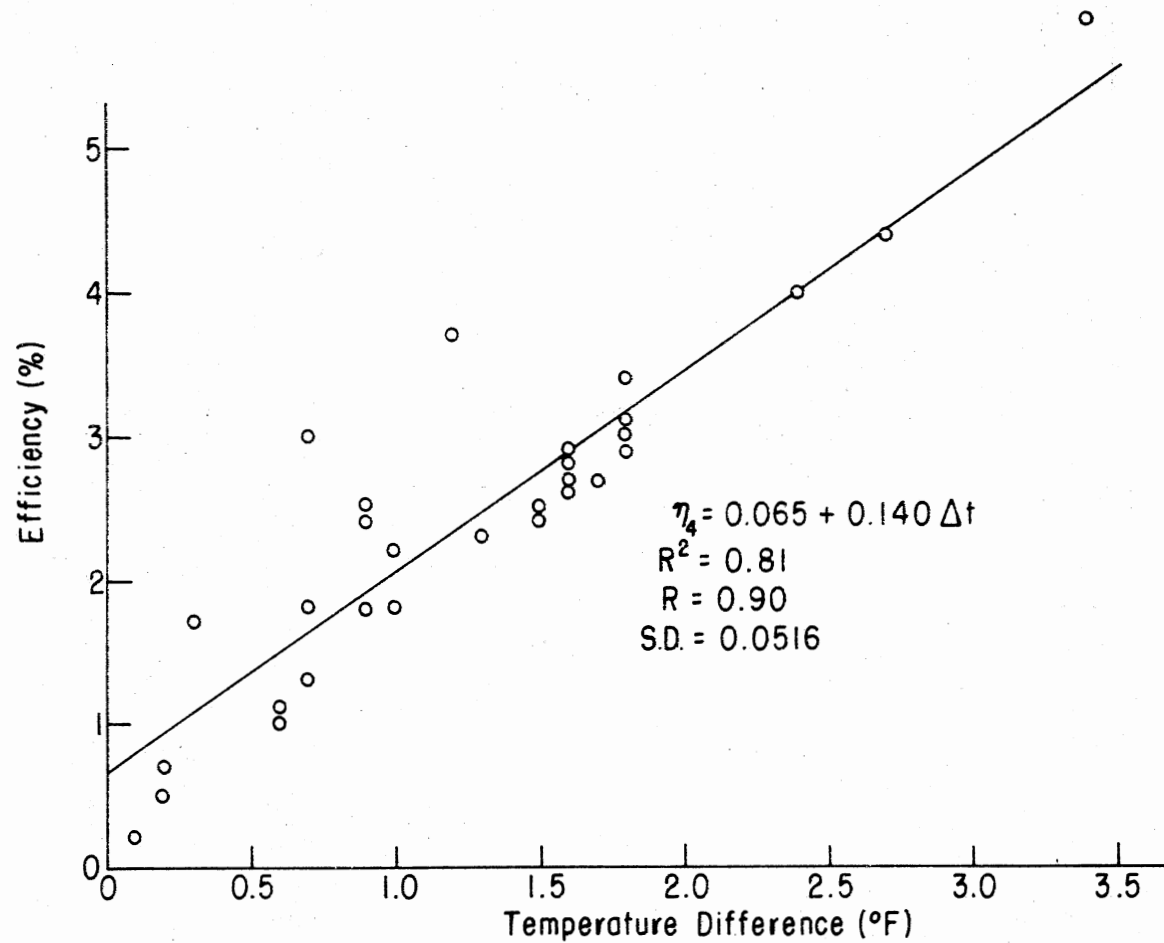


Figure 44. Daily Collection and Storage Efficiency for a 18 Hour Day Beginning at 6:00 a.m. with Infiltration Losses Included as a Function of Average Water Temperature Difference in Storage Media Between Beginning and End of Period

Table VIII presents a summary of efficiencies for the freshwater storage model, showing 15 hour and 24 hour efficiencies before correction and after correction for air infiltration into the system.

TABLE VIII

SUMMARY OF STORAGE EFFICIENCY FOR
FRESHWATER STORAGE MODEL

Date	Daily Solar Radiation ΣQ_{RAD} BTU/Day/Ft ²	Infiltration Energy Loss ΣQ_{INF} BTU/Day/Ft ²	Daily Temperature Change 24 Hour °F	15 Hour Temperature Change 6 am-9 pm °F	η_1 24 Hour Efficiency	η_2 24 Hour Eff. Corrected for Infiltration	η_3 15 Hour Efficiency	η_4 15 Hour Eff. Corrected for Infiltration
May								
17	1696	332	0.0	0.7	0.0	0.0	0.15	0.18
18	1081	332	0.5	0.7	0.17	0.25	0.24	0.30
19	1782	301	0.6	0.2	0.13	0.15	0.04	0.05
23	2509	348	-0.2	0.1	--	--	0.01	0.02
24	2304	345	2.6	1.8	0.42	0.49	0.29	0.34
25	2245	378	0.6	0.9	0.10	0.12	0.15	0.18
26	1649	322	0.4	0.9	0.09	0.11	0.20	0.24
27	377	213	-0.5	-0.1	--	--	--	--
29	2451	416	0.5	1.0	0.08	0.09	0.15	0.18
30	2544	397	-0.1	0.6	--	--	0.09	0.10
June								
1	1318	313	0.1	0.2	0.03	0.04	0.06	0.07
2	853	250	0.4	0.3	0.17	0.25	0.13	0.17
3	2036	431	0.4	1.0	0.07	0.09	0.18	0.22
4	1702	351	0.2	0.9	0.04	0.05	0.20	0.25
5	1377	336	-0.4	-0.1	--	--	--	--
6	1483	336	2.0	1.2	0.25	0.32	0.30	0.37
7	2522	435	0.0	0.0	0.0	0.0	0.0	0.0
8	2336	441	0.2	0.7	0.03	0.04	0.11	0.13
9	2363	425	0.4	0.6	0.06	0.08	0.09	0.11

TABLE VIII (Continued)

Date	Daily Solar Radiation ΣQ_{RAD} BTU/Day/Ft ²	Infiltration Energy Loss ΣQ_{INF} BTU/Day/Ft ²	Daily Temperature Change 24 Hour °F	15 Hour Temperature Change 6 am-9 pm °F	η_1 24 Hour Efficiency	η_2 24 Hour Eff. Corrected for Infiltration	η_3 15 Hour Efficiency	η_4 15 Hour Eff. Corrected for Infiltration
June								
13	2407	320	2.2	3.4	0.34	0.39	0.53	0.59
14	2539	309	1.5	2.4	0.22	0.25	0.35	0.40
15	2534	273	0.8	2.7	0.12	0.13	0.4	0.44
16	2551	249	1.1	1.6	0.16	0.18	0.26	0.26
17	2635	313	0.6	1.8	0.08	0.10	0.29	0.29
18	607	194	-1.7	-0.5	--	--	--	--
19	2480	346	0.8	1.8	0.12	0.14	0.31	0.31
23	2636	284	1.1	2.0	0.16	0.17	0.28	0.32
24	2343	318	0.8	1.3	0.13	0.15	0.21	0.23
25	2531	275	0.9	1.5	0.13	0.15	0.22	0.25
26	2638	292	0.7	1.5	0.10	0.11	0.22	0.24
27	1947	285	0.4	1.0	0.08	0.09	0.19	0.22
28	2510	352	0.9	1.6	0.13	0.16	0.24	0.27
29	2509	405	0.8	1.6	0.12	0.14	0.24	0.28
30	2352	367	0.4	1.6	0.06	0.07	0.25	0.30
July								
1	2462	308	0.2	1.8	0.03	0.03	0.27	0.30
2	2589	318	0.7	1.7	0.10	0.11	0.24	0.27

CHAPTER VI

SUMMARY AND CONCLUSIONS

Summary

The major objectives of this study were to develop a method for theoretically determining the temperature of a freshwater pond and to measure the efficiency of black polyethylene as a solar collector absorber. This required several assumptions to be made concerning heat losses from the model and absorption of heat by solar radiation.

A prediction equation was written by use of finite difference equations for a transient numerical conduction problem.

A storage and collection model was constructed to represent a vertical section of a 10,000 square foot pond. The storage model was six feet deep with a surface area of 36.1 square feet. A collector absorber constructed of six mil, black polyethylene was placed on the water surface with a clear polyethylene being placed over the absorber and supported by air. Operation of the experiment began on May 17, 1978, with data being collected for 47 days. The temperatures of the ambient air, air inside the polyethylene dome, at the surface of the water and depths of 1 inch, 6 inches, 10 inches, 18 inches, 24 inches, 36 inches, and 72 inches below the surface were recorded. Average water temperature increased at a rate of 0.3° F per day or 9° F per month for May, June, and July with efficiencies of the polyethylene absorber ranging from 10 to 50% on a daily basis. Prediction of temperature distribution resulted

in errors as high as 33% and was due mainly to an incorrect specification of the surface boundary condition concerning the heat loss from the surface of the model.

Conclusions

The prediction of temperature distribution in the freshwater storage model is dependent upon accurate definition of the surface boundary condition. The surface boundary condition includes heat loss due to convection, radiation, evaporation, and air infiltration. Differences as high as 33% between predicted and observed temperatures occurred due to the surface boundary condition being inaccurately specified. An 8% difference occurred when the surface heat loss was decreased by 44% during nighttime hours and increased by 33% during daytime hours.

Efficiencies of the black polyethylene absorber ranged from 10% to 50% and compare favorably with conventional flat-plate collectors. Air infiltration from the inflated structure reduced collection and storage efficiencies by 10%. The black polyethylene absorber deteriorated under ultraviolet rays of the sun after 47 days of use. Therefore, polyethylene is not recommended as an absorber on the surface of freshwater ponds because of its short life.

The average water temperature increased at a rate of 0.3° F per day for the months of May and June, 1978, which is equivalent to a heat gain in the storage model of 3,348 BTU/ft²-month.

Condensation on the underside of the clear polyethylene cover reduced solar radiation transmittance through the cover by 14%.

SELECTED BIBLIOGRAPHY

1. Brunt, D. "Notes on Radiation in the Atmosphere." Royal Meteorological Society, Quarterly Journal, 58:408-411, 1932.
2. Carlson, Glenn Alvin. "An Analysis of Floating Styrofoam Cover for Evaporation Suppression." Unpublished Master's Thesis, 1970.
3. Chepurniy, N. and S. B. Savage. "An Analytical and Experimental Investigation of a Laboratory Solar Pond Model." ASAE Paper No. 74-WA/Sol-3.
4. Dake, Jonas M. K. and Donald B. F. Harleman. "Thermal Stratification in Lakes: Analytical and Theoretical Studies." Water Resources Research, 5(2):484-495, 1969.
5. Donn, William L. Meteorology. McGraw-Hill Book Company, New York, 1965.
6. Duffie, John A. and William A. Beckman. Solar Energy Thermal Processes. John Wiley and Sons, Inc., New York, 1974.
7. Eaton, Elmer R. "Floating Plastic Reservoir Covers in the Arctic." Solar Energy, 8(4):116, 1964.
8. Garg, H. P. "Effect of Dirt on Transparent Covers in Flat-Plate Solar Energy Collectors." Solar Energy, 15:299-302, 1974.
9. Godbey, L. C., T. E. Bond and H. F. Zornig. "Solar and Long Wavelength Energy Transmission of Materials." ASAE Paper No. 77-4013, 1977.
10. Grevskott, G. "The Use of Water Reservoirs, Lakes and Bays for Shallow Pond Collectors and Submerged Hot Water Storage." Solar Energy, 19:777-778, 1977.
11. Hsieh, C. K. and Avil K. Rajvanshi. "The Effect of Dropwise Condensation on Glass Solar Properties." Solar Energy, 19:389-393, 1977.
12. Jaeger, J. C. and C. H. Johnson. "Note on Diurnal Temperature Variation." Geofisica Pura E Applicata, 24:104-106, 1953.

13. Keener, H. M., M. A. Sabbath, G. E. Meyer and W. L. Roller. "Plastic Film Solar Collectors for Grain Drying." Proceedings Solar Grain Drying Conference. Urbana, Illinois. Available from the National Technical Information Service, January 11-12, 1977, pp. 56-77.
14. Kline, Gerald L. "Solar Collector Performance." Proceedings Solar Grain Drying Conference. Urbana, Illinois. Available from the National Technical Information Service, January 11-12, 1977, pp. 50-55.
15. McAdams, William H. Heat Transmission. McGraw-Hill Book Company, New York, 1954.
16. Myers, Glen E. Analytical Methods in Conduction Heat Transfer. McGraw-Hill Book Company, 1971.
17. Parker, Jerald D., James H. Boggs and Edward F. Blick. Introduction to Fluid Mechanics and Heat Transfer. Addison-Wesley Publishing Company, Inc., 1969.
18. San Martin, Robert L. and Gary J. Fjeld. "Experimental Performance of Three Solar Collectors." Solar Energy, 17:345-349, 1975.
19. Schlag, J. H., D. C. Ray, A. P. Sheppard and J. M. Wood. "Inexpensive Solar Collectors for Agricultural Requirements." Solar Energy, 20:89-91, 1978.
20. Snider, D. M. and R. Viskanta. "Radiation Induced Thermal Stratification in Surface Layers of Stagnant Water." Journal of Heat Transfer, Trans. of ASAE, February, 1975, 35-40.
21. Tabor, H. "Large-Area Solar Collectors for Power Production." Solar Energy, 7(4):189-194, 1963.
22. Umarov, G. Ya, M. K. Asamov, B. M. Achilov, T. K. Sarros, E. Zh. Narov and N. A. Tsagaraeva. "Modified Polyethylene Films for Solar Stills." Geliotekhnika, 12(2):29-33, 1976.
23. Walker, John N. and Donald C. Slack. "Properties of Greenhouse Covering Materials." Trans. of the ASAE, 1970, pp. 682-684.
24. Weinberger, Hershel. "The Physics of the Solar Pond." Solar Energy, 8(2), 45-56, 1964.

VITA²

Dennis Leroy Datin

Candidate for the Degree of
Master of Science

Thesis: MODEL OF A FRESHWATER POND USED FOR COLLECTION AND STORAGE OF SOLAR ENERGY

Major Field: Agricultural Engineering

Biographical:

Personal Data: Born in Guthrie, Logan County, Oklahoma, November 8, 1949, the son of Marion Leroy and Alice Winifred (Dreessen) Datin; married to Colette Louise Reiche (Slattengren) on April 20, 1979, in Oakland, California.

Education: Graduated from Guthrie High School, Guthrie, Oklahoma, in 1968; received a Bachelor of Science degree in Agricultural Engineering from Oklahoma State University in May, 1972; completed requirements for the Master of Science degree from Oklahoma State University in December, 1979.

Professional Experience: Metrologist for the State of Oklahoma, Department of Agriculture from July, 1972, to February, 1975; Missionary for The Church of Jesus Christ of Latter-day Saints in Alberta, Canada, from March, 1975, to March, 1977; Graduate Research Assistant for the Agricultural Engineering Department of Oklahoma State University from May, 1977, to July, 1979.

Professional Organizations: Student member of American Society of Agricultural Engineers; American Society of Heating, Refrigerating and Air-conditioning Engineers.